Cool-Season Regime Transition and Its Impact

On Precipitation in the Northeastern United States

Abstract of

a thesis presented to the Faculty

of the University at Albany, State University of New York

in partial fulfillment of the requirements

for the degree of

Master of Science

College of Arts & Sciences

Department of Earth and Atmospheric Sciences

HEATHER M. ARCHAMBAULT

2005

Cool-Season Regime Transition and Its Impact

On Precipitation in the Northeastern United States

A thesis presented to the Faculty

of the University at Albany, State University of New York

in partial fulfillment of the requirements

for the degree of

Master of Science

College of Arts & Sciences

Department of Earth and Atmospheric Sciences

HEATHER M. ARCHAMBAULT
2005

Acknowledgements

I would like to thank my co-advisors, Lance Bosart and Dan Keyser, for their guidance, insight, and support throughout this research endeavor. I am grateful for the opportunity to work on such a relevant and interesting project, and I truly appreciate the time they have devoted to helping me improve as a scientist. I also wish to thank NOAA for their financial support of this research through the Collaborative Science and Technology Applied Research (CSTAR) program (Grant # NA07WA0458).

Thanks are due to Rich Grumm at the Central Pennsylvania Weather Forecast Office for his important role in the initiation of this research. I'd especially like to acknowledge Anantha Aiyyer, whose programming expertise greatly facilitated the compilation of datasets for this project. Anantha also proved to be an invaluable resource while I was working on the statistical portion of the project. In addition, I'd like to thank Alicia Wasula, Tom Galarneau, Ron McTaggert-Cowen, and Alan Srock for helping me generate the figures used in this thesis.

I appreciate all the assistance I received from Kevin Tyle and David Knight; without their technical support, this research would not have been possible. I'd also like to acknowledge Lynn Hughes, Diana Patton, Sharon Baumgardner, Sally Marsh, and especially Celeste Iovinella for their help in handling various administrative issues.

I would like to thank the faculty and all my fellow graduate students, especially Tom Galarneau and Joe Kravitz, for making this department such a fun and intellectually stimulating place to work. Special thanks goes to Scott Runyon for being so supportive and for keeping my stress level in check by constantly making me laugh.

Finally, I'd like to thank my wonderful family for their unconditional love and support. My mother and father deserve special recognition for being the best role models I could imagine, and also for encouraging my lifelong obsession with snowstorms, hurricanes, and other natural disasters.

Table of Contents

1. Introduction

1.1 Overview

Past research has indicated that reconfigurations of the large-scale flow may alter regional weather patterns due to shifts in storm tracks and associated eddy transports of heat, momentum, and vorticity. Meteorological wisdom also suggests that high-impact weather events tend to occur during large-scale flow reconfigurations. Therefore, if this wisdom is valid, certain types of large-scale flow reconfigurations, or regime transitions, may be associated with an increased probability of a significant precipitation event impacting the northeastern United States (U.S.).

Up until this point, no known study has explored relationships between regime transitions and Northeast precipitation. To address this need, this research seeks to identify relationships between phase transitions of weather regimes such as the North Atlantic Oscillation (NAO) and the Pacific/North American (PNA) pattern and cool-season precipitation in the Northeast. These relationships will be explored through the use of a statistical climatology and composite analyses of NAO and PNA phase transitions.

1.2 Literature Review

1.2.1 The North Atlantic Oscillation

Documented observations suggesting the existence of the NAO, a low-frequency atmospheric oscillation over the North Atlantic, date back to the 18th century, when Crantz (1765) noted that mild (cold) Greenland winters tend to coincide with cold (mild) northern European winters (van Loon and Rogers 1978). The term “North Atlantic Oscillation” was first used by Walker and Bliss (1932) to describe this phenomenon. They noted that the positive phase of the NAO is characterized by lower-than-average sea level pressure (SLP) near Iceland and higher-than-average SLP over the Azores and northwestern Europe. These large-scale atmospheric conditions were found to be associated with strong westerlies in the North Atlantic, below-normal temperatures over the Greenland-Labrador area and the Middle East, and above-normal temperatures over the eastern U.S. and northwestern Europe. Conversely, Walker and Bliss (1932) noted that the negative phase of the NAO is characterized by higher-than-average SLP near Iceland and lower-than-average SLP over the Azores and northwestern Europe. These conditions were found to be associated with weak westerlies in the North Atlantic, above-normal temperatures in the Greenland-Labrador area and the Middle East, and below-normal temperatures in the eastern U.S. and northwestern Europe.

Van Loon and Rogers (1978) examined large-scale atmospheric patterns associated with the “seesaw” in winter temperatures between Greenland and northwestern Europe by defining two states of the temperature seesaw that were analogous to the two phases of the NAO described by Walker and Bliss (1932). The first state, “Greenland Below” (GB), is similar to the positive NAO phase and occurs when the mean January surface temperature in Jakobshavn, Greenland, is below normal while the mean temperature in Oslo, Norway, is above normal. The second state, “Greenland Above” (GA), is similar to the negative NAO phase and occurs when the mean January temperature in Jakobshavn is above normal while the mean temperature in Oslo is below normal. Van Loon and Rogers (1978) observed that January temperature anomalies over the southern Mediterranean, the Middle East, Central America, and western North America tend to be of the same sign as the temperature anomaly over Greenland, while the January temperature anomaly over eastern North America tends to be of the same sign as the temperature anomaly over Europe.

In addition to identifying temperature patterns associated with the two states of the temperature seesaw, van Loon and Rogers (1978) identified SLP patterns associated with each state. They observed that SLP near Iceland tends to vary oppositely with SLP near the Azores and the Aleutians. These variations led van Loon and Rogers (1978) to infer that Atlantic westerlies tend to vary inversely with the strength of the Pacific westerlies during both states of the temperature seesaw. Finally, van Loon and Rogers (1978) noted that one phase of the atmospheric circulation seesaw tends persist for several decades at a time.

Wallace and Gutzler (1981) objectively identified winter teleconnection patterns in the Northern Hemisphere (NH) using one-point spatial correlations represented on correlation maps. The maps demonstrated that geopotential heights at certain points are strongly correlated not only with the geopotential heights in surrounding regions, but also with geopotential heights in remote regions. Their work identified a dipole pattern similar to the NAO described by van Loon and Rogers (1978) using both 500 hPa geopotential height data and SLP. Correlations between 1000–500 hPa thickness and the SLP differences between the two centers of the NAO dipole verified that temperatures over Greenland tend to be negatively correlated with temperatures over the eastern U.S. and northern Africa, and positively correlated with temperatures over Scandinavia. One notable difference between Wallace and Gutzler's (1981) work and van Loon and Rogers's (1978) work was that Wallace and Gutzler did not find a relationship between Icelandic and Aleutian SLP.

While Wallace and Gutzler (1981) employed a teleconnections method to identify and characterize the NAO, Barnston and Livezey (1987) used rotated empirical orthogonal function (REOF) analyses to establish the NAO as both a statistically stable and physically meaningful representation of large-scale atmospheric variability. Barnston and Livezey (1987) identified the NAO as having a strong center near western Greenland, with a strong north–south gradient of large zonal extent to the south. They found that the NAO pattern explains the highest or second-highest amount of large-scale 700 hPa geopotential height variance in nine months of the year, and is the only large-scale circulation pattern in the NH that is active year-round. Thus, they concluded that the NAO is the most significant contributor to low-frequency geopotential height variability in the NH.

In addition to illustrating the pervasiveness of the NAO in the northern hemispheric large-scale circulation, Barnston and Livezey (1987) demonstrated that the NAO dipole pattern tends to contract northward during winter and expand southward during summer, likely in response to the annual solar insolation cycle. They also found that the location of the NAO dipole pattern varies longitudinally throughout the year, with the October, February, and April NAO patterns deviating most from the mean NAO pattern.

Hurrell (1995) examined atmospheric decadal variability in the NH and used singular vector analysis to show that the NAO explains nearly 75% of the total squared variance of seasonal mean SLP and surface temperature anomalies. He noted that the tendency of the NAO to be in a positive phase since the mid-1970's has significant implications for regional weather because of the implied associated shift in storm tracks and synoptic eddy activity. Figure 1.1 shows the difference between evaporation and precipitation for strongly positive NAO winters minus the difference between evaporation and precipitation for negative or normal NAO winters (Hurrell 1995). This figure shows that the positive (negative) phase of the NAO is associated with suppressed (enhanced) precipitation over Greenland, the Mediterranean and central and southern Europe, and enhanced (suppressed) precipitation near the east coast of the U.S. and in a region from Iceland to Scandinavia.

Hurrell (1995) also noted that the NAO pattern can influence ocean surface conditions because these conditions are governed by wind-induced changes in air–sea energy fluxes. Thus, a persistent anomalous NAO pattern could alter the extraction of heat from the ocean by the atmosphere. In addition, potential long-term changes in evaporation and precipitation and the melting of sea ice associated with a persistent anomalous NAO pattern may affect the rate of deep water formation in the North Atlantic and the ocean thermohaline circulation.

Research by Groenert (2002) indicates that daily values of the NAO index are not well correlated with daily precipitation in the Northeast during the cool season. However, this research suggests a possible relationship between phase transitions of the NAO and Northeast precipitation events. Specifically, Groenert (2002) found that more than 70% of negative-to-positive NAO phase transitions were associated with a precipitation event in the Northeast, while 47% of positive-to-negative NAO phase transitions were associated with a precipitation event in the Northeast.

Franzke et al. (2003) found that the development of the positive and negative phases of the NAO pattern may be associated with anticyclonic and cyclonic wave breaking, respectively (see Thorncroft et al. 1993). Wave breaking is defined as a reversal in the sign of the north-south potential temperature gradient on the dynamic tropopause (DT), the height in the atmosphere at which potential vorticity (PV) is equal to two PV units. This modeling study showed that the location of an initial perturbation over the Pacific Ocean determines the phase of the NAO that evolves; the positive phase of the NAO appears to be initiated by a low-latitude perturbation, while the negative phase of the NAO appears to be initiated in high latitudes. According to Franzke et al. (2003), the development of the positive NAO pattern is associated with two separate anticyclonic wave breaking events along the west coast of North America and over the midlatitude and subtropical North Atlantic, respectively, that are linked through downstream development. Franzke et al. (2003) argue that the evolution of the negative NAO pattern is simpler and may be associated with a single in-situ cyclonic wave breaking event on the poleward side of the climatological jet.

The modeling results of Franzke et al. (2003) show that a zonally symmetric basic state is not sufficient for the development of the NAO pattern; a zonally varying background flow is critical for replicating the correct spatial scale and sense of wave breaking for the observed NAO pattern. In addition, Franzke et al. (2003) found a discrepancy between the e-folding time scale of approximately six days found in their simulations and the 10-day e-folding time scale observed in previous studies. They speculated that not allowing consecutive wave breaking events in their simulations may have resulted in the simulated life cycle of the NAO pattern being too short, which would be consistent with findings that transient eddy fluxes associated with wave breaking events maintain low-frequency anomalies and also retard the propagation of Rossby waves.

Benedict et al. (2004) helped confirm that the NAO pattern evolves through wave breaking by showing the composite evolution of potential temperature on the dynamic tropopause (DT) during the development of both a positive and negative NAO pattern. Their observations show that only one cyclonic wave breaking event is necessary to generate the high-over-low potential temperature anomaly structure on the DT characteristic of the negative NAO pattern, and that more than one anticyclonic wave breaking event is required to generate the low-over-high potential temperature anomaly structure on the DT characteristic of the positive NAO pattern. Benedict et al. (2004) note that as a precursor to the development of a negative or positive NAO pattern, transient high-frequency waves break upstream of the NAO domain and project onto low-frequency waves in the NAO domain. Thus, Benedict et al. (2004) contend that the physical entity of the NAO grows and is maintained by remnants of transient high-frequency wave breaking. Benedict et al. (2004) note that once there is no longer an influx of high-frequency transient waves to continue the wave breaking process and the projection of high-frequency waves onto low-frequency waves in the NAO domain, the NAO pattern will begin to decay.

1.2.2 Comparison of the North Atlantic Oscillation to the Arctic Oscillation/North American Annular Mode

Some recent papers address the argument that the NAO is essentially equivalent to a dominant annular mode of low-frequency atmospheric variability in the NH most commonly called the Arctic Oscillation (AO). A comprehensive paper by Wallace (2000) contrasted the spatial similarities between the NAO and AO (referred to in his paper as the NH ‘annular mode’, or NAM) with the stark differences in the paradigms with which they are associated.

Wallace (2000) argued that most documented methods for identifying the NAO can be grouped into two types of approaches. The first approach uses SLP time series from a pair of observing stations to identify the NAO. NAO indices generated using this approach typically represent the meridional SLP gradient, and thus, the strength of the surface westerlies across the Atlantic. A second approach uses principal component analysis to obtain the dominant patterns of variability in the NH SLP field. In this second approach, the leading mode of atmospheric variability recovered from the analysis is not correlated with succeeding modes in time or space and is considered to be reliable.

Wallace (2000) noted that a dominant mode of atmospheric variability in the NH was documented in the early to mid-20th century by Rossby (1939), Rossby and Willett (1948), Namias (1950), and others using an entirely different approach than the methods used to identify the NAO. This apparent large-scale pattern cycle called the “zonal-index cycle” was based upon the perspective that low-frequency variability of the general circulation can be divided into a zonally symmetric component and an eddy component. The procedure for identifying this mode of atmospheric variability involved the subtraction of the midlatitude zonally averaged SLP from SLP averaged over the polar cap. A high-index cycle corresponds to strong sea-level westerlies, while a low-index corresponds to a breakdown in sea-level westerlies.

Rossby and Willett (1948) described four stages of the zonal-index cycle, which tend to follow sequentially in time. The first stage is the high index stage, characterized by a strong circumpolar vortex located to the north of its climatological position. The second stage of the zonal-index cycle is characterized by the circumpolar vortex and jet stream located near or south of their climatological latitudes. The third stage of the cycle is the low-index stage and is characterized by strong troughs and ridges in the circumpolar vortex and jet stream. Finally, the fourth stage of the zonal-index cycle is characterized by a re-establishment of the circumpolar vortex at higher latitudes. Wallace (2000) and others have pointed out that the high-index stage resembles the positive phase of the NAM, while the low-index stage resembles the negative phase of the NAM.

Wallace (2000) noted that despite the different approaches for identifying NH low-frequency variability, many types of NAO indices are very highly correlated with NAM indices.   Thus, Wallace (2000) contended that the NAO is actually a more regional representation of the NAM. According to Wallace (2000), some of the redundancy between the two identified modes is due to the fact that the leading mode of NH low-frequency variability cannot be represented as well using SLP data from only a few stations as it can by projecting the full hemispheric seasonal-mean SLP fields onto their spatial correlation patterns. Principal component analysis is shown to provide a better depiction of the time-dependence behavior of the spatial pattern derived from station-based indices than do the indices themselves. Therefore, according to Wallace (2000), that the NAO is found to be distinct from the NAM only when the NAO is defined strictly by a particular station-based index, rather than by the corresponding correlation of regression pattern in the SLP field, is further evidence that the NAO and NAM are different representations of the same entity.

Another reason that Wallace (2000) felt that the NAO could be equivalently represented as an annular mode is the similarity of the NAM to the leading mode of atmospheric variability in the Southern Hemisphere (SH). Wallace called this mode the SH Annular Mode (SAM) [often referred to as the Antarctic Oscillation (AAO)]. Wallace (2000) noted that those favoring the use of the NAO instead of the NAM to describe the main cause of low-frequency variability in the NH point to the very weak SLP teleconnections between the North Atlantic and Pacific sectors in the NAM domain. Those favoring the use of the NAM, on the other hand, contend that like the SAM, the NAM is significant not because of the teleconnections it explains, but because of its polar symmetry and the large areal extent of its primary high-latitude centers of action.

As evidence of the need for scientists to choose one name for the phenomenon, Wallace (2000) pointed to what he considers to be two conflicting paradigms involving the leading mode of NH low-frequency variability that could hinder communication between scientists in different subfields, as well as between scientists and the public. According to Wallace (2000), those who favor the NAO: a) see the strong correlation between local NAO indices and various zonally averaged time series as evidence of the NAO's importance with respect to the zonally symmetric component of the general circulation; b) explain the weak correlations between North Atlantic and North Pacific sectors as caused by Rossby wave trains that extend across the pole or as "direct connections between regional centers of action"; c) look to the North Pacific for a dynamic analogue; and d) view Atlantic sea surface temperature (SST) changes over the past few decades as primarily due to atmospheric-oceanic interactions related to the NAO.

Wallace (2000) contended that those who favor the use of annular modes: a) see the midlatitude geopotential height field as intrinsically zonally symmetric, with asymmetries mainly due to underlying land–sea distributions; b) explain the weak correlations between North Atlantic and North Pacific sectors as regional expressions of an oscillation in the geopotential height field between a single arctic center of action and an encircling midlatitude zonal belt; c) look to the SH for a dynamical analogue; and d) view Atlantic SST changes as a possible consequence of ozone depletion or the build-up of greenhouse gases forcing a tendency towards the positive phase of the NAM that, in turn, forces the observed SST anomalies.

Ambaum et al. (2001) directly addressed the issue of conflicting paradigms raised by Wallace (2000) by arguing that the NAO paradigm may be more physically relevant and robust in explaining NH variability than is the annular mode paradigm. Their first argument suggesting that the NAO is preferred to the AO is based upon the different analysis techniques used to identify the AO pattern versus the NAO pattern. The AO pattern is identified using EOF analysis, while the NAO pattern can be identified using one-point correlation analysis that identifies teleconnections between widely separated points. According to Ambaum et al. (2001), the difference in the two methods used to identify these patterns is important because EOF analysis is nonlocal; that is, the relationship between two separate points in a pattern identified by EOF analysis depends upon the entire dataset and not simply the data time series of the two particular points. On the other hand, the analysis used to identify teleconnections is local, meaning that the relationship between two separate points is completely characterized by the correlation between the time series of the two points.

According to Ambaum et al. (2001), this discrepancy between the two methods of analysis may discourage the use of the annular mode paradigm associated with the AO because SLP is not found to be significantly correlated at the Pacific and Atlantic centers of action of the AO pattern. In fact, the only significant correlation between centers of action in the AO pattern is between the Iceland and Azores regions, which correspond to the centers of action of the NAO pattern. Thus, the NAO pattern can be interpreted as a teleconnection pattern, while the AO pattern cannot.

Another argument given by Ambaum et al. (2001) in favor of using the sectoral paradigm associated with the NAO versus the AO paradigm is that the AO pattern does not emerge from EOF analyses of lower-tropospheric fields other than SLP that are dynamically related to the SLP (e.g., 850 hPa streamfunction), implying a possible physical inconsistency. Further, the AO pattern cannot be fully reproduced by EOF analysis when the domain is reduced to a small section of the NH such as a European–Atlantic sector. This lack of reproducibility implies that the apparent robustness of the AO as the leading mode of variability in the NH could be partially the result of the strong domain-shape dependence of EOF patterns. In contrast, the NAO could be identified as the leading mode of variability in the European–Atlantic sector using several different lower-tropospheric fields.

Ambaum et al. (2001) concluded that the NAO paradigm may be preferable to the AO paradigm because the NAO shows potentially predictable behavior in that it can be reproduced using different local analyses such as teleconnections and regional EOFs. However, they conceded that the AO may still be a valid annular mode mainly because of overwhelming evidence in the general circulation literature of a SH annular mode despite the absence of a SLP correlation between its midlatitude zonal sectors.

1.2.3 The Pacific/North American Pattern

In addition to the NAO pattern (or AO/NAM pattern), a second low-frequency circulation pattern called the Pacific/North American (PNA) pattern has been found to have a significant influence on NH low-frequency atmospheric variability. According to Wallace and Gutzler (1981), since the 1950’s, long-range forecasters had been aware of a preferred configuration of the midtropospheric geopotential height field within an arcing sector that extends from the mid-Pacific to eastern North America. These forecasters noted that positive midtropospheric geopotential height anomalies along the western coast of North America tend to coincide with negative midtropospheric geopotential height anomalies over the mid-Pacific ocean and the southeastern U.S. This anomaly configuration results in a highly amplified pattern. Long-range forecasters also noticed that negative geopotential height anomalies along the west coast of North America tend to correspond to positive geopotential height anomalies over the mid-Pacific Ocean and the southeastern U.S., resulting in a less amplified pattern. Thus, the phenomenon that the forecasters named the PNA pattern was identified as an alternation between a high-amplitude and a low-amplitude flow pattern across the Pacific Ocean and North America.

Wallace and Gutzler (1981) created composite 700 hPa geopotential height anomalies and 1000–700 hPa thickness anomalies from five winters that were characterized by below-normal temperatures in the eastern U.S. and by a strong 700 hPa ridge over the Pacific Northwest and the west coast of Canada. These composite maps were very similar, both showing a well-defined high-amplitude, or positive, PNA pattern. Looking at the composite thickness charts, Wallace and Gutzler (1981) found that, as with the NAO, the PNA pattern also influences winter temperatures over the eastern U.S..

Using one-point correlation maps, Wallace and Gutzler (1981) were able to identify a configuration of midtropospheric geopotential height anomalies nearly identical to the PNA pattern referenced in previous literature. Thus, the PNA pattern could be defined as a teleconnection pattern having four centers: one near Hawaii, a second over the North Pacific, a third over Alberta, and a fourth over the Gulf Coast of the U.S.. Wallace and Gutzler (1981) objectively defined the PNA pattern as a linear combination of normalized geopotential height anomalies at these four centers.

Wallace and Gutzler (1981) used this objective definition of the PNA pattern to create composites of the difference between the 1000–500 hPa mean thickness for the winter months having the 10 highest PNA values versus months with the 10 lowest values. These composites showed that the PNA pattern has a cold-core equivalent barotropic structure, with geopotential height anomalies corresponding to thickness anomalies.

Finally, Wallace and Gutzler (1981) identified the PNA pattern as the second eigenvector of the 500 hPa geopotential height correlation matrix during winter, corresponding to the second-largest influence on the variability of the 500 hPa geopotential height field in the NH winter. They note the fact that the PNA pattern can be reproduced using multiple analysis techniques, combined with the observation that anomalies associated with the PNA pattern tend to persist from month to month, help support the view that the PNA pattern is an important part of the NH circulation.

Barnston and Livezey (1987) used REOF analysis to identify the PNA pattern as a significant mode of wintertime low-frequency atmospheric variability. They found that, like the NAO pattern, the PNA pattern undergoes a seasonal progression: the strength of the influence of the PNA pattern increases in time while the separation between its centers of action decreases in time until the month of February, when it reaches its maximum strength and exhibits the shortest distance between centers. After February, the PNA pattern’s influence decreases as the separation between its centers increases. Structures bearing a resemblance to the PNA pattern were also found in the months of September and October, but an REOF analysis of November 500 hPa geopotential heights did not identify the PNA pattern in these months as having a significant influence on the midtropospheric geopotential height variability in the NH.

Leathers et al. (1991) sought to establish what influence the PNA pattern exerted on wintertime precipitation patterns in the U.S.. In their research, they used a definition of the PNA pattern that excluded the subtropical center of action located near Hawaii noted by Wallace and Gutzler (1981) and Barnston and Livezey (1987) because they were most interested in the propagation of energy associated with the PNA pattern across North America. The PNA index was regressed against standardized monthly mean precipitation for 344 regions in the U.S. The correlation coefficients that resulted were tested for statistical significance, with an attempt made to account for the spatial autocorrelation inherent in the precipitation database. To aid in the interpretation of the PNA index–precipitation correlation fields, monthly PNA index values were regressed against monthly mean 700 hPa geopotential heights over North America. The resulting correlation maps showed the position of the ridge–trough system over the U.S. associated with opposite extremes in the PNA index.

Leathers et al. (1991) found statistically significant correlations between the PNA index and monthly precipitation during the cool season, with the strongest correlations occurring in January. These correlations are shown in Fig. 1.2. For January, they found strong negative correlations between the phase of the PNA pattern and precipitation in two main regions, the upper Mississippi Valley and the northern Rockies. No meaningful correlation between the phase of the PNA pattern and precipitation was found over the Northeast, with the exception of a slight negative correlation across western sections of the Northeast during March. These correlations were considered to be physically reasonable and are explained in the next two paragraphs.

Leathers et al. (1991) noted that during the positive phase of the PNA pattern, the trough and the associated polar-front jet over the eastern U.S. are located farther to the south and east than their climatological positions. As a result, precipitation associated with disturbances forming along the jet occurs farther to the south and east than usual, leading to a suppression of precipitation in the upper Mississippi and Ohio Valleys. They argued that another contribution to the anomalously dry conditions associated with the positive PNA pattern is from the polar and arctic continental air masses that tend to dominate during a positive PNA weather regime. These types of air masses cut off the moisture feed from the Gulf of Mexico. Farther to the west over the Rockies, anomalous ridging associated with a positive PNA results in large-scale subsidence and compressional warming that suppresses precipitation there. They suggested that a positive PNA pattern might also limit precipitation in the Rockies by forcing the Pacific storm track to the north of the region.

Leathers et al. (1991) noted that during the negative phase of the PNA pattern, the polar-front jet is located farther to the north than usual over the eastern U.S., allowing maritime tropical air masses to spread north from the Gulf of Mexico at times. Across the West, a more zonally oriented storm track allows Pacific storms and their associated precipitation to cross the Rockies.

The relationships that Leathers et al. (1991) identified between the PNA pattern and regional precipitation for January were fairly representative of the relationships they found for November, December, and February. By March, the area of negative correlations between the PNA index and precipitation was shown to decrease greatly; only the area immediately surrounding the Ohio Valley and a small area in the southern Great Plains show statistically significant relationships. The rest of the autumn, winter, and spring months examined in their research (April, May, September, and October) did not exhibit statistically significant correlations between the PNA index and precipitation in the U.S..

Leathers et al. (1991) argued that although correlations between the PNA index and precipitation covered smaller regions and were generally weaker than correlations between the PNA index and temperature (also discussed in their paper), they were strong enough to show that the PNA pattern has an important influence on precipitation in certain regions of the U.S. during many cool-season months. This finding was consistent with research showing that during winter and early spring precipitation tends to be influenced more by synoptic-scale systems, while during the late spring and early fall precipitation may be influenced more by mesoscale type features. Thus, Leathers et al. (1991) hypothesized that the varying seasonal influence of the PNA pattern on precipitation may be a direct result of the varying seasonal influence of synoptic-scale systems on precipitation.

Cash and Lee (2001) were able to show that a linear stochastic model can accurately simulate the observed growth of the PNA pattern. Their model results showed that the most rapid amplification of the leading pattern of NH streamfunction variance at 300 hPa tends to evolved into a pattern resembling the negative PNA by Day 5. To verify the model results using observed data, Cash and Lee (2001) examined PNA pattern evolution during 40 winter seasons using the NCEP–NCAR reanalysis dataset. They found that the observed amplification of the PNA pattern is similar to the amplification simulated by their model: more than two-thirds of observed NH 300 hPa streamfunction anomaly patterns that were highly positively (negatively) correlated with the leading mode of NH streamfunction variance at 300 hPa evolved into a negative (positive) PNA pattern by Day 7.

Cash and Lee (2001) concluded from their model results that tropical convective heating occurring on the order of a few days likely plays an important role in triggering the observed PNA pattern. They also found that the growth of the PNA is dependent upon the location and configuration of the initial high-frequency streamfunction anomaly pattern relative to the low-frequency streamfunction pattern. Finally, Cash and Lee (2001) found that the timescale of the PNA is about 10 days, implying that studies examining the PNA through the use of monthly mean statistics may be unable to detect important aspects of PNA evolution.

A statistical study by Groenert (2002) indicated that daily values of the PNA index do not significantly contribute to the variability of precipitation over the

Northeast. However, two case studies of significant cool-season precipitation events impacting the Northeast implied that phase changes of the PNA may tend to occur in association with major precipitation events in the Northeast.

In addition to the NAO/AO/NAM and the PNA pattern discussed in detail above, many other large-scale patterns of NH low-frequency atmospheric variability have been documented in the literature. For example, Wallace and Gutzler (1981) and others identified the North Pacific Oscillation as an important mode of atmospheric variability akin to the NAO. Honda and Nakumura (2001) documented a late-winter interannual SLP oscillation between the Aleutian and Icelandic lows that they called the Aleutian low/Icelandic low seesaw. In an attempt to establish which of the numerous documented NH large-scale patterns or modes of variability are of most relevance to the NH extratropical circulation, Quadrelli and Wallace (2004a) created detailed EOF analyses of SLP fields, as well as EOF analyses of geopotential height and wind fields at several different levels in the atmosphere.

Quadrelli and Wallace (2004a) found that the first and second leading planetary-scale patterns in the NH SLP field closely resemble the AO/NAM and PNA pattern, respectively. Together, these patterns were found to account for over one-third of the variance of the monthly mean SLP field, and an even higher percentage of variance over longer time scales. Further, Quadrelli and Wallace (2004a) discovered that linear combinations of these two patterns could reconstruct many other previously identified NH extratropical large-scale patterns of variability in the SLP. These linear combinations were found to explain a large portion of the variance of geopotential height, surface air temperature, and precipitation for time scales longer than a month. Thus, the AO/NAM and PNA pattern were shown by Quadrelli and Wallace (2004a) to be the two most significant patterns of low-frequency variability in the NH wintertime extratropics.

1.2.4 Blocking

The alternation between zonal and blocked flow has long been considered an important feature of the NH large-scale circulation. Since blocking has been shown to significantly influence synoptic-scale features, atmospheric blocking should be considered an important type of flow regime in addition to lower-frequency circulation regimes such as the NAO, AO/NAM, and PNA. This section reviews some of the methods for the objective identification of atmospheric blocking that are documented in the literature.

Work by Lejenäs and Økland (1983) addressed the need for an objective way to identify atmospheric blocking. They noted that in previous studies, the process of identifying blocking was somewhat arbitrary because blocking had been identified by visually inspecting synoptic weather maps. One of the goals of their paper was to find an objective definition of blocking based upon the criteria used by Rex (1950a). Rex (1950a) identified a blocking regime as a synoptic situation having the following characteristics: a) the westerly flow is split into two branches; b) each branch of the flow transports appreciable mass; c) the two-branch structure of the jet extends over 45 degrees of longitude; d) the flow transitions sharply from low-amplitude to high-amplitude; and e) the above conditions persist for at least 10 days.

Lejenäs and Økland (1983) decided that a zonal index similar to the zonal index first introduced by Rossby (1939) to determine the strength of the upper-level westerlies would be an appropriate way to define blocking objectively. They chose to use the 500 hPa geopotential height difference between 40°N and 60°N to define blocking because of the documentation in past literature of the tendency for an anticyclone to be located near 60°N and a cyclone to be located near 40°N during a blocking event. A negative value of Lejenäs and Økland's (1983) blocking index, thus, indicated a blocking situation. An additional requirement imposed by Lejenäs and Økland (1983) was that the mean value of the index be negative over a distance of 30° longitude because they noted that negative blocking index values that were spatially isolated did not represent blocked flow.

A blocking study performed by Tibaldi and Molteni (1990) used an objective definition of blocking based upon the work of Lejenäs and Økland (1983). Their definition of blocking was based upon the strengths of the middle-latitude and the high-latitude 500 hPa geopotential height gradients (GHGS and GHGN, respectively) evaluated on 4° by 4° latitude–longitude grids:

$$\mathrm{GHGS} = [Z(\varphi_o) - Z(\varphi_s)]/(\varphi_o - \varphi_s),$$
$$\mathrm{GHGN} = [Z(\varphi_n) - Z(\varphi_o)]/(\varphi_n - \varphi_o),$$

where

$\varphi_n = 80°\mathrm{N} + \Delta$,
$\varphi_o = 60°\mathrm{N} + \Delta$,
$\varphi_s = 40°\mathrm{N} + \Delta$,
$\Delta = -4°, 0°$ or $4°$

Using these two definitions of 500 hPa geopotential height gradients, Tibaldi and Molteni (1990) considered the flow to be blocked if a) GHGS > 0 and b) GHGN < −10 meters per degree latitude for at least one value of Δ over a four-day period. They note that condition (a) is essentially equivalent to the condition for blocking prescribed by Lejenäs and Økland (1983). The addition of condition (b) ensured that non-blocking periods when the midlatitude westerly jet was displaced far to the south would not be counted as blocking events.

Pelly and Hoskins (2003a) suggested an alternative method for objectively identifying atmospheric blocking using a PV perspective. They found that the evolution of synoptic-scale and planetary-scale features associated with blocking events could be more clearly seen in the potential temperature field on the dynamic tropopause than in the upper-level geopotential height field. Their objective definition of blocking was based upon the following PV perspective on the evolution of blocking: A large subtropical mass of low PV air moves poleward in advance of a high-amplitude, slow-moving cyclone. This negative PV anomaly develops its own anticyclonic circulation and cuts off from its region of origin, causing upstream weather systems to elongate meridionally. As a result, the upstream systems deposit more low (high) PV air on the poleward (equatorward) side of the negative PV anomaly, thus reinforcing the block.

Based upon the above view of block evolution, and using the fact that low PV air aloft can be viewed as a positive potential temperature anomaly on the dynamic tropopause, Pelly and Hoskins (2003a) argued that blocking can be seen as a reversal in the normal meridional gradient in potential temperature on the dynamic tropopause. They objectively identified blocking at any given longitude as the difference in the spatially-averaged potential temperature on the dynamic tropopause to the north and south of a central blocking latitude. The central blocking latitude was allowed to vary as a function of longitude based upon the location of climatological maximum synoptic activity, where prior studies had shown blocking to occur most frequently. As in Tibaldi and Molteni (1990), conditions had to persist for four days to be considered a blocking episode.

Although NH blocking events may develop under almost any large-scale weather regime, blocking events have been linked to both the NAO/AO/NAM and the PNA patterns. For example, Dole (1986) pointed to a relationship between blocking in the eastern North Atlantic and in the central North Pacific and large-scale weather regimes resembling the NAO and the PNA pattern, respectively. He noted that persistent midtropospheric geopotential height anomalies seem to preferentially form over the central North Pacific, the eastern North Atlantic, and northern Russia. Persistent geopotential height anomalies over the central North Pacific are linked to a large-scale geopotential height anomaly pattern resembling the PNA pattern, while persistent geopotential height anomalies over the eastern North Atlantic are linked to a large-scale geopotential height anomaly pattern resembling the NAO pattern. According to Dole (1986), persistent positive (negative) geopotential height anomalies over the North Pacific tend to be associated with a negative (positive) PNA pattern and blocked (zonal) flow over the central North Pacific. Conversely, persistent positive (negative) geopotential height anomalies over the North Atlantic tend to be associated with a negative (positive) NAO pattern and blocked (zonal) flow over the eastern North Atlantic.

Shabar et al. (2001) used the blocking criteria detailed by Tibaldi and Molteni (1990) in order to explore the statistical and dynamical relationship between the NAO and blocking in the North Atlantic. They were able to demonstrate a statistically significant relationship between the NAO pattern and blocking, with linear regression analysis showing that the NAO pattern accounts for about 30% of the variation in North Atlantic wintertime blocking. They found that two-thirds more winter blocking days were observed during the negative phase of the NAO than during the positive phase. Blocking events occurring during the negative phase of the NAO were also found to be of longer duration; the average length of a blocking event during the negative phase of the NAO was found to be about 11 days, while the average length of a blocking event during the positive phase of the NAO was about six days.

In addition to establishing a statistical relationship between the NAO and North Atlantic blocking, Shabar et al. (2001) formed a conceptual model of the blocking/NAO relationship. Using a model, they found that zonally asymmetric thermal forcing modulated by the NAO is important in creating a favorable environment for blocking. Shabar et al. (2001) used these model results to support their conclusion that during the negative phase of the NAO, thermal forcing tends to act in concert with the resonance forcing of the regional physiography to create a favorable environment for the formation and persistence of North Atlantic blocks. In contrast, they concluded that for the positive phase of the NAO thermal forcing tends to reduce or destroy the resonance forcing of the regional physiography and creates an environment unfavorable for the development or persistence of blocks.

1.2.5 Planetary-/Synoptic-Scale Interactions during Regime Transitions

Much research has been devoted to the complex interactions between synoptic-scale disturbances and the planetary-scale flow during weather regime transitions. For example, Reinhold and Pierrehumbert (1982) used a two-layer channel model to explore the theory that the general behavior of the atmosphere could be understood as a flow driven by smaller-scale instabilities from one weather regime to another. This theory was based upon the idea of a feedback process in which planetary-scale flow organizes transients that, in turn, force the planetary-scale flow. Reinhold and Pierrehumbert (1982) cited, as an example, the observation made by Sanders and Gyakum (1980) in their paper on explosive cyclogenesis that planetary-scale ridges tended to amplify suddenly and produce blocking downstream of a region in which several successive explosively deepening cyclones had occurred. The concept of a significant synoptic-/planetary-scale feedback process suggested by Reinhold and Pierrehumbert (1982) supported the view of a weather regime as quasi-stationary period during which a balance results between the synoptic-scale and planetary-scale forcing.

Reinhold and Pierrehumbert (1982) suggested that the role of eddy transports organized by the planetary-scale flow is to stabilize the large-scale circulation during quasi-stationary equilibrium periods associated with weather regimes. During these periods, a small perturbation in the state of the large-scale pattern may induce net eddy transports that act against the sense of the perturbation and force the large-scale pattern back to its original state. Reinhold and Pierrehumbert (1982) found that transitions between weather regimes are associated with aperiodic, occasionally violent surges in the perturbation transports. Thus, they argued that transient disturbances provide an internal mechanism responsible for both the disruption and stabilization of weather regimes.

Colucci (1985) examined large-scale circulation changes accompanying synoptic-scale cyclogenesis for two cases involving blocking. His work was motivated by the idea that understanding interactions between synoptic-scale disturbances and the planetary-scale circulation would improve predictions of large-scale circulation changes during the passage of embedded smaller scale disturbances.

Results from Colucci (1985) suggested that blocking systems may become persistent anomalies if the forcing by the synoptic-scale perturbations is repeated in time and space. Cyclogenesis occurring near the long-wave trough axis was found to favor blocking cyclonic vortices, while cyclogenesis near the long-wave ridge axis favored blocking anticyclonic vortices. His research suggested that atmospheric blocking is a nonlinear, baroclinic process involving interaction between mobile, baroclinically active synoptic-scale disturbances and the planetary-scale circulation. Consistent with the results of Reinhold and Pierrehumbert (1982) discussed above, results from Colucci (1985) reinforced the idea that scale interactions, especially between the synoptic and planetary scales, are important to the maintenance of the general circulation. Colucci (1985) concluded that synoptic-scale disturbances “should not be viewed as passive byproducts in the atmospheric circulation, but as agents by which the character of the circulation can be considerably altered”.

Colucci (1987) continued his investigation into the connection between synoptic-scale cyclones and blocking episodes by examining surface cyclone and planetary wave activity over North America and the North Atlantic Ocean during three events in November 1980. The first event was the retrogression of a blocking anticyclone downstream of two intense cyclones, the second event was the weakening of this block and the subsequent development of an upper-level cyclonic vortex upstream, and the third event was the ejection of this cyclonic vortex downstream as the local midtropospheric flow became more zonally symmetric.

In his examination of the three events, Colucci (1987) found that cyclones associated with large PV advections did not result in downstream blocking when they were embedded in zonally symmetric flow. Colucci (1987) explained this result by suggesting that a planetary wave may be required to reach a critical amplitude before it can be reinforced by the cyclone waves. He argued that a cyclone embedded in fast zonally symmetric flow may not be able to produce a response in the planetary circulation despite associated large PV transports because forcing from such a cyclone would not persist in space and time. On the other hand, a cyclone embedded in relatively slow, high-amplitude flow might be able to produce a response in the planetary circulation because of the persistence of its associated PV transports.

Colucci (1987) also showed that the type of block that developed in response to synoptic-scale cyclogenesis might be dependent upon the proximity of the cyclone waves to planetary-scale troughs or ridges. Specifically, he found that a rapidly deepening cyclone upstream of a planetary-scale trough tends to produce a blocking cyclonic vortex. Conversely, a rapidly deepening cyclone upstream of a planetary-scale ridge tends to produce a blocking anticylonic vortex.

Reinhold and Yang (1993) studied the role of transients in the initiation and termination of weather regimes by using a quasi-geostrophic (QG) two-layer channel model to create idealized weather regime transitions. The model parameters were manipulated such that the model produced infrequent and dramatic regime transitions characterized by very different flow patterns so that it would be easy to tell the two regimes apart without the use of filtering. The first regime produced by the model was called the trough regime and consisted of a steady, neutrally tilted trough found upstream of a mountain with weak zonal flow. The second regime produced by the model was called the high-index regime and erratically varied between a zonal flow and a large-scale wave.

According to Reinhold and Yang (1993), this model showed two different mechanisms for regime transitions in which transient disturbances play very different roles. These two mechanisms were found to account for the basic framework of all model regime transitions, and were found to operate both independently and together.

One mechanism for weather regime transition was associated with synoptically triggered large-scale instability. Reinhold and Yang (1993) argued that the role of transients preceding a regime change associated with this type of mechanism is to maintain an environment in which the large-scale disturbance is stable to large-scale perturbations by reducing the baroclinicity of the atmosphere. Before the model regime transition occurred, large-scale instability increased in association with a change in the large-scale vertical structure. This increase in large-scale instability was not indicated by an easily identifiable precursor to regime change.

Reinhold and Yang (1993) found that the first type of regime change occurs when an individual synoptic weather event causes the large-scale instability to increase beyond a certain threshold, such that the synoptic-scale can no longer reduce the baroclinicity of the atmosphere. In this type of weather regime transition, the effectiveness of the synoptic-scale trigger depends more upon the flow stability than on the strength of the synoptic-scale trigger. Reinhold and Yang (1993) found that the time scale of a regime change associated with cases of synoptically triggered large-scale instability is just a few days because the change occurs on the time scale of baroclinicity.

The second mechanism for weather regime transition identified by Reinhold and Yang (1993) was found to be associated with regime-equilibrium instability. Reinhold and Yang (1993) argued that the role of transients preceding a regime change associated with this second type of mechanism is as a part of a regime equilibrium in which transients and the large-scale flow mutually influence and organize each other. Before the model regime transition occurs, the energy of the synoptic scale steadily increases. This increase in synoptic-scale energy is indicated by the development of a storm track and an increase in amplitude of the synoptic-scale waves prior to regime change.

Reinhold and Yang (1993) found that this second type of regime change occurs when the energy transport of the synoptic scale becomes either too large or too small to maintain an equilibrium between the large-scale and the transients. They believed that an example of this type of weather regime transition is the type observed by Colucci (1985) in which a series of mobile disturbances continued to pass until a disturbance came along that was so intense that it resulted in an enormous change in the planetary-scale flow. The synoptic-scale regime transition trigger in the model was found to be typically very strong for this type of regime transition and may often be associated with explosive cyclogenesis in the real atmosphere. The time scale of a regime change associated with cases of regime-equilibrium instability was found to vary depending on the rate at which the transient energy changed.

Higgins and Schubert (1994) studied the role of synoptic-scale eddies in the life cycles of persistent anticyclonic anomalies, or blocks, that tend to develop over the North Pacific using a global climate model. They found that their model was able to replicate many of the observed characteristics of both large-scale and synoptic-scale features involved in the development and maintenance of these blocking anticyclones. Several noteworthy results emerged from this research. The first result was that both positive and negative synoptic-scale temperature and wind anomalies are found to interact with the growing blocking anticyclones in the global climate model. The implication of this result is that the ability of a synoptic-scale feature to affect the evolution of a larger-scale anticyclone may depend more upon its amplitude and its distance from the large-scale anticyclone than upon its perturbation sign.

The second result from the research of Higgins and Schubert (1994) was that the role of synoptic-scale temperature and wind eddies seems to depend upon the stage of the development of the large-scale blocking anticyclone in the North Pacific. Early in the development of the block simulated by the model, increases in the kinetic energy of a blocking anticyclone are associated with a barotropic conversion of potential energy to kinetic energy from the synoptic-scale as well as from the planetary-scale flow. After the onset of a large-scale anticyclone, on the other hand, increases in the kinetic energy of the large-scale anticyclone are dominated by barotropic conversions of potential energy from the planetary-scale flow. The importance of synoptic-scale eddies in the initiation of large-scale anticyclonic circulation anomalies is found to be consistent with other studies showing that explosive synoptic-scale cyclogenesis always precedes the formation of large-scale anticyclones in the North Pacific.

1.3 Research Goals and Thesis Synopsis

The above literature review of some key aspects of the general circulation of the atmosphere shows that certain synoptic-scale processes, such as the onset of blocking forced by explosive cyclogenesis, often play a significant role in transitions between the phases of large-scale weather regimes such as the NAO/AO or PNA pattern. The literature also emphasizes that while synoptic-scale eddies may modulate the planetary-scale flow, so too can the large-scale flow modulate the synoptic-scale eddies. The complex feedback processes between the synoptic scale and the planetary scale require better documentation and understanding because of significant implications for atmospheric predictability. For example, Shabar et al. (2001) noted that models often fail to forecast the onset of blocking in the North Atlantic, particularly during the negative phase of the NAO.

This research attempts to enhance the understanding of synoptic- and planetary-scale interactions by examining regional precipitation trends during certain large-scale regimes and regime transitions. To this end, the goals of this thesis are to a) develop objective definitions for large-scale weather regimes and weather regime changes; b) establish statistical relationships between Northeast precipitation and weather regimes or weather regime transitions; c) construct composites to identify characteristic synoptic-scale forcing associated with weather regimes and weather regime transitions; and d) use statistical results and composite analyses to determine whether regime change/precipitation relationships are associative or cause and effect.

This thesis is organized as follows: Chapter 1 has provided a literature review of weather regimes such as the North Atlantic Oscillation, the Pacific/North American pattern, and blocking, as well as planetary- and synoptic-scale interactions during weather regime transitions. Chapter 2 discusses the data and methodology used in this research. Chapter 3 presents relationships between large-scale regimes and Northeast precipitation in the cool season; Chapter 4 presents relationships between large-scale regime transitions and Northeast precipitation; Chapter 5 discusses the implications of these relationships; and Chapter 6 contains a summary and concluding remarks.

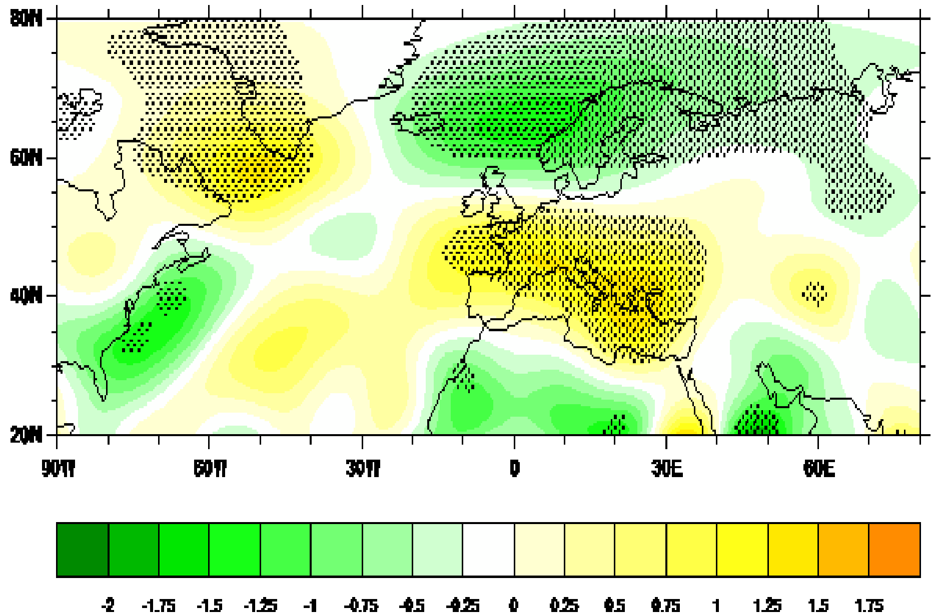

Fig. 1.1. The difference between evaporation and precipitation for strongly positive NAO winters minus the difference between evaporation and precipitation for normal or negative NAO winters. The contour interval is 0.5 mm day^{-1} and the stippling indicates values statistically significant from zero at the 95% confidence level using a *t*-test [from Hurrell (1995)].

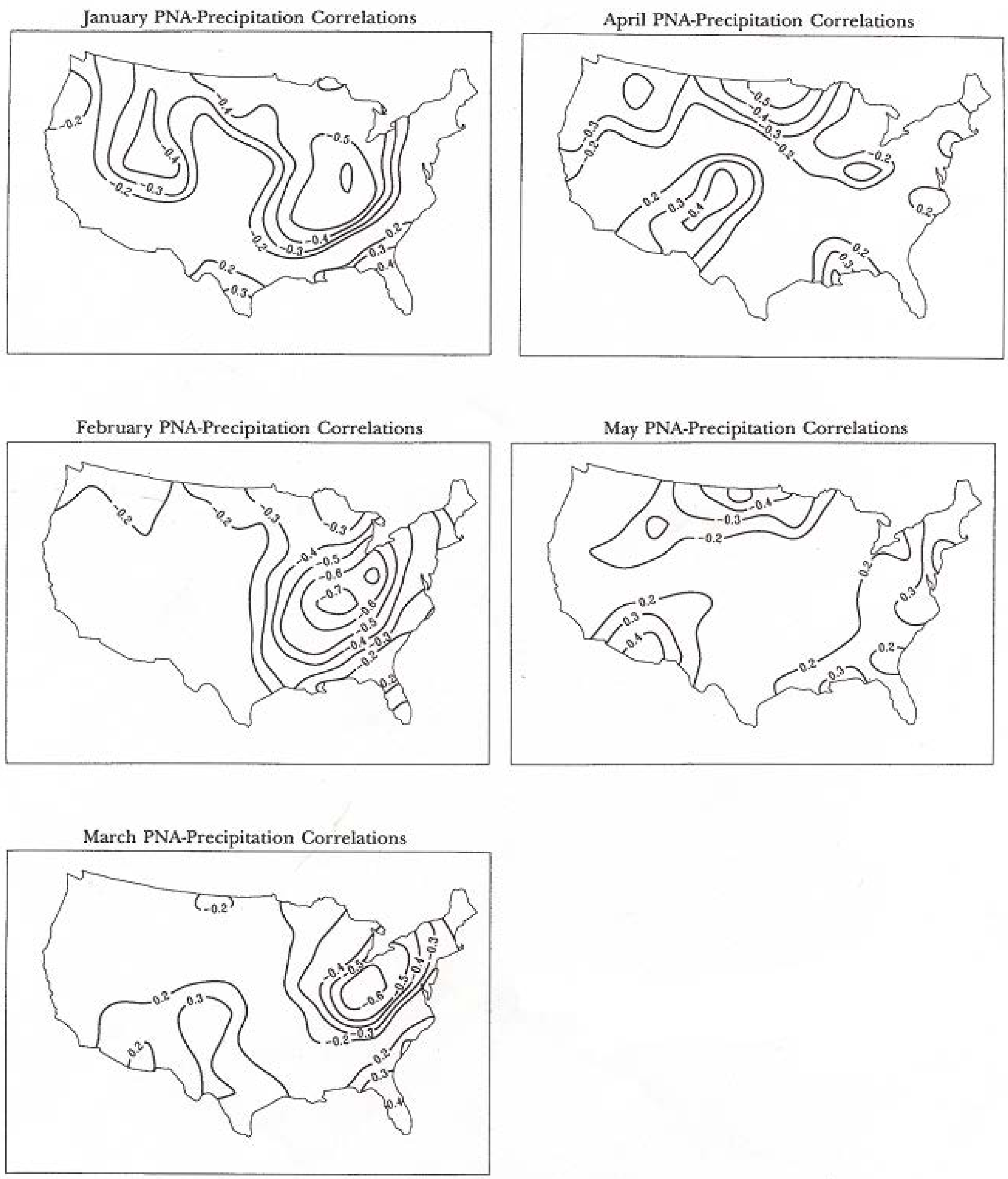

Fig. 1.2. Monthly maps of correlation coefficients between the PNA index and standardized divisional precipitation [From Leathers et al. (1991)].

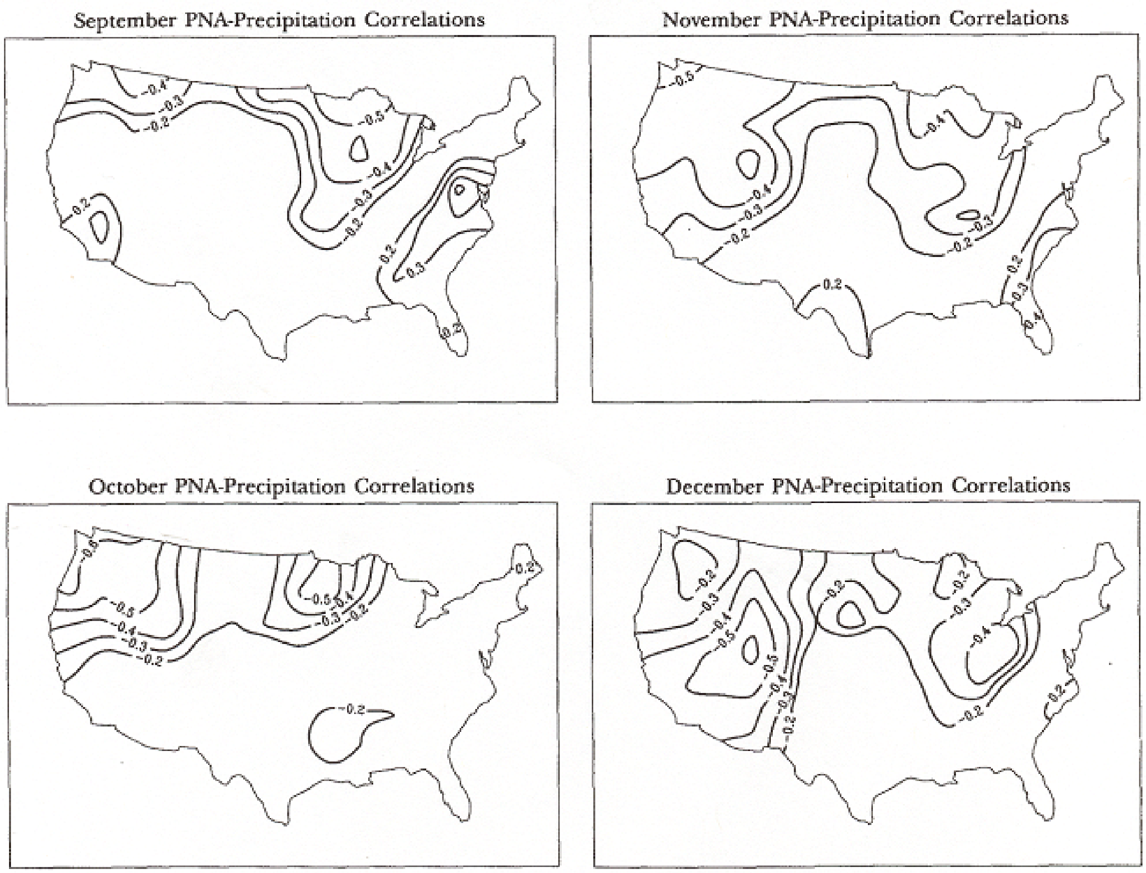

Fig. 1.2. *(Continued)*

2. Data and Methodology

2.1 Data Sources

Twice-daily (0000 and 1200 UTC) 500 hPa geopotential height data from the National Centers for Environmental Prediction–National Center for Atmospheric Research (NCEP–NCAR) reanalysis dataset (Kalnay et al. 1996) are used to identify large-scale regimes and regime changes in this study. In addition, 1000, 700, 500, and 300 hPa geopotential height and SLP data from the NCEP–NCAR reanalysis dataset are used to create composite analyses of regime transitions. The NCEP–NCAR reanalysis dataset is a global dataset gridded on a 2.5° latitude $\times$ 2.5° longitude mesh and is available on 17 isobaric levels from 1000 hPa to 10 hPa for the period 1948–2003.

The 24-h precipitation data used for analyzing Northeast precipitation during large-scale regimes and regime transitions are obtained from the NCEP Unified Precipitation Dataset (UPD) (Higgins et al. 2000). This dataset incorporates National Oceanic and Atmospheric Administration (NOAA) first-order station precipitation measurements, daily cooperative observation measurements, and River Forecast Center data, representing over 13,000 stations in the U.S. after 1992. Radar-derived precipitation estimates from the Weather Surveillance Radar-1988 Doppler (WSR–88D) network have been incorporated into the UPD in recent years, allowing for precipitation estimates on immediate coastal waters (Groenert 2002). The UPD contains 24-h (1200–1200 UTC) precipitation for the domain of 20^{o}–60^{o}N and 140^{o}–60^{o}W. It is gridded on a

0.25° latitude $\times$ 0.25° longitude mesh and is available for the period 1948–2003. The UPD may be obtained at ftp://ftpprd.ncep.noaa.gov/pub/precip/wd52ws/unified/.

2.2 Definition of a Large-Scale Regime

Many types of large-scale patterns referenced in the general circulation literature may be considered to be regimes. Some examples of large-scale regimes are high- and low-index flows (e.g., Rossby 1939; Rossby and Willett 1948; Namias 1950), blocking (e.g., Rex 1950a; Colucci 1985; Colucci 1987), persistent high and low pressure circulation anomalies (e.g., Dole 1986), and teleconnection patterns such as the NAO and PNA (e.g., Wallace and Gutzler 1981; Barnston and Livezey 1987). In this study, large-scale regimes are objectively defined using teleconnection indices for several reasons. First, research studies have shown that teleconnection patterns significantly influence extratropical NH large-scale variability (e.g., Barnston and Livezey 1987, Ambaum et al. 2001; Quadrelli and Wallace 2004a). Second, the phases of teleconnection patterns can be associated with specific regional regimes (e.g., Leathers et al. 1991; Hurrell 1995). Third, teleconnection indices are widely used as first-order approximations of large-scale patterns. Teleconnection indices are easily accessible online at the NOAA–Cooperative Institute for Research in Environmental Sciences (CIRES) Climate Diagnostics Center (CDC) website (http://www.cdc.noaa.gov/map/wx/indices.shtml), and at the NOAA/National

Weather Service (NWS) Climate Prediction Center (CPC) website (http://www.cpc.ncep.noaa.gov/products/precip/CWlink/all_index.html).

Following Groenert (2002), the positive and negative phases of the NAO and the PNA have been chosen to represent four different large-scale regimes. The NAO pattern is used instead of the AO/NAM pattern in this research because the more regional spatial extent and the proximity of the domain of the NAO to the northeastern U.S. imply that the NAO may have a greater influence on precipitation in the northeastern U.S. than does the AO/NAM.

For use in the objective identification of large-scale regimes and regime transitions, daily indices of the NAO and PNA are produced for a 56-year period from 1 January 1948 through 31 December 2003 using daily 500 hPa geopotential height data from the NCEP–NCAR reanalysis dataset. The spatial domains used to calculate the daily teleconnection indices are the same domains used by the CDC and correspond to the loading pattern identified through REOF analysis of NH 500 hPa geopotential height (Barnston and Livezey 1987). Examples of the loading patterns of the positive phase of the NAO and the positive phase of the PNA obtained through REOF analysis are shown in Figs. 2.1 and 2.2, respectively.

Identical to the domains used by the CDC to calculate daily NAO indices, the two domains used to calculate NAO indices for this study are shown in Fig. 2.3 as the North (N) domain (55°–70°N, 70°–10°W) and the South (S) domain (35°–45°N, 70°–10°W). The four domains of the PNA used in this study are also identical to the PNA domains used by the CDC. The PNA domains are shown in

Fig. 2.4 as the Hawaii (HI) domain (15°–25°N, 180°–140°W), the Alaska (AK) domain (40°–50°N, 180°–140°W), the Pacific Northwest (NW) domain (45°–60°N, 125°–105°W), and the southeastern U.S. (SE) domain (25°–35°N, 90°–70°W).

The procedure to compute a time series of daily normalized NAO indices is as follows: First, daily values of area-weighted domain-average 500 hPa geopotential height are computed for the N and S domains of the NAO using 0000 UTC and 1200 UTC data. Second, the daily domain-average 500 hPa geopotential height data are normalized by subtracting 15-day long-term (i.e., for the entire time series) climatological geopotential heights centered on each day of the year from the daily geopotential heights and dividing by the 15-day long-term standard deviation (Wilks 1995, p. 81). Third, a time series of normalized NAO indices are created by subtracting the N domain daily normalized geopotential heights from the S domain daily normalized geopotential heights. Finally, a daily time series of standardized and normalized NAO indices is obtained by dividing the daily values of the NAO index time series by the standard deviation of the entire index time series.

For the purposes of this study, a positive NAO regime corresponds to a NAO index value greater than or equal to +1 standard deviation from the mean of the entire index time series, while a negative NAO regime corresponds to a NAO index value less than or equal to −1 standard deviation from the mean. The spatial pattern of the NAO shown in Fig. 2.1 can be interpreted as showing the composite 500 hPa geopotential height anomaly field for a positive NAO regime.

From a synoptic perspective, then, a positive NAO regime is indicative of a strong latitudinal midtropospheric geopotential height gradient over the North Atlantic relative to climatology. Assuming that the speed of the actual wind is close to the speed of the geostrophic wind at in the middle troposphere, a positive NAO regime corresponds to stronger-than-average midtropospheric westerlies over the North Atlantic. Conversely, a negative NAO index value indicates a weak latitudinal midtropospheric geopotential height gradient over the North Atlantic relative to climatology, and may be associated with weaker-than-average midlevel westerlies over the North Atlantic.

The procedure to compute a time series of daily normalized PNA indices is similar to the procedure used to compute the time series of daily normalized NAO indices. First, a daily time series of the differences in normalized geopotential heights between the HI and AK domains is obtained by repeating steps 1–3 of the procedure for calculating the NAO time series, with the HI domain replacing the S domain and the AK domain replacing the N domain. Second, a daily time series of the differences in normalized geopotential heights between the NW and SE domains is obtained by again repeating steps 1–3 with the NW domain replacing the S domain and the SE domain replacing the N domain. Third, a time series of normalized PNA indices is created by adding the daily values of the HI − AK time series to the daily values of the NW − SE time series. Finally, a time series of standardized and normalized PNA indices is obtained by dividing the daily values of the PNA index time series by the standard deviation of the entire time series.

Similar to a positive and negative NAO regime, a positive PNA regime corresponds to a PNA index value greater than or equal to +1 standard deviation from the mean, while a negative PNA regime corresponds to a PNA index value less than or equal to −1 standard deviation from the mean. The spatial pattern of the PNA shown in Fig. 2.2 can be interpreted as showing the mean 500 hPa geopotential height anomaly field for a positive PNA regime. From a synoptic perspective, then, a positive PNA regime indicates an amplified pattern with respect to climatology, with a positive midtropospheric geopotential height anomaly centered over Alberta, Canada and a negative midlevel geopotential height anomaly centered over the southeastern U.S. Conversely, a negative PNA regime indicates a zonal pattern with respect to climatology, with a negative midtropospheric geopotential height anomaly centered over Alberta, Canada, and a positive midtropospheric geopotential height anomaly centered over the southeastern U.S.

The normalized NAO and PNA index time series calculated for use in this study are highly linearly correlated with the CPC's NAO and PNA index time series, respectively, which may be downloaded at ftp://ftpprd.ncep.noaa.gov/pub/cpc/cwlinks/. The CPC's normalized daily NAO and PNA indices are constructed by projecting the daily 0000 UTC 500 hPa NH geopotential height anomalies onto the loading patterns of the NAO and PNA (Figs. 2.1 and 2.2, respectively). Simple linear regression of the two NAO time series for a 54-year period from 1 January 1950 through 31 December 2003 yields a correlation coefficient of 0.84, while simple linear regression of the two PNA time series for the same period yields a correlation coefficient of 0.81.

2.3 Definition of a Large-Scale Regime Transition

Based on the definitions of large-scale regimes detailed above, a regime transition is defined as a transition from a negative to positive regime or positive to negative regime over a seven-day period. The requirement of a regime transition time of seven days is chosen in order to identify only the most rapid regime transitions, which may be more easily linked to transient synoptic-scale disturbances. In addition, the requirement of a seven-day regime transition period is consistent with research indicating an intrinsic time scale of about 10 days for the NAO (Feldstein 2003) and PNA (Cash and Lee 2001).

2.4 Calculation of Northeast Precipitation Anomalies

For use in determining composite Northeast precipitation anomalies during large-scale regimes and regime transitions, normalized seven-day running precipitation anomalies are calculated for the Northeast from the UPD 24-h precipitation data using the following procedure. First, a 56-year time series (1 January 1948–31 December 2003) of running seven-day domain-average precipitation totals is created using the Northeast domain shown in Fig. 2.5. Second, since seven-day domain-average Northeast precipitation totals are found to be positively skewed over time, a simple square-root power transformation, $T(x) = x^{1/2}$ (Wilks 1995, p. 39), is applied to the time series of running seven-day domain-average Northeast precipitation totals to create a precipitation time series with an approximately normal distribution. Finally, the transformed seven-day running precipitation totals for each day in the 56-year time series are standardized by first subtracting from each day's transformed seven-day running precipitation total the climatological mean of the transformed precipitation total centered on that date, and then dividing by the climatological standard deviation of the transformed precipitation total centered on that date.

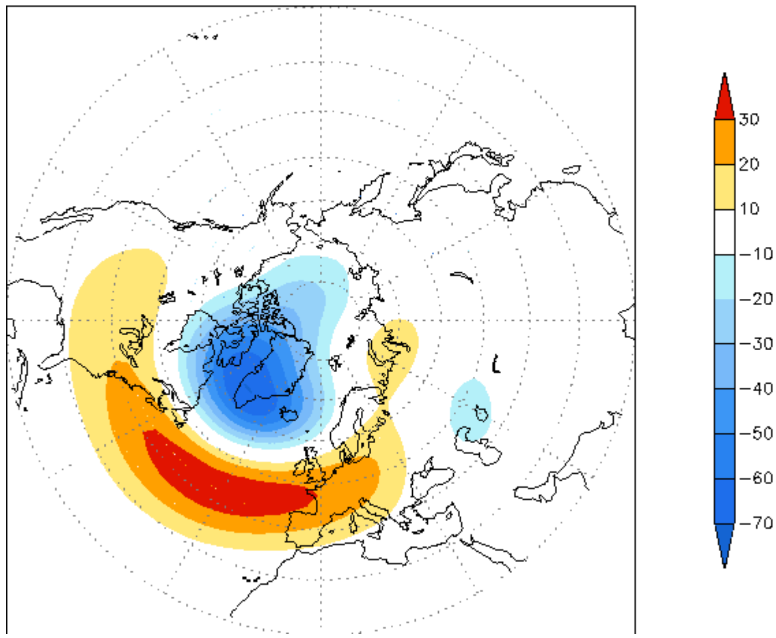

Fig. 2.1. The loading pattern of the NAO shown as the first-leading REOF of NH mean monthly 500 hPa geopotential height (from the CPC). Units are nondimensional.

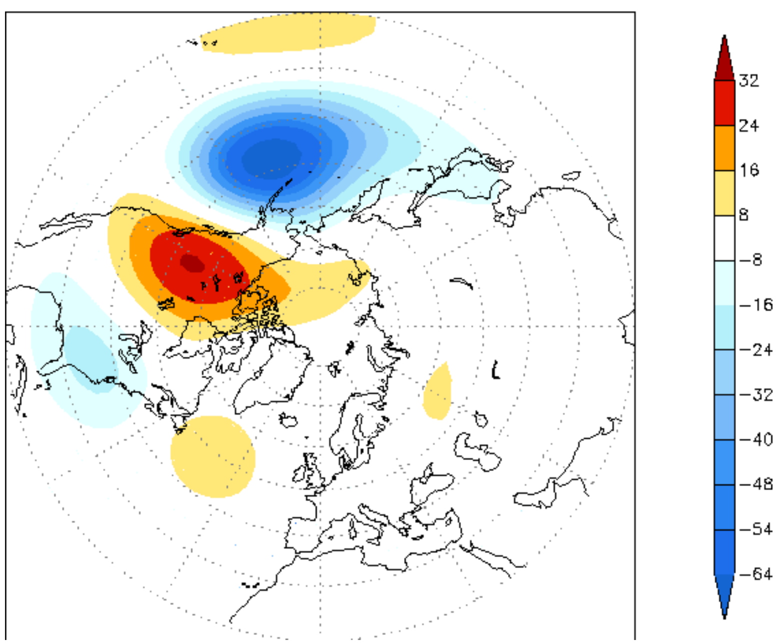

Fig. 2.2. The loading pattern of the PNA shown as the second-leading REOF of NH mean monthly 500 hPa mean monthly height (from the CPC). Units are nondimensional.

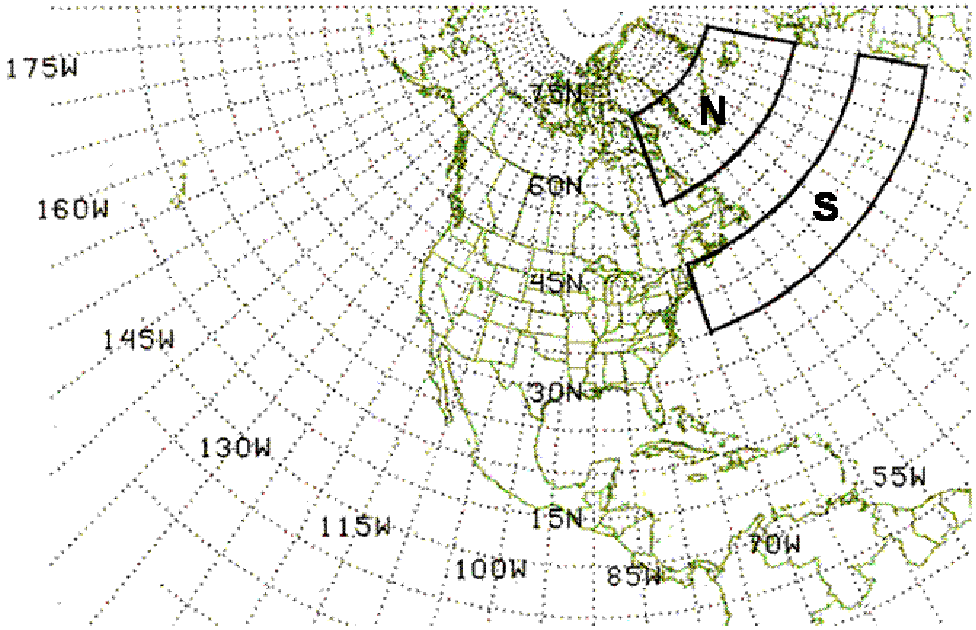

Fig. 2.3. The N and S domains of the NAO used to create a daily NAO time series.

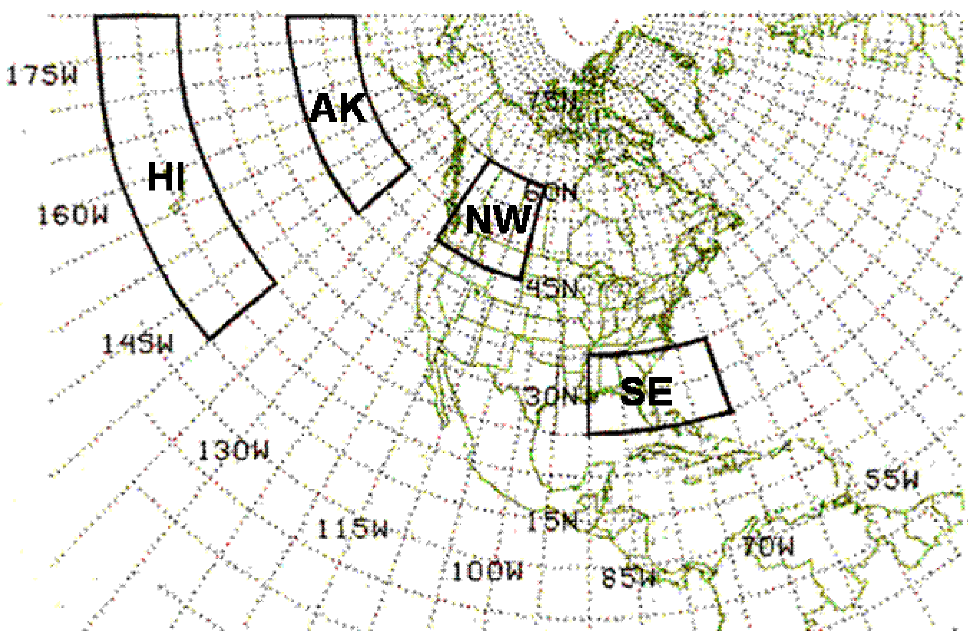

Fig. 2.4. The HI, AK, NW, and SE domains of the PNA used to create a daily PNA time series.

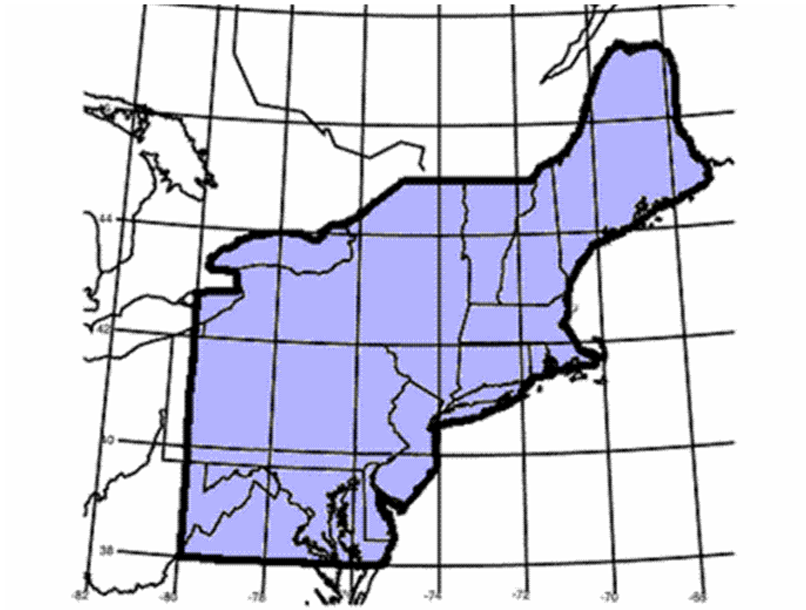

Fig. 2.5. The domain used to calculate Northeast precipitation anomalies.

3. Relationships between Large-Scale Regimes and Northeast Precipitation in the Cool Season

3.1 Overview

In this chapter, statistical relationships between large-scale regimes and Northeast precipitation in the cool season are illustrated through graphs of composite Northeast precipitation anomalies during persistent positive and negative NAO and PNA regimes. The statistical significance of these precipitation anomalies is evaluated using a two-tailed Student's t-test (Wilks 1995, 121–125). To examine whether the NAO and PNA tend to be in a certain phase during major precipitation events in the Northeast, the values of NAO and PNA indices during the top 24-h cool-season precipitation events are also presented.

The relationships between large-scale regimes and Northeast precipitation are interpreted synoptically using three types of composite analyses. Each composite analysis shows the atmospheric structure during the top five 24-h (1200 UTC–1200 UTC) cool-season precipitation events in a 56-year period (1948–2003) that were associated with a particular large-scale regime. The first type of analysis exhibits midtropospheric structure as represented by geopotential height and geopotential height anomalies on a 500 hPa surface. The geopotential heights are plotted from data valid at the midpoint of each of the five 24-h precipitation events (+12 h from the start of the events). The composite geopotential height anomalies at 500 hPa are two-day anomaly averages centered at the midpoints of the 24-h precipitation events and are calculated from a 29-year (1968–1996) climatology.

The second kind of composite analysis shows the position and strength of the jet stream at the midpoint of the precipitation events by displaying geopotential height and wind speeds on a 300 hPa surface. The third type of analysis provides a QG approximation of vertical motion (with friction and diabatic effects neglected) at the midpoint of the precipitation events by displaying advection of absolute vorticity by the thermal wind (e.g., Sutcliffe 1947; Trenberth 1978; Atallah and Bosart 2003). The variables plotted in this analysis are 700 hPa absolute vorticity, 1000–500 hPa thickness (showing the thermal wind), and SLP (showing surface features).

3.2 Statistical Relationships

3.2.1 Northeast Precipitation Anomalies during Persistent Large-Scale Regimes in the Cool Season

To determine whether persistent large-scale regimes influence precipitation amounts in the Northeast during the cool season, composite Northeast precipitation anomalies during regimes lasting seven days were calculated and are displayed in Fig. 3.1. Results indicate that persistent positive NAO and negative PNA regimes tend to be associated with slightly enhanced Northeast precipitation, while persistent negative NAO and positive PNA regimes are linked to slightly suppressed Northeast precipitation. The most statistically significant composite precipitation anomaly is the positive anomaly associated with negative PNA regimes at the 99.9% level, while the other two statistically significant composite precipitation anomalies are the positive anomalies associated with positive NAO regimes and positive PNA regimes, both significant at the 90.0% level.

3.2.2 Teleconnection Indices during Major Northeast Precipitation Events in the Cool Season

In addition to exploring the influence of persistent large-scale regimes on Northeast precipitation in the cool season, this research seeks to determine whether particular phases of the NAO and PNA are favored during major cool-season precipitation events in the Northeast. To establish whether such connections exist, the 25 greatest 24-h (1200 UTC–1200 UTC) cool-season precipitation events in the Northeast were calculated from the UPD and are displayed in Table I. Interestingly, the dates of the top 25 precipitation events suggest that major Northeast precipitation events tend to occur during the early part of the cool season, with nearly half (12) of the 25 greatest cool-season precipitation events in the Northeast occurring in November, and more than a quarter (7) occurring in December.

The values of the NAO and PNA indices during these 25 cool-season precipitation events in the Northeast were plotted and are displayed in Figs 3.2a and 3.2b, respectively. Figure 3.2a shows that 15 of 25 (60%) top precipitation events in the Northeast occurred when the NAO index was positive. During top cool-season precipitation events in the Northeast, the mean NAO index value was +0.11 and the median NAO index value was +0.27, indicating that the distribution of NAO index values for top Northeast precipitation events in the cool season is slightly negatively skewed.

While Fig. 3.2a suggests a weak relationship between major precipitation events in the Northeast and the phase of the NAO, Fig. 3.2b suggests a robust relationship between major Northeast precipitation events and the phase of the PNA, with mean and median values of the PNA index during top cool-season precipitation events found to be +0.50 and +0.44, respectively. These values show that the distribution of PNA index values for the top 25 24-h precipitation events in the Northeast is slightly positively skewed. Of the top 25 precipitation events in the Northeast, the PNA was in a positive phase during 17 events (68% of the time).

Research results indicating that the NAO shows a slight tendency to be positive during major precipitation events in the Northeast (Fig. 3.2a) seem consistent with results suggesting that Northeast precipitation is slightly enhanced during persistent positive NAO regimes (Fig. 3.1). However, that the PNA shows a strong tendency to be positive during major precipitation events in the Northeast (Fig. 3.2b) seems to contradict results suggesting that precipitation in the Northeast is suppressed during persistent positive PNA regimes and enhanced during persistent negative PNA regimes (Fig. 3.1).

The apparent paradoxical relationship between persistent negative PNA regimes and enhanced Northeast precipitation may be explained by the fact that a negative PNA pattern is associated with a stronger-than-average midtropospheric southwesterly flow across the Northeast as implied by higher-than-average 500 hPa geopotential heights across the southeastern U.S. (e.g., Wallace and Gutzler 1981). This type of flow pattern might favor precipitation in the Northeast because it could allow moisture to spread northward from the Gulf of Mexico (Leathers et al. 1991). The relationship between major Northeast precipitation events and the positive phase of the PNA, on the other hand, may be explained by the fact that cool-season coastal storms impacting the Northeast tend to be forced by strong dynamics and often occur in association with an anomalously deep 500 hPa trough over the eastern U.S. (e.g., Kocin and Uccellini 2004, 101–105) that is characteristic of a positive PNA pattern. Thus, major but relatively few precipitation events in the Northeast may be favored when the PNA is in a positive phase, while minor but more numerous events may be favored when the PNA is in a negative phase.

3.3 Composite Analyses of Cool-Season Northeast Precipitation Events Associated with Large-Scale Regimes

3.3.1 Events Associated with Positive NAO Regimes

The dates and precipitation amounts associated with the top five precipitation events that occurred on days when the NAO was strongly positive (index values greater than +2.0) are displayed in Table II. The mean of the five domain-average 24-h precipitation amounts is 2.0 cm, while the mean of the maximum 24-h precipitation amounts associated with each of the five events is 6.0 cm. Since smoothing processes used to construct the UPD tend to reduce observed precipitation maxima (e.g., DeLuca 2004, section 2.2), the mean of the actual precipitation maxima occurring with these events is likely higher than 6.0 cm. The greatest of these five events, beginning at 1200 UTC 30 December 1948, is ranked #17 in the list of top 25 24-h cool-season precipitation events occurring in the Northeast (Table I).

In order to determine characteristic midtropospheric signatures of major cool-season precipitation events in the Northeast associated with positive NAO regimes, a composite analysis of 500 hPa geopotential heights and geopotential height anomalies was created using the dates in Table II. The analysis (Fig. 3.3a) shows a composite meridional geopotential height anomaly dipole characteristic of a positive NAO regime, with a region of below-normal 500 hPa geopotential heights centered close to 60°N, 20°W, and a region of above-normal 500 hPa geopotential heights centered around 45°N, 55°W. These respective anomalies over the North Atlantic are associated with a stronger-than-average latitudinal 500 hPa geopotential height gradient, indicative of a stronger-than-average midtropospheric westerly jet. Across the U.S., the composite midtropospheric flow is relatively zonal, and only a weak trough can be seen over the Northeast in the 500 hPa geopotential height field.

A composite analysis of the upper-tropospheric jet structure during the top Northeast precipitation events associated with strong positive NAO regimes (Fig. 3.3b) shows an anticylonically curved jet streak extending from the Northeast U.S. northeastward to Newfoundland and then eastward across the central North Atlantic. The 300 hPa jet maximum across the North Atlantic is collocated with the strong 500 hPa geopotential height gradient shown in Fig. 3.3a, and places the Northeast in the right-entrance region of the jet streak.

Figure 3.3c shows composite QG forcing for ascent for major Northeast precipitation events associated with a strong positive NAO pattern. A 700 hPa absolute vorticity maximum centered over northern New York and southwesterly thermal wind over the region suggest that QG forcing for ascent is located mainly over the southern portion of the province of Quebec, Canada, and northern Maine. The 1000–500 hPa thickness pattern shows a neutrally to slightly "positively" (northeast-to-southwest) tilted thermal trough over the Ohio Valley, west of a weak surface low with an approximate 1008 hPa SLP minimum centered over eastern New England. Strong surface southeasterly geostrophic winds to the northeast of the surface low are associated with strong warm air advection across northeastern New England and are suggestive of a significant influx of moisture from the Atlantic.

3.3.2 Events Associated with Negative NAO Regimes

Dates and precipitation amounts associated with the top five precipitation events that occurred when the NAO was strongly negative (index values less than −2.0) are displayed in Table III. The period beginning at 1200 UTC 21 January 1979 is ranked #12 on the list of top 25 24-h cool-season precipitation events occurring in the Northeast (Table I). The mean of the five domain-average 24-h precipitation amounts associated with strong negative NAO precipitation events is 1.9 cm, similar to the 2.0 cm mean domain-average precipitation amount associated with strong positive NAO events. However, the mean of the five maximum UPD 24-h precipitation amounts associated with each of the five negative NAO events is 8.2 cm, 36% greater that the average maximum 24-h precipitation amount of 6.0 cm associated with positive NAO events. The difference between average maximum precipitation amounts suggests that precipitation-enhancing mesoscale features may be more likely to develop during negative NAO precipitation events than during positive NAO precipitation events.

Composite 500 hPa geopotential heights and anomalies during major precipitation events in the Northeast associated with strong negative NAO regimes are shown in Fig. 3.4a. In contrast to the strong negative-over-positive 500 hPa geopotential height anomaly dipole associated with positive NAO storms (Fig. 3.3a), negative NAO storms are associated with a strong positive-over-negative 500 hPa geopotential height anomaly dipole over the North Atlantic, a pattern characteristic of blocking. The composite positive geopotential height anomaly over southern Greenland is greater in amplitude than the negative geopotential height anomaly located farther to the south and east of southern Greenland, with maximum geopotential height departures over Greenland exceeding +36 dam. In contrast to the positive NAO regime, the blocking pattern characteristic of a negative NAO regime is associated with an inferred weaker-than-average midtropospheric westerly jet across the North Atlantic. The relatively weak jet associated with negative NAO storms may indicate that these types of storms are slow-moving and can produce prolonged events of precipitation, thus yielding precipitation totals comparable to totals produced by more strongly forced but faster-moving storms such as those that tend to occur during positive NAO regimes.

In addition to the negative geopotential height anomaly associated with the southern center of the negative NAO dipole, a negative geopotential height anomaly is located in the base of a closed 500 hPa low over the Northeast. The closed 500 hPa low associated with negative NAO precipitation events in the Northeast (Fig. 3.4a) contrasts dramatically with the weak open 500 hPa trough associated with positive NAO precipitation events in the Northeast (Fig. 3.3a).

A composite analysis of the upper-tropospheric jet structure during major precipitation events associated with strong negative NAO regimes (Fig. 3.4b) shows a prominent 300 hPa jet streak over the southeastern U.S. The location of this jet streak across the southeastern U.S. places the Mid-Atlantic and perhaps the southern portion of the Northeast in the left-exit region of the jet streak. Across the North Atlantic, the blocking pattern seen in the geopotential height field at 500 hPa (Fig. 3.4a) also can be seen at the 300 hPa level (Fig.

3.4b). This pattern corresponds to a relatively weak 300 hPa jet over the North Atlantic that is displaced southward in comparison to the relatively strong 300 hPa jet associated with positive NAO precipitation events (Fig. 3.3b).

Composite QG forcing for ascent for major Northeast precipitation events occurring during strongly negative NAO regimes is shown in Fig. 3.4c. The location of an absolute vorticity maximum at 700 hPa over eastern New York and the presence of south-southwesterly thermal wind in the composite analysis indicate forcing for ascent over New England. The 1000–500 hPa thickness pattern shows a negatively tilted thermal trough over the eastern U.S. just to the west of a moderately strong surface low with an approximate 1000 hPa SLP minimum that is collocated with the left-exit region of the 300 hPa jet streak (Fig. 3.4b). Strong surface southeasterly geostrophic winds are evident along the New England coast, implying an influx of Atlantic moisture into the Northeast.

3.3.3 Events Associated with Positive PNA Regimes

Dates and precipitation amounts associated with the top precipitation events that occurred when the phase of the PNA was strongly positive (index values greater than +2.0) are displayed in Table IV. The mean of the five domain-average 24-h precipitation amounts associated with strong positive PNA events is 2.3 cm, a higher amount than the mean domain-average precipitation amounts associated with strong positive NAO and strong negative NAO regimes. Three of these events are ranked among the top 25 24-h precipitation events in the Northeast during the cool season: The event beginning on 1200 UTC 9 January 1978 is ranked #2, the event beginning on 15 November 1995 is ranked #20, and the event beginning on 30 November 1963 is ranked #22 on the list of top 25 24-h cool-season precipitation events occurring in the Northeast (Table I). The mean of the five UPD maximum 24-h precipitation amounts associated with strong positive PNA regimes is 6.9 cm, higher than the mean maximum precipitation amount associated with strong positive NAO regimes but lower than the mean maximum precipitation amount associated with strong negative NAO regimes.

Composite 500 hPa geopotential heights and geopotential height anomalies during major Northeast precipitation events associated with strong positive PNA regimes are shown in Fig. 3.5a. The 500 hPa geopotential height anomaly field shows a longitudinally oriented series of alternating positive and negative anomalies characteristic of the positive phase of the PNA, with two regions of negative geopotential height anomalies centered near 45°N, 160°W and 35°N, 80°W and two regions of positive geopotential height anomalies centered close to 45°N, 110°W and 50°N, 60°W. The composite 500 hPa geopotential height pattern shows a trough over the North Pacific to the south of Alaska, a ridge over western North America, a negatively tilted trough over the eastern U.S., and a ridge northeast of the Canadian Maritimes.

A composite analysis of the upper-tropospheric jet structure during the top five precipitation events associated with strong positive PNA regimes (Fig 3.5b) shows one primary 300 hPa jet streak off the Northeast coast. The position of this jet streak suggests that northern sections of the Northeast may be located in the left-exit region of the jet streak.

Quasi-geostrophic forcing for ascent associated with the top five Northeast precipitation events occurring during strong positive PNA regimes is shown in Fig. 3.5c. An absolute vorticity maximum centered over northern New York at 700 hPa is associated with QG forcing for ascent over northern New England. The 1000–500 hPa thickness pattern for positive PNA precipitation events resembles the thickness pattern associated with negative NAO precipitation events (Fig. 3.4c), with a negatively tilted thickness trough located over the Great Lakes. This thickness trough is just to the west of a strong surface cyclone over western Maine with an approximate SLP minimum of 992 hPa. A strong surface pressure gradient perpendicular to a strong 1000–500 hPa thickness gradient indicates both strong warm air advection to the north of the surface low over eastern Canada and strong cold air advection to the south and southwest of the low off the southern New England coast and over western portions of the Northeast, respectively.

3.3.4 Events Associated with Negative PNA Regimes

Dates and precipitation amounts associated with the top precipitation events that occurred when the phase of the PNA was strongly negative (index values less than −2.0) are displayed in Table V. The mean of the five domain-average 24-h precipitation amounts associated with strong negative PNA events is 1.5 cm, the lowest of the mean domain-average amounts associated with any of the four types of regime precipitation events in the Northeast. Predictably, none of the five events is ranked among the top 25 24-h precipitation events to affect the Northeast during the cool season. The mean of the five UPD maximum 24-h precipitation amounts associated with strong negative PNA regimes is just 4.4 cm, the lowest of the average maximum precipitation amounts of the average maximum amounts associated with any of the four types of regime precipitation events.

Composite 500 hPa geopotential heights and geopotential height anomalies during major Northeast precipitation events associated with strong negative PNA regimes (Fig. 3.6a) show a strikingly different 500 hPa composite geopotential height pattern than the composite pattern for positive PNA events (Fig. 3.5a). The composite 500 hPa geopotential height pattern associated with negative PNA precipitation events in the Northeast is much less amplified across the U.S., with two areas of positive geopotential height anomalies centered near 50°N, 150°W and 35°N, 70°W, and an area of negative geopotential height anomalies centered close to 50°N, 110W°. Of the three main regions of geopotential height anomalies, the area with the greatest geopotential height anomaly magnitude is collocated with a Rex-block type structure in the geopotential height field just south of Alaska, around 50°N, 150°W. The 500 hPa geopotential height anomaly pattern shown in Fig. 3.6a indicates midtropospheric ridging off the eastern U.S. coast and a very weak short-wave trough over the eastern Great Lakes east of a broader trough over the western U.S. Higher-than-average 500 hPa geopotential heights across the Southeast combined with lower-than-average geopotential heights across the West suggest an enhanced midtropospheric southwesterly flow from the western Gulf Coast to the eastern Great Lakes. As mentioned previously in section 3.2, this enhanced flow from the Gulf of Mexico might play an important role in contributing to precipitation in the Northeast.

A composite analysis of the upper-tropospheric jet structure during major precipitation events associated with strong negative PNA regimes (Fig 3.6b) shows a split-flow pattern across the western U.S., with the northern branch of the flow originating from the North Pacific and the southern branch from the tropical Pacific. Farther east, the two branches of the jet merge, likely contributing to the presence of a jet streak extending from the Ohio Valley to the eastern New England coast. Based upon the position of the jet streak, the Northeast does not appear to be located in the left-exit or right-entrance region of the jet streak. The composite zonal pattern across the U.S. at 300 hPa for the top five negative PNA precipitation cases contrasts sharply with the highly amplified 300 hPa pattern associated with the top five positive PNA precipitation cases (Fig. 3.5b).

Quasi-geostrophic forcing for ascent associated with the top five Northeast precipitation events occurring during strong negative PNA regimes is shown in Fig. 3.6c. Northern sections of the Northeast U.S. are experiencing cyclonic vorticity advection by the thermal wind in association with a 700 hPa absolute vorticity maximum centered over the eastern Great Lakes. The composite surface cyclone associated with a negative PNA precipitation event has an approximate SLP minimum of 1008 hPa and is considerably weaker than the surface cyclone associated with a positive PNA precipitation event, which has an approximate SLP minimum of 992 hPa (Fig. 3.5c). This difference in the strength of the surface cyclone may be explained by the more amplified flow pattern and, thus, stronger dynamics associated with positive PNA Northeast precipitation events.

3.4 Summary

Statistical results show that persistent negative PNA and positive NAO regimes are associated with enhanced precipitation in the Northeast during the cool season, while positive PNA and negative NAO regimes are associated with suppressed precipitation in the Northeast. Calculation of the signs of the NAO and PNA indices during major 24-h Northeast precipitation events in the cool season indicates that the phase of the PNA tends to be positive during these events. Major precipitation events seem to occur independently of the phase of the NAO.

Composite analyses show that synoptic-scale features associated with major cool-season precipitation events in the Northeast tend to vary greatly depending upon the type of large-scale regime in place. A summary of the differences in synoptic-scale features of precipitation events for each of the four large-scale regimes follows below.

Positive NAO events

1. The Northeast is located in the right-entrance region of a strong North Atlantic jet streak.

2. The large-scale flow across the U.S. is zonal during these events, and the 500 hPa trough affecting the Northeast is relatively weak.

3. A weak surface cyclone appears to be favored during these events. Quasi-geostrophic forcing for ascent is located primarily over eastern Canada and parts of northern New England.

Negative NAO events

1. The Northeast is located in the left-exit region of a jet streak centered off the southeastern coast of the U.S..

2. Contrasting with the zonal flow associated with positive NAO precipitation events, the flow during negative NAO precipitation events is highly amplified from the eastern U.S. to the eastern North Atlantic. A deep closed low at 500 hPa is located over the Northeast.

3. A weak surface cyclone appears to be associated with these types of events. Quasi-geostrophic forcing for ascent is located mainly over New England.

Positive PNA events

1. The Northeast is located in the left-exit region of a jet streak centered off the Mid-Atlantic coast.

2. Positive PNA precipitation events are associated with highly amplified flow from western North America to the western North Atlantic. A closed low at 500 hPa is located over the Northeast.

3. A strong surface cyclone appears to be associated with these types of events. Quasi-geostrophic forcing for ascent is located primarily over northern New England.

Negative PNA events

1. The Northeast is not located in a left-exit or right-entrance region of the jet streak extending from the Ohio Valley to the southern New England coast.

2. The flow pattern associated with negative PNA storms is zonal, similar to the flow associated with positive NAO storms. A weak 500 hPa trough is located over the Northeast.

3. A weak surface cyclone appears to be favored during these types of events. Quasi-geostrophic forcing for ascent is found primarily over northern sections of the Northeast.

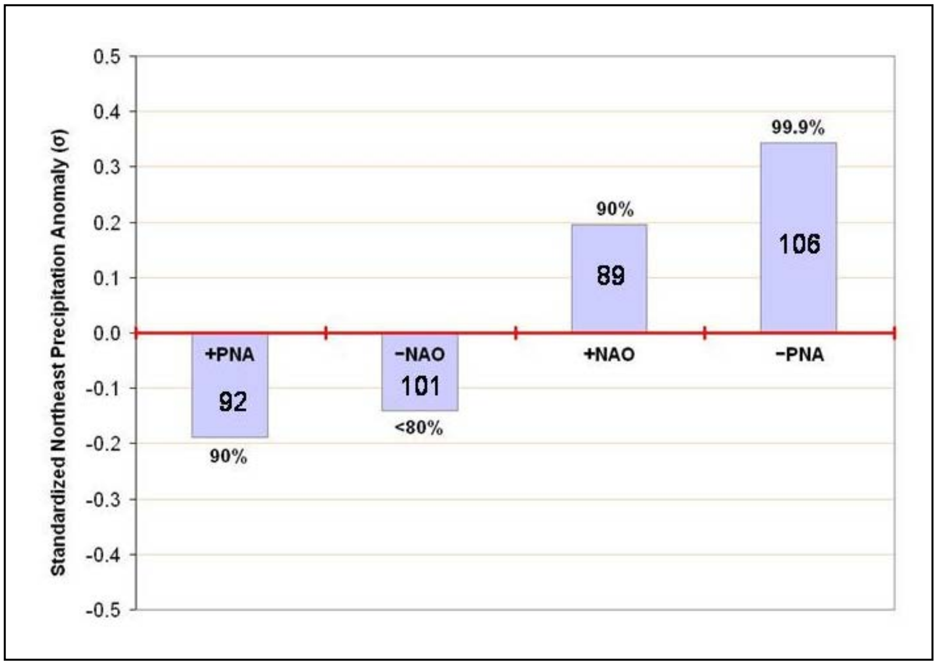

Fig. 3.1. Composite standardized cool-season Northeast precipitation anomalies corresponding to persistent large-scale regimes. Percentages above and below bars indicate statistical significance of precipitation anomalies as determined by a two-tailed t-test; the number of independent events in each category is shown inside the bars.

	Start of Event (1200 UTC)	Mean Northeast 24-h Precipitation (mm)			Start of Event (1200 UTC)	Mean Northeast 24-h Precipitation (mm)
1.	11/28/1993	32.3		14.	12/04/1990	26.9
2.	01/09/1978	31.1		15.	11/12/1995	26.7
3.	11/09/1996	30.4		16.	03/14/1994	26.6
4.	11/20/2003	29.8		17.	12/30/1948	26.3
5.	12/21/1973	29.0		18.	04/02/1970	26.0
6.	12/02/1996	28.9		19.	12/05/1993	25.1
7.	11/07/1963	28.9		20.	11/15/1995	25.0
8.	12/13/1983	28.7		21.	11/25/1983	24.6
9.	01/08/1998	28.1		22.	11/30/1963	24.1
10.	01/26/1978	28.1		23.	11/20/1948	23.8
11.	11/26/1950	27.8		24.	12/11/1952	23.7
12.	01/21/1979	27.7		25.	11/28/1959	23.6
13.	11/03/1951	27.1				

TABLE I. Dates and mean Northeast precipitation amounts (mm) for the top 25 24-h (1200 UTC–1200 UTC) cool-season precipitation events in the Northeast for a 56-year period (1948–2003).

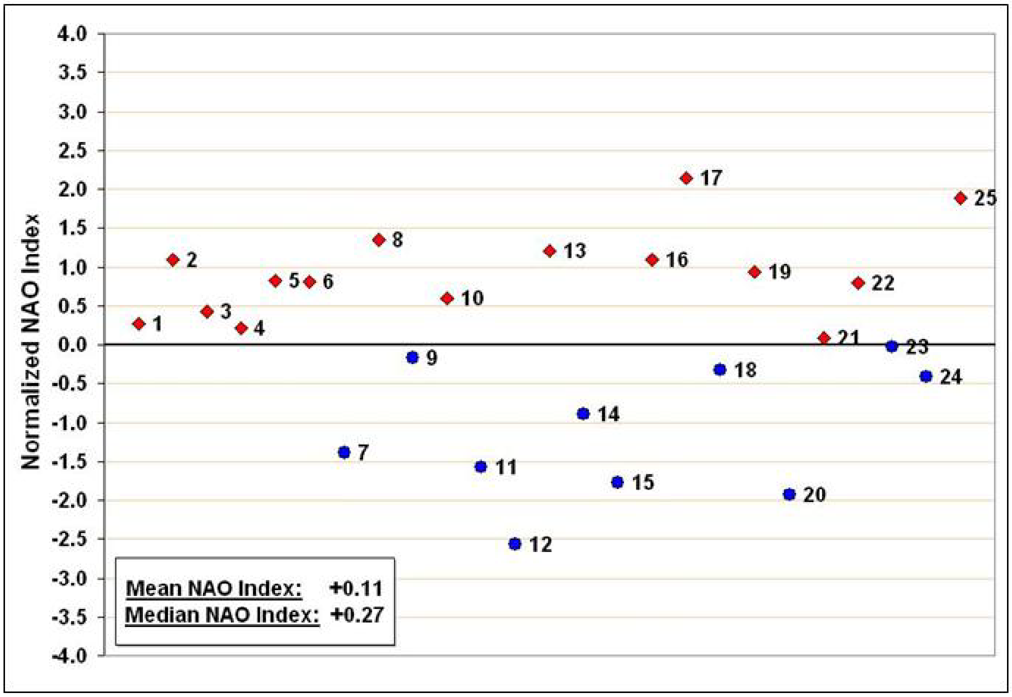

Fig. 3.2a. Normalized NAO index values during the top 25 cool-season precipitation events in the Northeast. Numbers to the right of the points indicate the rank of the precipitation events.

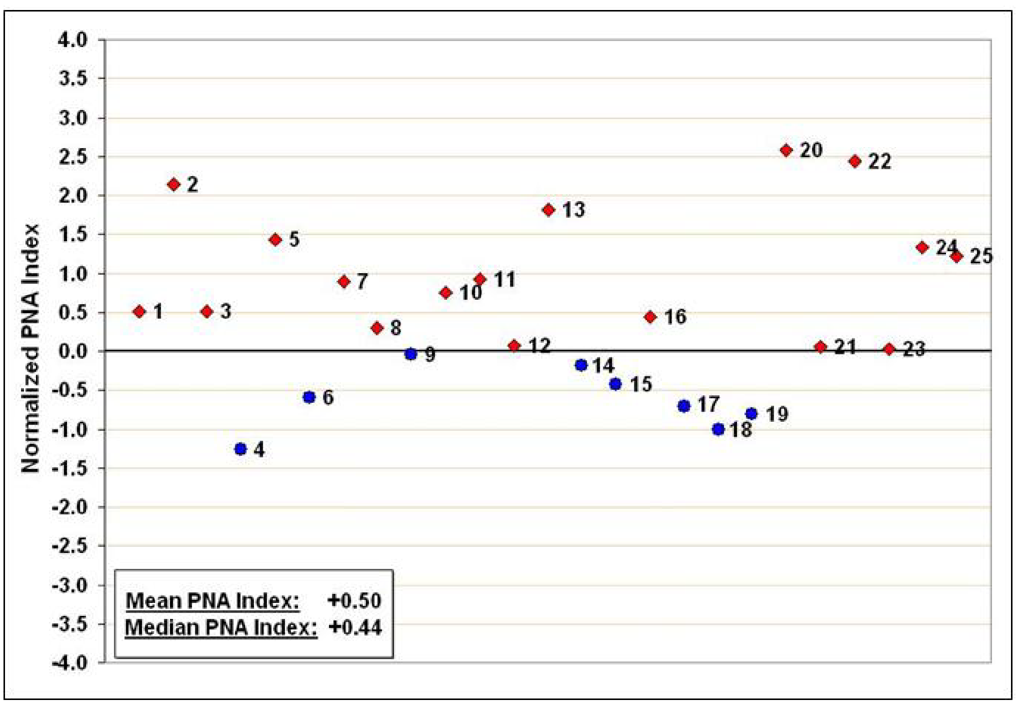

Fig. 3.2b. Same as in Fig. 3.2a, except normalized PNA index values.

	Start of Event (1200 UTC)	Mean Northeast 24-h Precipitation (mm)	Max Northeast 24-h Precipitation (mm)	NAO Index
1.	12/30/1948	26.3	86.5	+2.1
2.	3/10/1994	23.3	52.8	+2.1
3.	11/21/1986	19.0	64.6	+2.1
4.	1/15/1999	16.8	41.7	+2.2
5.	3/3/1972	15.9	55.0	+2.1

TABLE II. Dates, mean and maximum Northeast precipitation amounts (mm), and NAO index values for the top five cool-season precipitation events in the Northeast associated with strong positive NAO regimes.

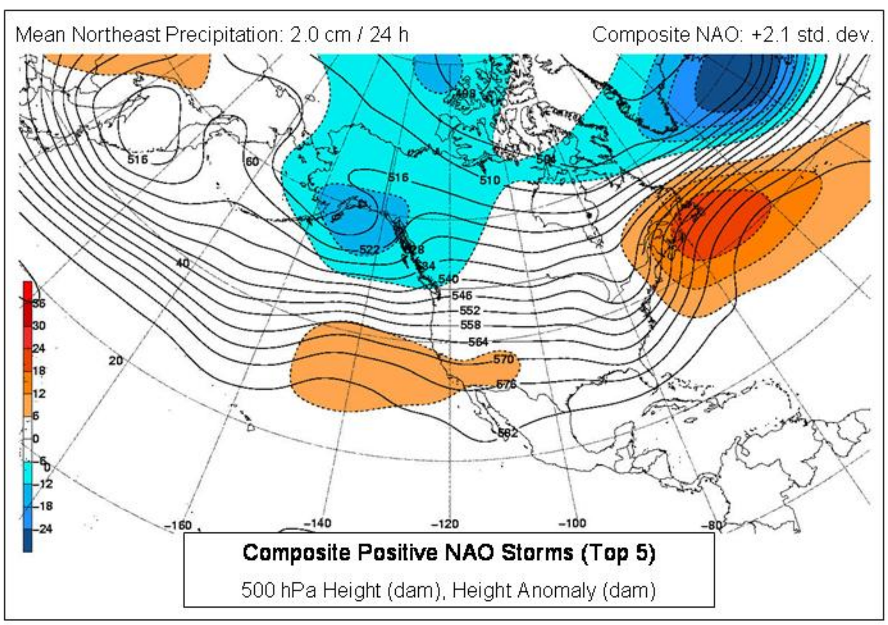

Fig. 3.3a. Composite 500 hPa geopotential heights (dam) and anomalies (dam) corresponding to the top five cool-season precipitation events in the Northeast associated with strong positive NAO regimes. Geopotential heights are contoured every 6 dam; anomalies are contoured every 6 dam and are shaded as indicated.

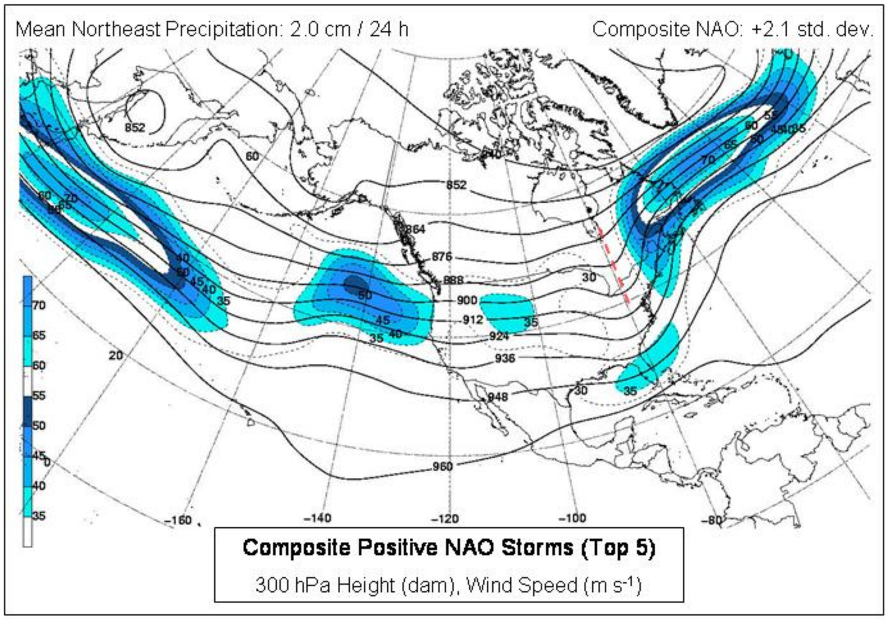

Fig. 3.3b. Composite 300 hPa geopotential heights (dam) and wind speed (m s^{-1}) corresponding to the top five cool-season precipitation events in the Northeast associated with strong positive NAO regimes. Geopotential heights are contoured every 12 dam. Wind speed is contoured every 5 m s^{-1} starting at 30 m s^{-1}; shading begins at 35 m s^{-1}.

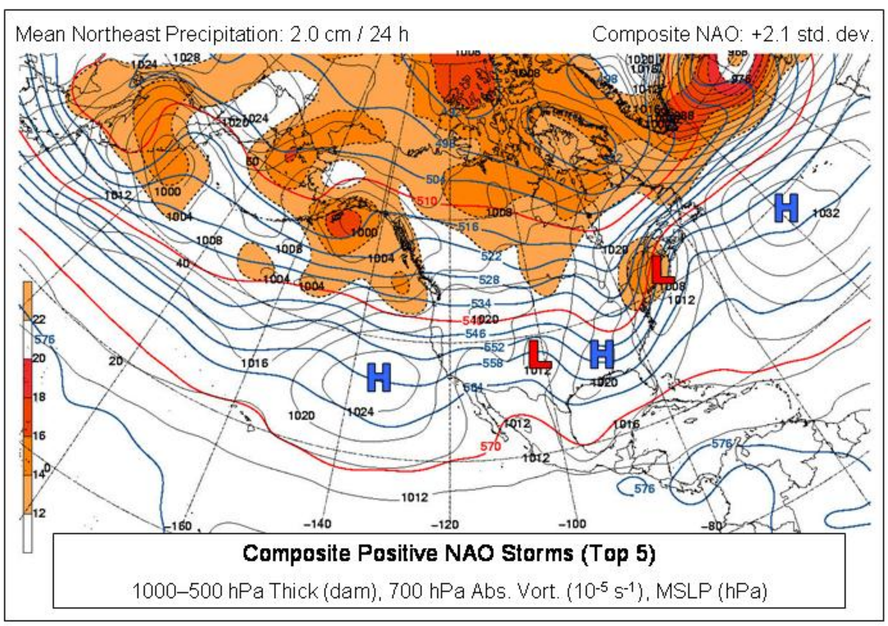

Fig. 3.3c. Composite 1000–500 hPa thickness (dam), 700 hPa absolute vorticity (10^{-5} s^{-1}), and SLP (hPa) corresponding to the top 5 cool-season precipitation events in the Northeast associated with strong positive NAO regimes. Thickness is contoured every 6 dam in blue; isobars are contoured every 4 hPa in black. Absolute vorticity is contoured in intervals of 2 x 10^{-5} s^{-1}; shading begins at 12 x 10^{-5} s^{-1}.

	Start of Event (1200 UTC)	Mean Northeast 24-h Precipitation (mm)	Max Northeast 24-h Precipitation (mm)	NAO Index
1.	1/21/1979	27.7	90.4	−2.6
2.	1/25/1979	19.4	78.8	−2.8
3.	11/16/1983	15.9	78.6	−2.1
4.	4/4/1987	15.7	71.9	−2.2
5.	3/22/1980	14.2	87.6	−2.6

TABLE III. Same as in Table II, except for cool-season precipitation events in the Northeast associated with strong negative NAO regimes.

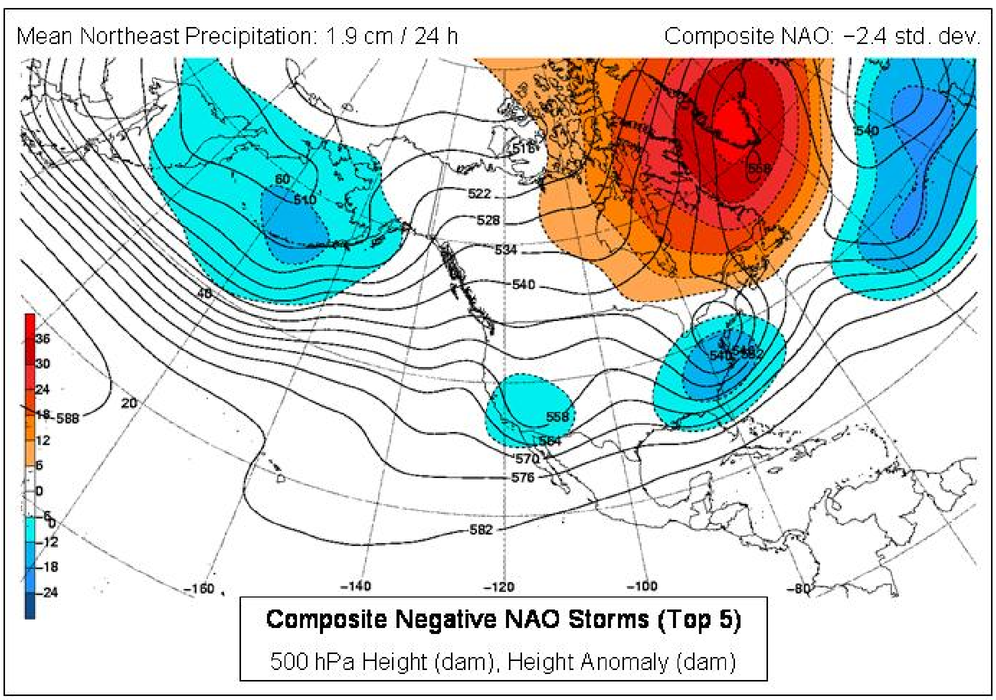

Fig. 3.4a. Same as in Fig. 3.3a, except for top five cool-season precipitation events in the Northeast associated with strong negative NAO regimes.

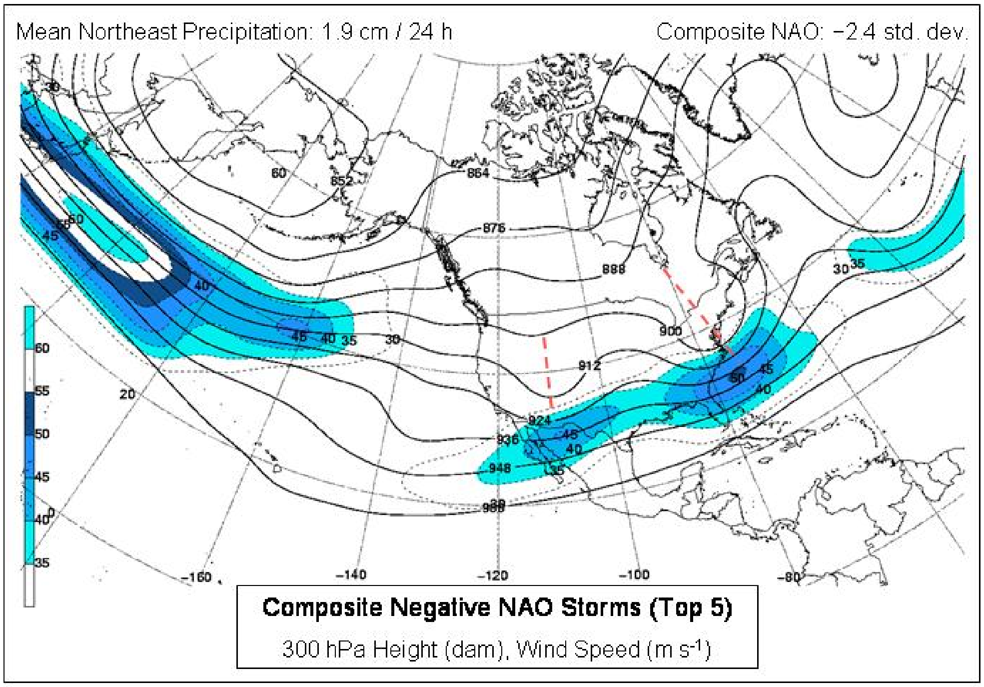

Fig. 3.4b. Same as in Fig. 3.3b, except for top five cool-season precipitation events in the Northeast associated with strong negative NAO regimes.

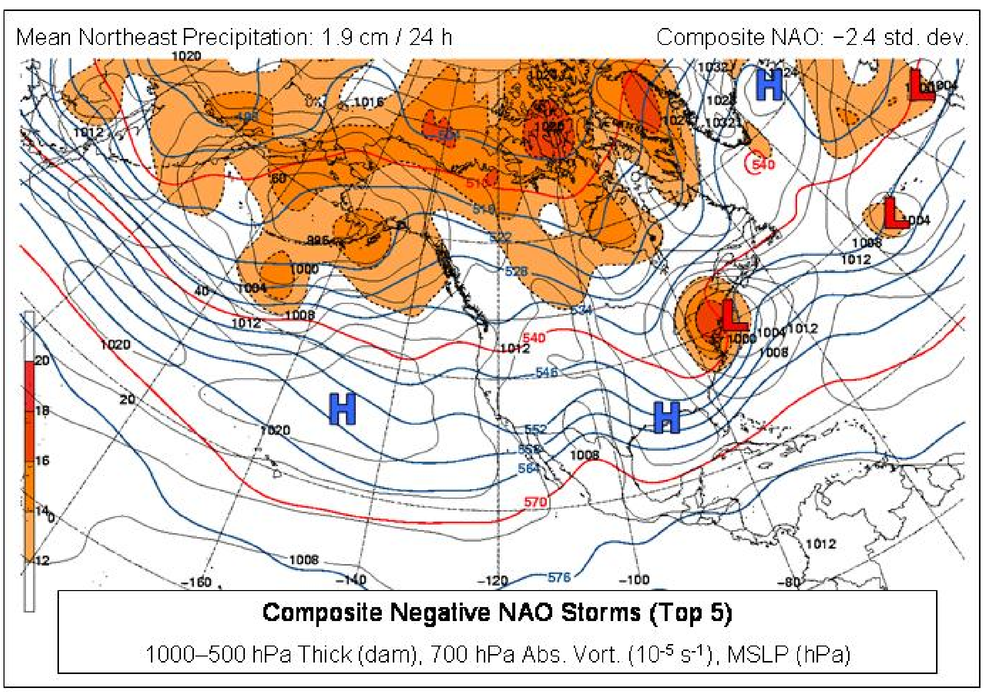

Fig. 3.4c. Same as in Fig. 3.3c, except for top five cool-season precipitation events in the Northeast associated with strong negative NAO regimes.

	Start of Event (1200 UTC)	Mean Northeast 24-h Precipitation (mm)	Max Northeast 24-h Precipitation (mm)	PNA Index
1.	1/9/1978	31.1	73.0	+2.1
2.	11/15/1995	25.0	89.3	+2.6
3.	11/30/1963	24.1	70.5	+2.5
4.	3/3/1994	18.9	62.2	+2.2
5.	11/11/1983	17.5	49.5	+2.3

TABLE IV. Same as in Table II, except for cool-season precipitation events in the Northeast associated with strong positive PNA regimes.

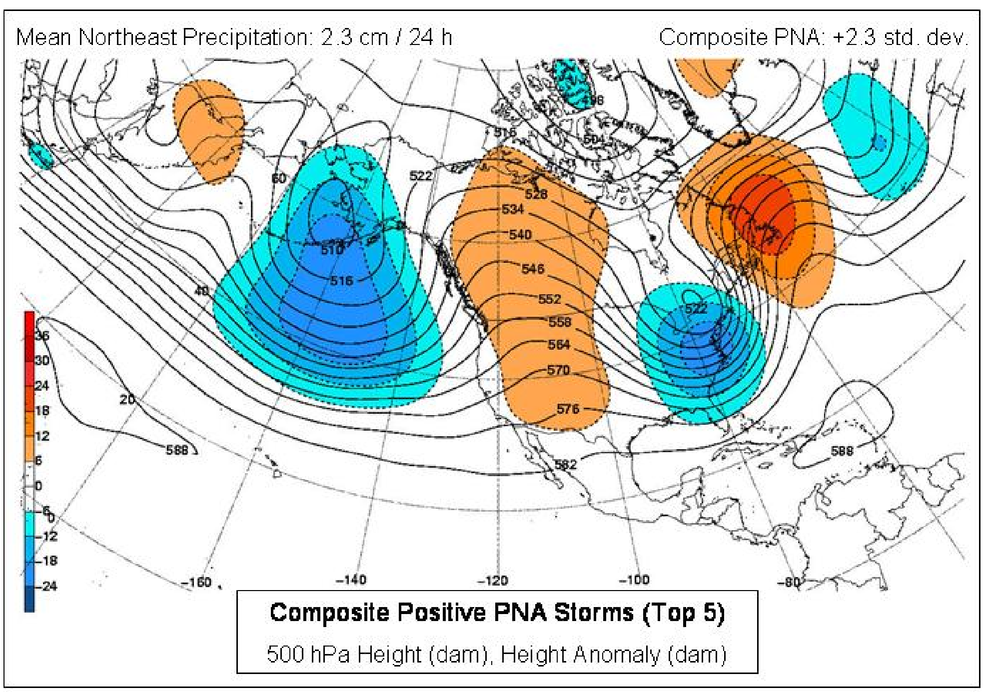

Fig. 3.5a. Same as in Fig. 3.3a, except for top five cool-season precipitation events in the Northeast associated with strong positive PNA regimes.

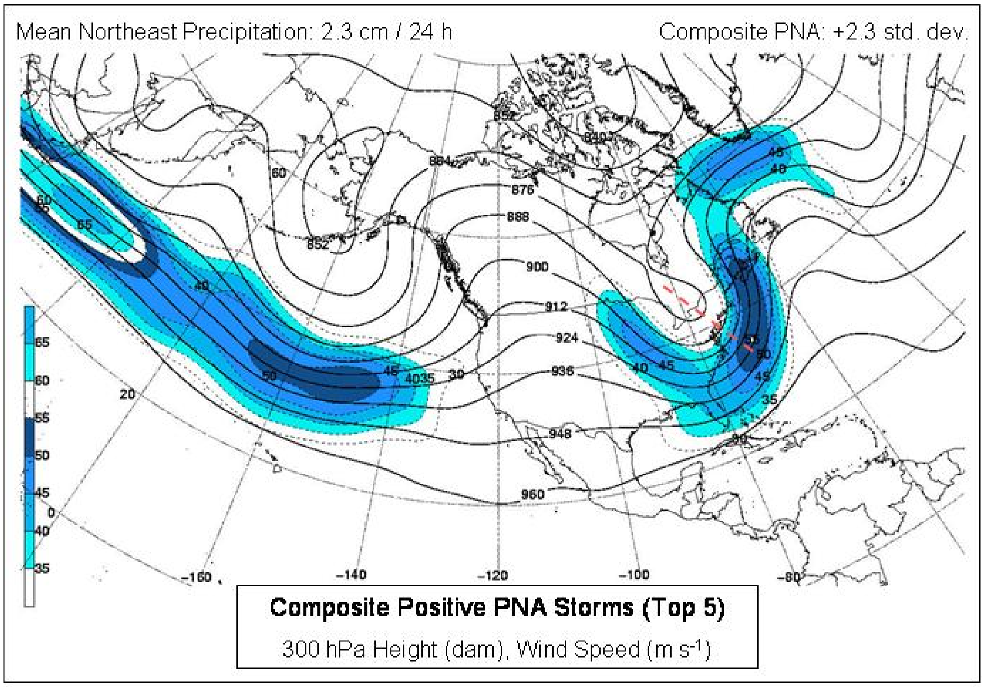

Fig. 3.5b. Same as in Fig. 3.3b, except for top five cool-season precipitation events in the Northeast associated with strong positive PNA regimes.

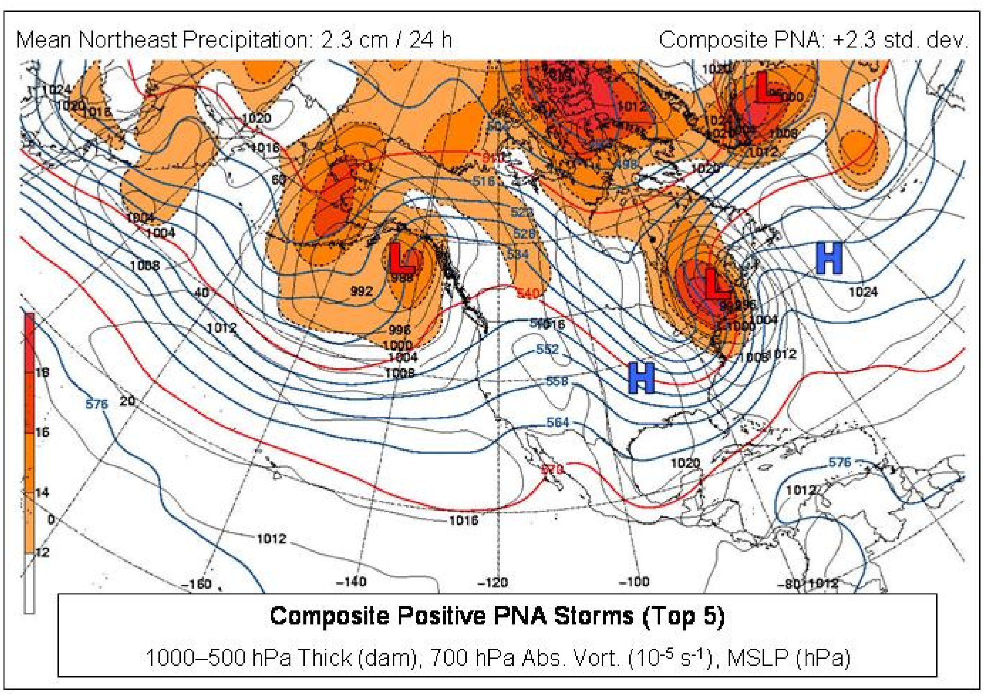

Fig. 3.5c. Same as in Fig. 3.3c, except for top five cool-season precipitation events in the Northeast associated with strong positive PNA regimes.

	Start of Event (1200 UTC)	Mean Northeast 24-h Precipitation (mm)	Max Northeast 24-h Precipitation (mm)	PNA Index
1.	2/24/1962	17.4	38.9	−2.3
2.	12/24/1990	15.6	38.9	−2.0
3.	3/22/1955	15.3	47.6	−2.1
4.	2/10/1959	14.0	47.9	−2.5
5.	3/5/1985	12.8	48.4	−2.8

TABLE V. Same as in Table II, except for cool-season precipitation events in the Northeast associated with strong negative PNA regimes.

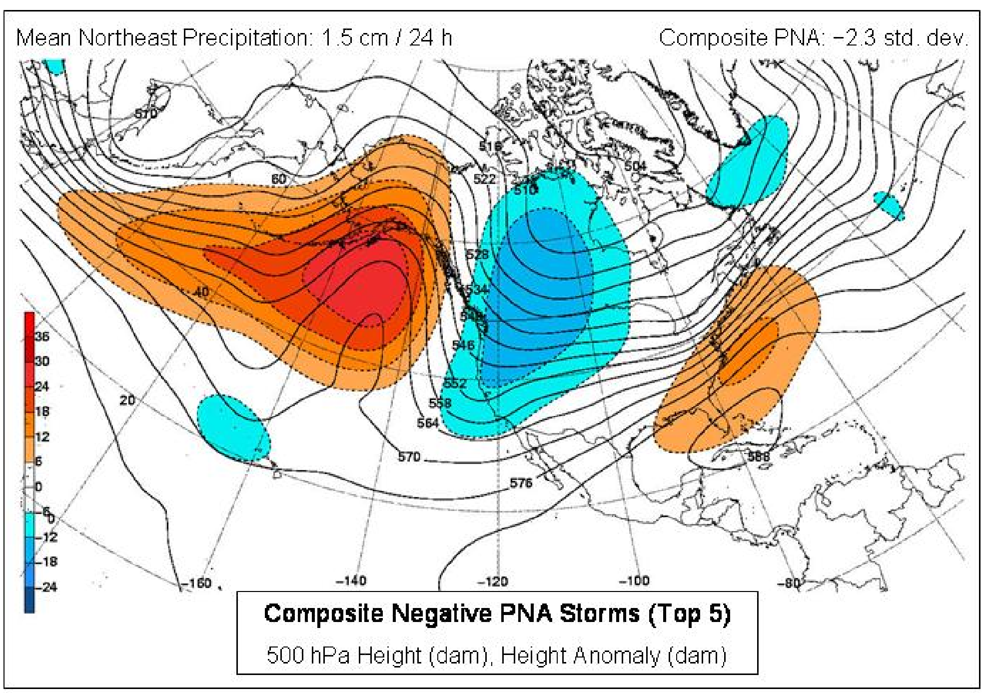

Fig. 3.6a. Same as in Fig. 3.3a, except for top five cool-season precipitation events in the Northeast associated with strong negative PNA regimes.

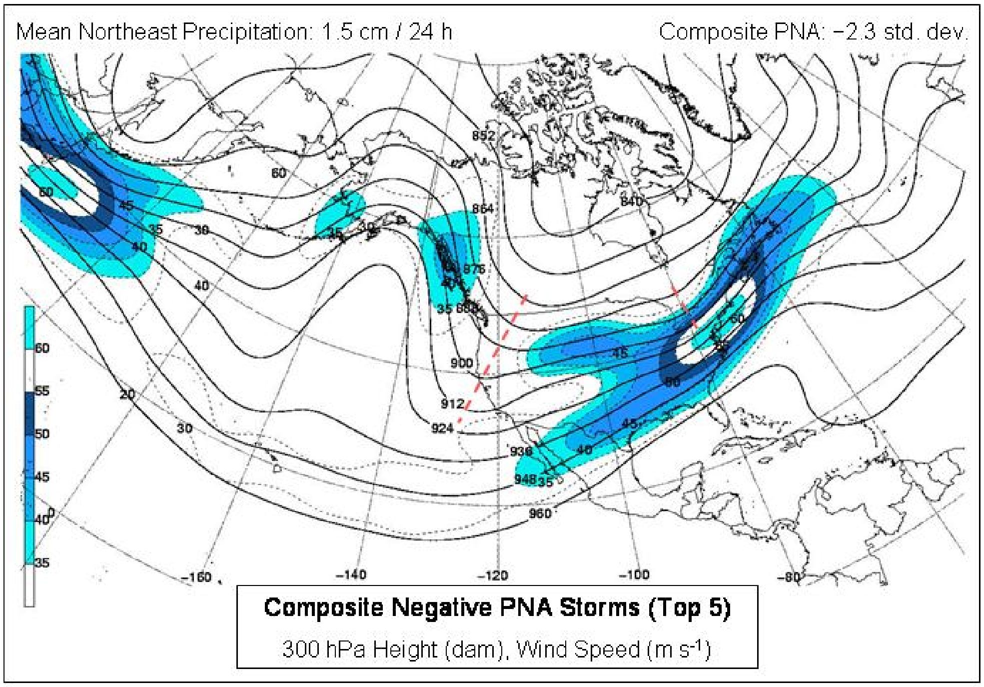

Fig. 3.6b. Same as in Fig. 3.3b, except for top five cool-season precipitation events in the Northeast associated strong negative PNA regimes.

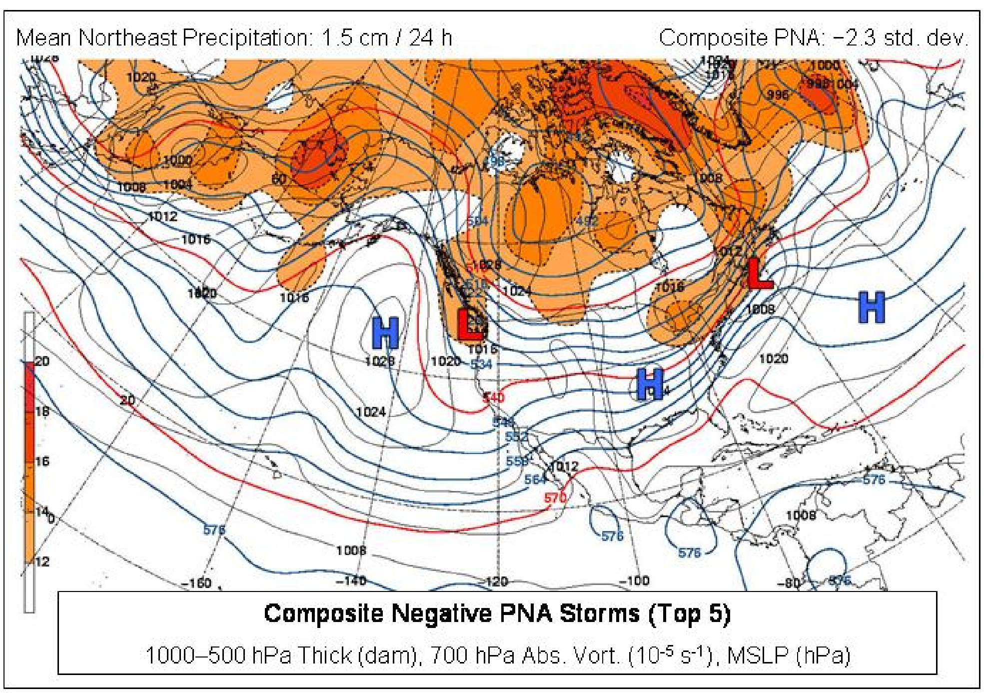

Fig. 3.6c. Same as in Fig. 3.3c, except for top five cool-season precipitation events in the Northeast associated strong negative PNA regimes.

4. Relationships between Large-Scale Regime Transitions and Northeast Precipitation in the Cool Season

4.1 Overview

This chapter presents statistical relationships between four kinds of large-scale regime transitions and Northeast precipitation during the cool season. To examine first-order changes in the large-scale pattern during major precipitation events in the Northeast, the seven-day tendencies of NAO and PNA indices centered on top 24-h cool-season precipitation events in the Northeast are also presented.

The relationships between certain large-scale regime transitions and Northeast precipitation are interpreted synoptically using the same three types of composite analyses shown in Chapter 3. The analyses show atmospheric structure from Day 1 through Day 7 of two types of regime transitions, positive-to-negative NAO transitions and negative-to-positive PNA transitions. The first type of composite analysis shows 500 hPa geopotential heights and anomalies, the second shows 300 hPa geopotential heights and wind speeds, and the third shows QG forcing for vertical motion and sea level pressure.

The five positive-to-negative NAO and negative-to-positive PNA regime transitions with the greatest 24-h Northeast precipitation events beginning at the transition midpoints (1200 UTC on Day 4) were chosen to be included in each set of composite analyses. Instead of centering composite analyses on 0000 UTC as in Chapter 3, each composite analysis in Chapter 4 is a daily mean composite analysis created from an average of 0000, 0600, 1200, and 1800 UTC data. Daily mean composite analyses were used to examine regime transitions so that daily changes in the large-scale pattern could be easily related to daily changes in the composite daily teleconnection indices.

4.2 Statistical Relationships

4.2.1 Northeast Precipitation Anomalies during Large-Scale Regime Transitions in the Cool Season

To examine whether precipitation in the Northeast significantly deviates from climatology during large-scale regime transitions, precipitation anomalies during seven-day regime transitions (defined in section 2.3 as seven-day NAO or PNA index changes of two standard deviations, centered on zero) were calculated and are displayed in Fig. 4.1. Figure 4.1 shows that precipitation is enhanced in the Northeast during transitions from positive to negative NAO regimes and during transitions from negative to positive PNA regimes. Conversely, precipitation tends to be suppressed during transitions from positive to negative PNA regimes and during transitions from negative to positive NAO regimes. Using a two-sided Student's t-test, the most statistically significant composite precipitation anomaly associated with regime transitions is found to be the negative anomaly linked to positive-to-negative PNA regime transitions at the 99.9% level, while the next most statistically significant composite precipitation anomaly is the positive anomaly associated with positive-to-negative NAO regime transitions at the 99.5% level.

To examine the variation of the relationships between regime transitions and Northeast precipitation during the cool season, precipitation anomalies associated with the regimes transitions were calculated for each month of the cool season (Fig. 4.2). Anomalies associated with positive-to-negative NAO transitions and negative-to-positive NAO transitions stratified by month (Fig. 4.2a) suggest that the relationship between positive-to-negative NAO transitions and enhanced Northeast precipitation shown in Fig. 4.1 is valid throughout the cool season, with the exception of February and March. Regime transitions from negative to positive NAO appear to be associated with suppressed Northeast precipitation in the latter part of the cool season, during March and April, but do not seem to influence Northeast precipitation during other times of the cool season.

An apparent monthly variation in the strength of the relationships between certain regime transitions and Northeast precipitation is also seen in Fig. 4.2b, which presents monthly relationships between PNA regime transitions and precipitation. Figure 4.2b suggests that the association between positive-to-negative PNA transitions and below-normal precipitation in the Northeast shown in Fig. 4.1 is valid primarily in December, January, and March. Figure 4.2b also suggests that the association between negative-to-positive PNA transitions and above-normal precipitation in the Northeast shown in Fig. 4.1 is valid mainly in November, March, and April.

Although the strength of the relationships between regime transitions and Northeast precipitation tends to vary monthly as shown in Fig. 4.2, this monthly variability in the strength of the relationships may be an artifact of the relatively restrictive definition of regime transition used in this research. Calculating composite precipitation anomalies from a greater sample of regime transitions might produce more consistent relationships between regime transitions and precipitation from month to month.

4.2.2 Teleconnection Index Tendencies during Major Northeast Precipitation Events in the Cool Season

In addition to exploring the influence of large-scale regime transitions on Northeast precipitation in the cool season, this research sought to determine the first-order behavior of the large-scale pattern during major cool-season precipitation events in the Northeast. To examine this behavior, normalized seven-day NAO and PNA index tendencies were calculated for the same top 25 24-h cool-season precipitation events used to determine relationships between major precipitation events and the signs of the NAO and PNA in section 3.2. Figure 4.3a shows seven-day NAO index tendencies for the top 25 24-h cool-season precipitation events in the Northeast, while Fig. 4.3b shows seven-day PNA index tendencies for the top 25 24-h cool-season precipitation events.

Results shown in Fig. 4.3a indicate that the NAO index frequently exhibits a negative tendency during the period surrounding a major 24-h precipitation event in the Northeast during the cool season. The NAO index was negative during 18 of 25 major precipitation events (72% of the time), and the mean seven-day tendency during the 25 precipitation events was −0.45. The median seven-day NAO tendency during the 25 precipitation events was −0.60, indicating that the distribution of NAO tendencies is positively skewed. These results suggest a strong relationship between major precipitation events in the Northeast and the seven-day tendency of the NAO index, and are consistent with results shown in Fig. 4.1 suggesting that precipitation in the Northeast tends to be enhanced during positive-to-negative NAO transitions in the cool season.

A strong relationship was also found between major precipitation events in the Northeast and the seven-day tendency of the PNA index. Figure 4.3b shows that the PNA index exhibited a positive tendency during 17 of 25 major precipitation events (68% of the time), with a mean seven-day index tendency of +0.77. A median seven-day tendency of +0.74 indicates that the distribution of seven-day PNA tendencies during top precipitation events in the Northeast is not significantly skewed. These results, combined with results shown in Fig. 4.3a, suggest that the NAO index tends to decrease and the PNA index tends to increase during major precipitation events in the Northeast. The tendency of the PNA index to increase during major precipitation events appears consistent with results indicating that enhanced precipitation can be expected in the Northeast during negative-to-positive PNA transitions in the cool season (Fig. 4.1).

4.3 Composite Analyses of Large-Scale Regime Transitions Associated with Cool-Season Precipitation Events in the Northeast

4.3.1 Positive-to-Negative NAO Regime Transitions

Since positive-to-negative transitions of the NAO appear to be linked to enhanced precipitation in the Northeast (Figs. 4.1 and 4.2a), and since the NAO index tends to decrease during major precipitation events in the Northeast (Fig. 4.3a), composite analyses were created to explore why transitions from a positive NAO regime to a negative NAO regime appear to be associated with enhanced precipitation in the Northeast. A list of the dates of the five regime transitions used in the composite analyses and the associated Northeast precipitation amounts (mm) are shown in Table VI. The mean of the five domain-average 24-h precipitation amounts was 2.0 cm, while the mean of the maximum 24-h precipitation amounts associated with each of the five events was 6.5 cm. Two of these five precipitation events are among the top 25 all-time 24-h (1200 UTC to 1200 UTC) cool-season events in the Northeast; the event that occurred at the midpoint of the 6–12 November 1996 transition (from 1200 UTC 9 November to 1200 UTC 10 November) is ranked #3, while the event that occurred at the midpoint of the 27 November–3 December 1963 transition (from 1200 UTC 30 November to 1200 UTC 1 December) is ranked #22 (Table I).

Composite analyses for Day 1 of positive-to-negative NAO transitions having a mid-transition storm are shown in Fig. 4.4. Figures 4.4a and 4.4b show a zonal flow pattern at 500 hPa and 300 hPa, respectively, from the west coast of the U.S. to the eastern North Atlantic. A weak trough is evident at both 300 hPa and 500 hPa over the Great Basin of the U.S. The presence of a jet streak at 300 hPa in the northwest flow of the trough indicates that this trough should deepen with time. Farther west across the North Pacific, the mid and upper-tropospheric pattern is slightly more amplified, with a series of short-wave troughs and ridges extending zonally across the North Pacific. This pattern suggests that downstream development associated with a Rossby wave train might be underway over the North Pacific. The pattern over the North Atlantic, on the other hand, is relatively zonal due to a high-latitude negative 500 hPa geopotential height anomaly centered over Greenland and a midlatitude positive 500 hPa geopotential height anomaly centered off the northwest coast of Spain. This pattern is characteristic of a positive NAO regime, although the strength of the 500 hPa geopotential height anomaly associated with the northern center of the NAO dipole is greater than the strength of the 500 hPa anomaly associated with the southern center of the NAO dipole.

The sea level pressure field displayed in Fig. 4.4c shows two weak low pressure centers to the lee of the Rockies. This region of low pressure is likely tied to the mid and upper-tropospheric troughs at 500 hPa (Fig. 4.4a) and 300 hPa (Fig. 4.4b), and also may be orographically forced by the Rockies.   Warm air advection into the weak 1000–500 hPa thickness ridge (Fig. 4.4c) ahead of the area of surface low pressure and cold air advection into the 1000–500 hPa thickness trough behind the area of surface low pressure suggest that the 1000–500 hPa thickness pattern may amplify with time.

Farther to the east, the Northeast is influenced by a westward extension of the Bermuda High (Fig. 4.4c). Slight warm air advection over the Northeast is implied by the sea level pressure and 1000–500 hPa thickness fields, but little or no QG forcing for ascent is evident there. Over the North Atlantic, strong cold air advection east of Newfoundland and Labrador and south of Greenland suggests decreasing 1000–500 hPa thicknesses in that region. Since no significant thermal advection is evident farther south, a decrease in 1000-500 hPa thickness, and, thus, a fall in 500 hPa geopotential heights in this region may maintain the positive NAO regime in the short term.

Composite analyses for Day 2 of the positive-to-negative NAO transition are displayed in Fig. 4.5. Figures 4.5a and 4.5b show that mid and upper-tropospheric troughs, respectively, previously over the Great Basin on Day 1 have moved just east of the Rockies and deepened. At the same time, ridges at 500 hPa and 300 hPa have developed over the eastern U.S. and the overall pattern across the U.S. has become more amplified. The jet maximum at 300 hPa that was centered off the Pacific Northwest on Day 1 has remained offshore, though the axis of the jet has become somewhat more meridionally oriented as the upper-tropospheric ridge builds off the west coast of the U.S. Farther east, a weaker jet streak is located in west-southwesterly flow just east of the base of the trough over the Plains. A split-flow pattern is apparent at 300 hPa (Fig. 4.5b) and 500 hPa (Fig. 4.5a) across central North America. Across the North Pacific, a series of short-wave troughs and ridges is still evident, while over the North Atlantic the mid- and upper-tropospheric pattern has remained relatively zonal.

Consistent with the zonal pattern across the North Atlantic, the composite NAO index on Day 2 is +1.0, a NAO index change of only −0.2 standard deviations from Day 1 to Day 2.

Likely related to the split-flow pattern that has developed aloft, the sea level pressure pattern (Fig. 4.5c) on Day 2 shows that the two centers of low pressure just east of the Rockies on Day 1 have diverged; the northern area of low pressure has moved northeast to the Canadian border and the southern area of low pressure has tracked southeast to the Mexican border. Both cold air and warm air advection associated with these areas of low pressure can be expected to amplify the 1000–500 hPa thickness pattern across the U.S. In addition, the presence of QG forcing for ascent in advance of the northern system indicates that diabatic heating associated with precipitation may contribute to the amplification of the thickness ridge south of the Hudson Bay. Farther west over the eastern North Pacific, on the northwest side of surface high pressure off the west coast of the U.S., strong warm air advection associated with a cyclone in the Gulf of Alaska is likely helping to amplify the 1000–500 hPa thickness ridge over western Canada.

Meanwhile, over the Northeast, the combination of a westward extension of the Bermuda High to the East Coast and approaching low pressure over the Northern Plains is producing warm air advection. However, a composite mean Northeast precipitation amount only 0.2 cm in a 24-h period beginning at 1200 UTC on Day 2 indicates a dry pattern over the Northeast.

By Day 3 (Fig. 4.6), the mid and upper-tropospheric geopotential height patterns have amplified further (Figs. 4.6a and 4.6b, respectively). The 500 hPa ridge over western Canada has amplified due to ongoing warm air advection, and is associated with geopotential height anomalies of +12 dam (Fig. 4.6a). Farther east, the trough that was just east of the Rockies on Day 2 has reached the Plains and is associated with geopotential height anomalies of –12 dam. In addition, the 500 hPa ridge that built over the Northeast on Day 2 has amplified further, and now contains geopotential height anomalies of +12 dam. Despite the marked amplification of the pattern across North America, the flow pattern across the North Atlantic is still relatively zonal, as indicated by the composite NAO index of +0.9 on Day 3. However, the region of negative 500 hPa geopotential height anomalies associated with the northern center of the positive NAO dipole has begun to weaken slightly and drift to the west. Although cold air advection is ongoing over the western North Atlantic, the magnitude and areal extent have lessened slightly from Day 2 to Day 3 (Figs. 4.5c and 4.6c)

In association with the amplification of the pattern over North America on Day 3, three significant jet streaks are now evident 300 hPa (Fig. 4.6b). An anticylonically curved jet streak previously offshore has moved over British Columbia on the northern side of the ridge, a second short and straight jet streak has strengthened over the western Gulf Coast just east of the base of the 300 hPa trough over the Plains, and a third anticylonically curved jet streak has formed over Quebec.

One area of surface low pressure that has moved east from southern Texas (Fig. 4.6c) appears to be associated with the poleward-exit region of the jet streak over the western Gulf Coast. The other low pressure center that was located over the Northern Plains on Day 2 has since moved north and is now over southern Hudson Bay. This region of low pressure does not appear to be coupled to a jet streak aloft (Fig. 4.6b), and is located in relatively zonal 500 hPa flow well north of the sharpest part of the trough (Fig. 4.6a); thus, the surface circulation may be expected to weaken with time.

Persistent warm (cold) air advection into the thickness ridge (trough) on the northwest (southeast) side of the surface high pressure over the western U.S., combined with warm air advection occurring over the Northeast on the western side of the Atlantic high, should allow the midtropospheric pattern to continue to amplify over North America (Fig. 4.6c). In addition, QG forcing for ascent over the Great Lakes and the southwestern portion of Quebec implies that precipitation-induced diabatic heating may also help to build the ridge over eastern North America.

By Day 4, the day that marks the beginning of a 24-h period of significant precipitation in the Northeast, the mid and upper-tropospheric geopotential height patterns (Figs. 4.7a and 4.7b, respectively) have continued to amplify across much of North America. While the 500 hPa ridge across western North America has dampened somewhat, the 500 hPa trough and ridge farther east across central and eastern North America, respectively, have strengthened. The deep 500 hPa trough over the Missouri Valley contains climatological geopotential height departures of –18 dam, while the 500 hPa ridge over Labrador contains climatological geopotential height departures of +18 dam. The apparent downstream transfer of energy from western North America to eastern North America over a short period of time may represent the eastward propagation of a Rossby wave packet.

As the mid and upper-tropospheric pattern amplifies, so too does the intensity of the 300 hPa jet streak that was centered over the western Gulf Coast on Day 3 (Fig. 4.7b). Now located over the southeastern U.S., the jet streak contains wind speeds in excess of 50 m s^{-1}. Farther north, the jet streak previously centered over Quebec on Day 3 is still in the same region, but is more anticyclonically curved, with the tail of the jet streak extending southward to the eastern Great Lakes. The location of the entrance region of this jet, combined with the location of the exit region of the jet over the southeastern U.S., implies that the western portion of the Northeast and northwestern portion of the Mid-Atlantic are in the right-entrance region of one jet and the left-exit region of another.

The surface pressure field displayed in Fig. 4.7c shows that the surface low over the Northeast is, in fact, collocated with the left-exit region of the southern jet streak and the right-entrance region of the northern jet streak. The asymmetrical shape of the 1004 hPa isobar surrounding the low pressure center suggests the possibility that at least two relative pressure minima are impacting the Northeast. The southward extension of the 1004 hPa isobar along the Mid-Atlantic coast may imply the presence of a coastal low, while the westward bulge of the 1004 hPa isobar into eastern Michigan may indicate the presence of an interior surface low. This type of pattern suggests the redevelopment of a surface low east of the Appalachians as the initial low center tied to the main 500 hPa trough weakens while the entire system crosses the Appalachians.

Several factors appear to contribute to the precipitation event that produced an average 24-h composite precipitation total of 2 cm over the Northeast from 1200 UTC on Day 4 to 1200 UTC on Day 5. The location of the Northeast under the right-entrance and left-exit regions of two upper-level jet streaks (Fig. 4.7b) appears to favor the formation of a surface low pressure system over the Northeast. Warm air advection associated with the surface low pressure system over the Northeast is also likely contributing to a broad area of upward motion and precipitation (Fig. 4.7c). The Atlantic appears to be providing moisture for this storm, with an implied onshore geostrophic wind at the surface (Fig. 4.7c) and implied anomalous south-southeasterly geostrophic winds at 500 hPa (Fig. 4.7a) along the southern New England coast. The diabatic heating associated with the heavy precipitation event in the Northeast on Day 4, combined with strong warm air advection over the Northeast, should help amplify the pattern over the western North Atlantic, and, thus, effect a transition from a positive to negative NAO regime over the next few days.

Composite analyses for Day 5 (Fig. 4.8) show that a regime transition is indeed beginning to occur over the North Atlantic at this time. The closed 500 hPa low associated with below-normal geopotential heights that was anchored over Greenland during the first half of the regime transition has now drifted well to the north and west of the region (Fig. 4.8a). In its place, the 500 hPa ridge previously located over Labrador on Day 4 has moved east into the western Atlantic. This 500 hPa ridge has also strengthened, with 500 hPa geopotential height anomalies greater than +24 dam. In addition, farther to the east, a significant 500 hPa trough has developed, with geopotential height anomalies in excess of −12 dam. The amplification of the pattern across the central and eastern North Atlantic, combined with a weakening of the 500 hPa trough over the eastern U.S., provides further evidence that downstream development may play an important part in the overall pattern amplification associated with positive-to-negative NAO transitions. In conjunction with this pattern amplification, the composite NAO index has dropped from +0.6 on Day 4 to −0.3 by Day 5.

The amplification of the pattern over the western North Atlantic by Day 5 appears to be linked to the development and track of the surface cyclone that brought heavy precipitation to the Northeast on Day 4 and Day 5 (Fig. 4.8c). As the surface cyclone moves northward away from the Northeast on Day 5, associated warm air advection to the north and northwest of the low helps to build the thickness ridge across eastern Canada, while cold air advection to the south of the low helps to deepen the thickness trough across the Great Lakes. The track of the cyclone to the north appears to be both a response to and a cause of the developing blocking pattern over the North Atlantic. As the jet streak that was over northern Quebec on Day 4 moves northward with the building 300 hPa ridge, the equatorward jet entrance region moves northward, thus favoring the surface low to be located farther to the north (Fig. 4.8b).

By Day 6 of the seven-day transition from a positive-to-negative NAO regime, a blocking pattern has developed across the North Atlantic (Figs. 4.9a and 4.9b). The NAO index has dropped by one standard deviation between Day 5 to Day 6, from −0.3 to −1.3. This development of a negative NAO regime is associated with a high-amplitude 500 hPa ridge to the east of Greenland and a closed 500 hPa low just west of Europe (Fig. 4.9a). The trough over the eastern U.S. has weakened further as energy associated with the Rossby wave train appears to continue to propagate eastward. The Northeast is experiencing a dry westerly geostrophic flow at 300 hPa (Fig. 4.9b) and 500 hPa (Fig. 4.9a), and a southwesterly geostrophic flow and the surface (Fig. 4.9c), consistent with a composite domain-average Northeast precipitation amount of 0.1 cm on Day 6. The area of low pressure that brought heavy precipitation to the Northeast on Day 4 and Day 5 has continued to move northward and is located over the Hudson Strait just north of Quebec.

On Day 7, the final day of the regime transition, a blocking pattern over the North Atlantic has been established, with geopotential height anomalies of +30 dam just east of Greenland (Fig. 4.10a). To the east of the blocking anticyclone, negative geopotential height anomalies of −24 dam are associated with a closed low at 500 hPa to the west of Portugal. Meanwhile, across North America, a weak broad trough remains over the eastern half of the U.S., with a more amplified ridge in place over western North America.

The pattern at 300 hPa (Fig. 4.10b) is similar to the 500 hPa pattern. A Rex block is located over the central North Atlantic, with a jet streak situated in the base of a broad trough over the eastern U.S. At the surface, high pressure has become established to the east of Greenland and low pressure to the west of Portugal. Since the surface high (low) is located nearly directly beneath the ridge (trough) at 300 hPa, this negative NAO pattern appears to be equivalent barotropic.

A summary of the composite transition from a positive to negative NAO regime associated with a major precipitation event in the Northeast follows below:

1. The pattern at the onset of the transition is relatively zonal over North America and the North Atlantic.

2. By the midpoint of the transition, the pattern over North America and the western North Atlantic is beginning to amplify in association with strong warm (cold) air advection on the northwest (southeast) side of a strong surface high over the western U.S., as well as strong warm air advection over the Northeast in advance of an area of low pressure. This area of low pressure is collocated with the poleward exit region of a jet streak centered over the southeastern U.S. and an equatorward entrance region of a jet streak centered over eastern Canada.

3. At the end of the transition, the pattern over the North Atlantic has become blocked, with a highly amplified mid and upper-tropospheric ridge located just east of Greenland and a closed midtropospheric low just to the west of Portugal. Farther west, a high-latitude ridge has developed over western North America and a broad trough has formed over eastern North America.

4.3.2 Negative-to-Positive PNA Regime Transitions

Because negative-to-positive transitions of the PNA are associated with enhanced precipitation in the Northeast, and because the PNA index tends to increase surrounding major precipitation events in the Northeast, composite analyses were created for negative-to-positive PNA transitions with major precipitation events in the Northeast beginning at their midpoints. As was done to create composite analyses of positive-to-negative NAO regime transitions, five negative-to-positive PNA regime transitions with the greatest midtransition precipitation events (24-h events beginning at 1200 UTC on Day 4 of the seven-day transitions) were selected. A list of the dates of the five transitions used in the composite analyses and the precipitation amounts associated with the Northeast storms is shown in Table VII. The mean of the domain-average precipitation amounts associated with these five events is 1.6 cm, slightly less than the 2.0 cm mean of the domain-average precipitation amounts associated with the positive-to-negative NAO precipitation events. The average maximum precipitation amount associated with the negative-to-positive PNA regime transition precipitation events is 6.0 cm, also somewhat less than the 6.5 cm average maximum precipitation amount associated with the NAO regime transition precipitation events. One of these precipitation events, the event occurring at the midpoint of the negative-to-positive PNA transition beginning on 1 December 1990 is ranked #14 in the top 25 all-time 24-h cool-season events in the Northeast (Table I).

Composite analyses for Day 1 of the negative-to-positive PNA transitions having a midtransition storm are shown in Fig. 4.11. Similar to the pattern characteristic of the positive phase of the NAO (Fig. 4.4a), a relatively zonal pattern is evident from the eastern North Pacific to the central North Atlantic at 500 hPa (Fig. 4.11a). Despite the lack of amplified midtropospheric troughs or ridges over North America, in some regions, 500 hPa geopotential heights deviate noticeably from climatology. For instance, positive geopotential height anomalies in excess of +12 dam are located across the Northeast in association with a weak 500 hPa ridge, while negative geopotential heights anomalies in excess of −12 dam are centered over British Columbia in association with a weak 500 hPa trough.

At 300 hPa (Fig. 4.11b), the negative PNA pattern is also relatively zonal, with a jet streak stretching eastward along the northern edge of the ridge that is over the eastern U.S. Almost everywhere outside of eastern North America, winds at 300 hPa are below 35 m s^{-1} from the Dateline to the eastern North Atlantic, although a strong jet streak is located just west of the Dateline. Beneath the 500 and 300 hPa ridges over the eastern U.S., a surface high pressure system is centered just off the Mid-Atlantic coast, promoting dry weather over the Northeast (Fig. 4.11c). Farther west, a weak area of low pressure on the lee side of the Rockies is located just east of a midtropospheric trough (Fig. 4.11a).

By Day 2, the weak 500 hPa trough over the West has amplified somewhat, although the low 500 hPa geopotential heights associated with the trough do not deviate appreciably from climatology (Fig. 4.12a). The northern extension of the 500 hPa trough over Alberta and British Columbia is, on the other hand, associated with negative geopotential height anomalies in excess of −12 dam. Farther east, the Northeast remains under the influence of a weak ridge at both 500 hPa (Fig. 4.12a) and 300 hPa (Fig. 4.12b).

At the surface (Fig. 4.12c), high pressure off the Eastern Seaboard continues to influence the Northeast and the rest of the eastern U.S. The closed low just to the lee of the Rockies at Day 1 has disappeared, leaving a weak area of relatively low pressure between high pressure centered off the eastern U.S. coast and high pressure centered just off the southwestern coast of the U.S.

The 500 hPa pattern on Day 3 of the negative-to-positive PNA regime transition (Fig. 4.13a) shows that the weak trough located just east of the Rockies on Day 2 has strengthened and moved into the central Plains. The pattern has also amplified farther to the west as a 500 hPa ridge builds over southern California. Across the eastern U.S., the ridge that was centered over the Northeast on Day 1 and Day 2 has remained nearly stationary. This stationary ridge over the Northeast might help to explain the deepening of the trough east of the Rockies by Day 3; the pattern may be forced to "buckle" due to the impediment of eastward movement by the stationary ridge over the Northeast.

At 300 hPa (Fig. 4.13b), the jet streak located along the northern edge of the ridge over the eastern U.S. has strengthened and now contains wind speeds of 45 m s^{-1}. A weak wind maximum has also developed on the west side of the amplifying trough over the Plains. At the surface (Fig. 4.13c), a closed area of low pressure has regenerated just in advance of the trough at 500 hPa (Fig. 4.13a) and 300 hPa (Fig. 4.13b). Some warm air advection and slight cyclonic vorticity advection by the thermal wind, implied in Fig. 4.13c, are likely contributing to QG forcing for ascent over the Missouri Valley and toward the western Great Lakes. Farther west, strong warm air advection is acting to build the 1000–500 hPa thickness ridge over the west coast of Canada. The amplification of the ridge in this area over the next few days will prove to be critical in the development of a positive PNA pattern.

By Day 4, the day when a 24-h period of significant precipitation begins in the Northeast, the ridge located over the Northeast on Day 3 has moved slightly eastward and has amplified (compare Figs. 4.14a,b with their counterparts in Figs. 4.13a,b). Figure 4.14 shows that maximum geopotential height anomalies associated with the ridge at 500 hPa are in excess of +18 dam. The 500 hPa trough located over the Plains on the previous day has edged slightly farther east while maintaining its strength.

At 300 hPa (Fig. 4.14b), the persistent jet streak over eastern Canada on the north side of the ridge near the East Coast has become more anticylonically curved by Day 4, while a new jet streak has formed over the Southeast on the east side of the trough over the Midwest. As a result, the Northeast appears to be located beneath the poleward exit region of the jet streak centered over the Southeast, and beneath the equatorward entrance region of the jet streak centered over eastern Canada. Conditions are favorable for surface cyclogenesis in the Northeast, since this region appears to be influenced by strong upper-tropospheric dynamical forcing. As anticipated, Fig. 4.14c shows that a surface low pressure center is indeed located between the equatorward jet entrance region and poleward jet exit region over the Northeast.

Strong warm air advection on Day 4 indicated in Fig 4.14c is likely producing significant QG forcing for ascent over the Northeast while geostrophic onshore flow at the surface in advance of the cyclone provides an influx of moisture into the Northeast. In addition, northern portions of the Northeast are experiencing weak QG forcing for upward motion. The main area of strong warm air advection observed over British Columbia on Day 3 has now shifted east somewhat, but still appears to be contributing to the amplification of the 1000–500 hPa thickness ridge over western Canada.

On Day 5, the day marking the end of the 24-h precipitation event in the Northeast, the 500 hPa ridge across western North America has become more amplified (Fig. 4.15a). Across the East, a broad, rather weak trough is present in association with a surge of cold air over the Northeast in the wake of exiting a surface low pressure system (Fig. 4.15c).

At 300 hPa (Fig. 4.15b), a jet streak is located on the east side of a weak short-wave trough exiting the Northeast and is the only apparent jet streak affecting the U.S. As the short-wave trough at 300 hPa exits the Northeast, a second very weak short-wave trough has developed just east of the northern High Plains. When this weak short-wave trough enters the broader, longer wave trough over the eastern U.S. over the next few days, the short-wave trough can be expected to deepen. Cyclogenesis present in the Gulf of Alaska appears to be linked to the poleward-exit region of a potent 300 hPa jet streak just west of the Dateline in the North Pacific that has steadily moved eastward throughout the period (Fig. 4.15b).

On Day 6 (Fig. 4.16), likely a result of downstream development, the pattern over North America has amplified, with negative geopotential height anomalies in excess of −6 dam at 500 hPa associated with a trough centered over the Midwest (Fig. 4.16a). In addition to the amplification of the trough across the central and eastern U.S., the ridge at 500 hPa has amplified from Day 5 to Day 6, with a large area of +12 dam geopotential height anomalies located over the Pacific Northwest and British Columbia at the latter time.

At 300 hPa (Fig. 4.16b), a jet streak remains over the Northeast, but a new jet streak has developed on the western side of the Midwest trough as this trough and the upstream ridge continue to amplify. In association with the Midwest trough, a weak surface low with little accompanying warm air advection is located over the Great Lakes (Fig. 4.16c). Across western North America, strong warm air advection continues to contribute to the amplification of the ridge along the western Canadian coastline and thus to the development of a positive PNA regime.

On Day 7 (Fig. 4.17), the last day of the transition of the pattern from negative to positive PNA, the 500 hPa composite analysis (Fig. 4.17a) shows that a classic positive PNA pattern has been established, with a deeper mid and upper-tropospheric trough replacing the weaker trough associated with the mid-transition precipitation event in the Northeast (Fig. 4.14a). Upstream of the trough, a strong ridge remains in place over western North America, while downstream of the trough, a split-flow pattern has developed at both 500 hPa (Fig. 4.17a) and 300 hPa (Fig. 4.17b) in association with a developing ridge over the North Atlantic. This eastward amplification of the 300 hPa and 500 hPa pattern from Day 5 to Day 7 appears suggestive of downstream development associated with a Rossby wave packet.

At 300 hPa, the jet streak located over the Northeast on Day 6 has strengthened and become more meridionally oriented by Day 7, extending from the Southeast coast northeastward to Newfoundland (4.17b). The jet streak that was located over the northern High Plains on Day 6 has remained in the same location, though it has weakened somewhat. Cold air advection associated with a weak clipper-like low pressure system near Lake Ontario (Fig. 4.17c) has allowed a second surge of cold air to become established over the Northeast, thus completing the transition to a positive PNA pattern. The location of the clipper low suggests that it is forced primarily by the 500 hPa and 300 hPa troughs just to the west rather than by the secondary circulation associated with the jet streak at 300 hPa, since it is not located underneath a poleward exit region or an equatorward entrance region of a jet streak

A summary of the composite transition from a negative to positive PNA regime associated with a midtransition major precipitation event in the Northeast follows below:

1. As is the case during positive-to-negative NAO transitions, a surface low pressure system over the Northeast associated with a major midtransition

precipitation event is linked to the poleward exit region of a jet streak centered over the southeastern U.S. and the equatorward entrance region of a jet centered over eastern Canada.

2. Two separate processes appear to bring about the transition of the pattern from a negative PNA to positive PNA regime. First, persistent warm air advection acts to amplify the ridge over western North America. Second, a cold surge in the wake of the midtransition Northeast precipitation event appears to precondition the atmosphere for a second, stronger cold surge in the East at the end of the transition period.

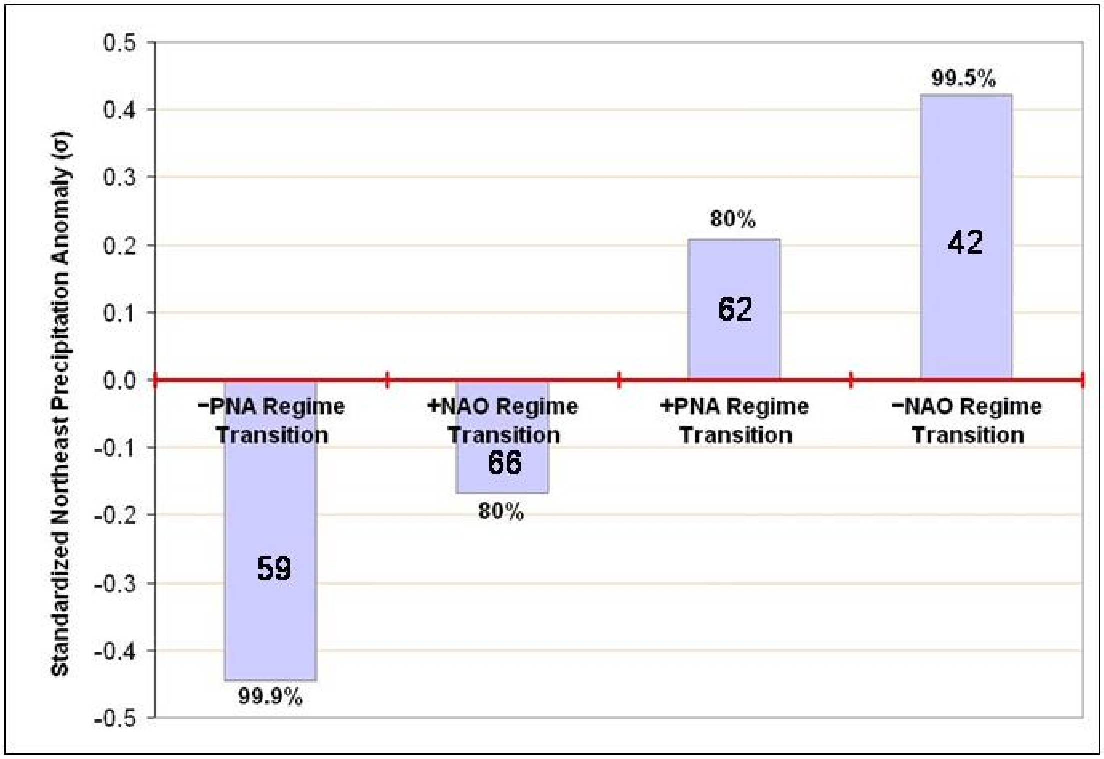

Fig. 4.1. Composite standardized cool-season Northeast precipitation anomalies during large-scale regime transitions. Percentages above and below bars indicate statistical significance of precipitation anomalies as determined by a two-tailed t-test; the number of independent events in each category is shown inside the bars.

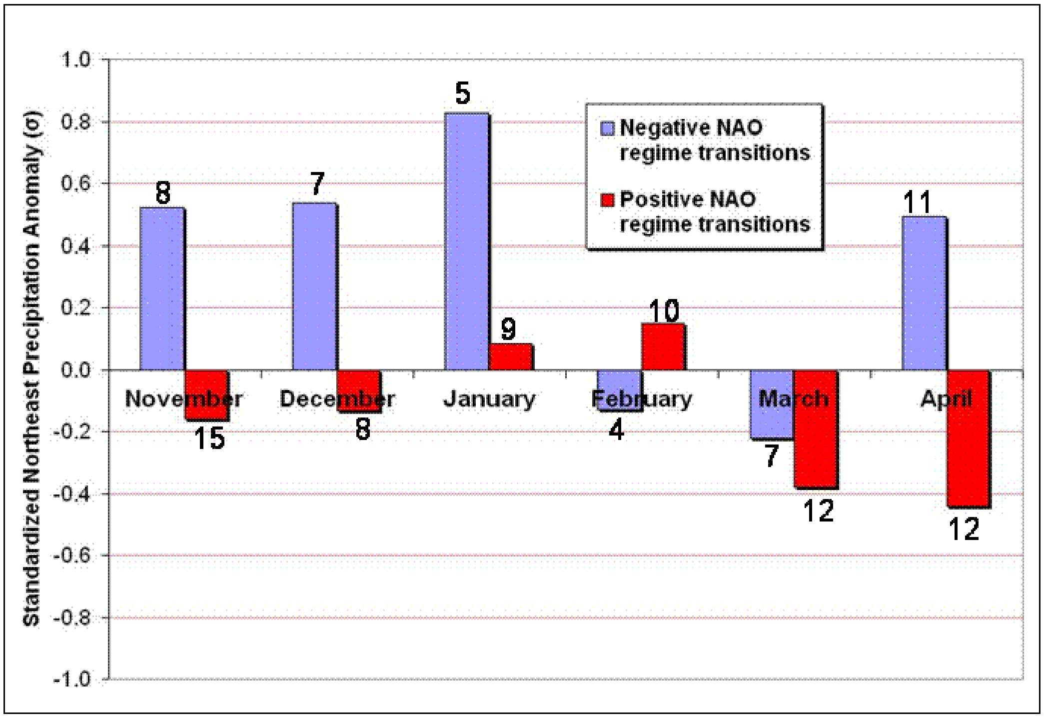

Fig. 4.2a. Composite standardized cool-season Northeast precipitation anomalies during large-scale NAO regime transitions by month. The number of independent events occurring in each month is shown above and below the bars.

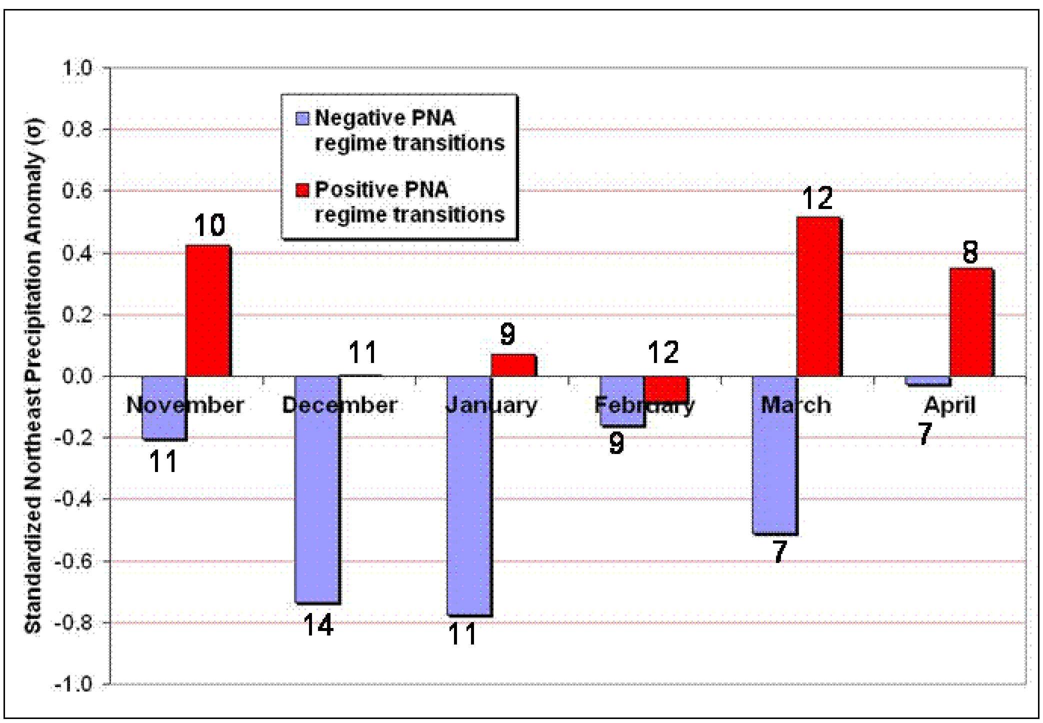

Fig. 4.2b. Same as in Fig. 4.2a, except for PNA regime transitions.

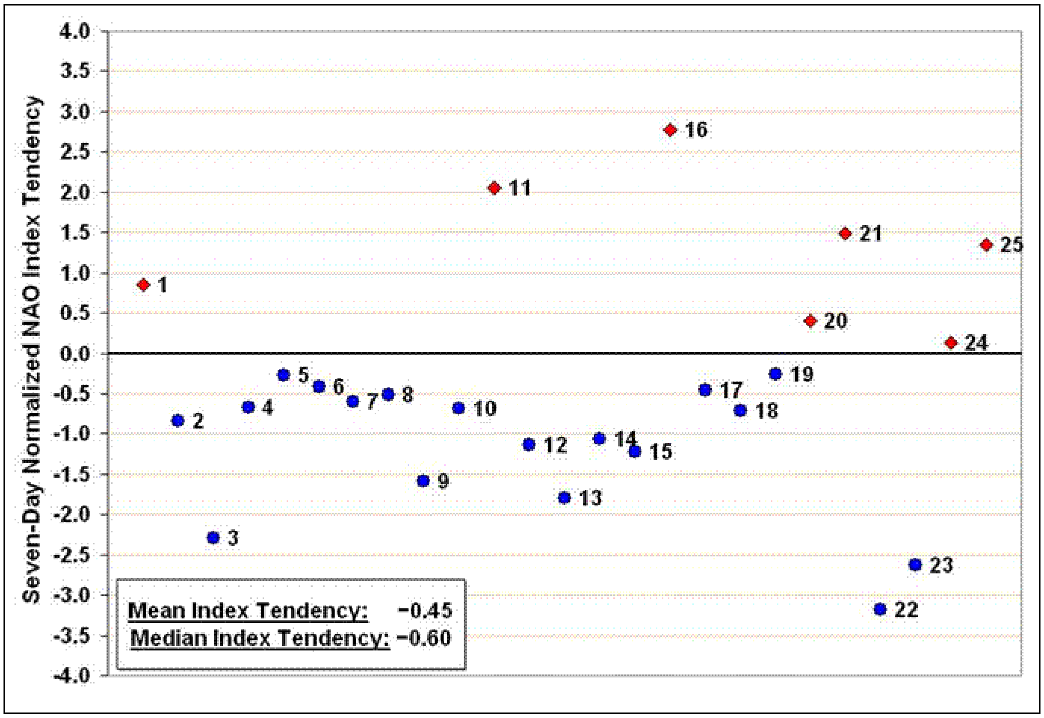

Fig. 4.3a. Normalized seven-day NAO index tendencies centered on the top 25 24-h cool-season precipitation events in the Northeast. Numbers to the right of the points indicate the rank of the precipitation events.

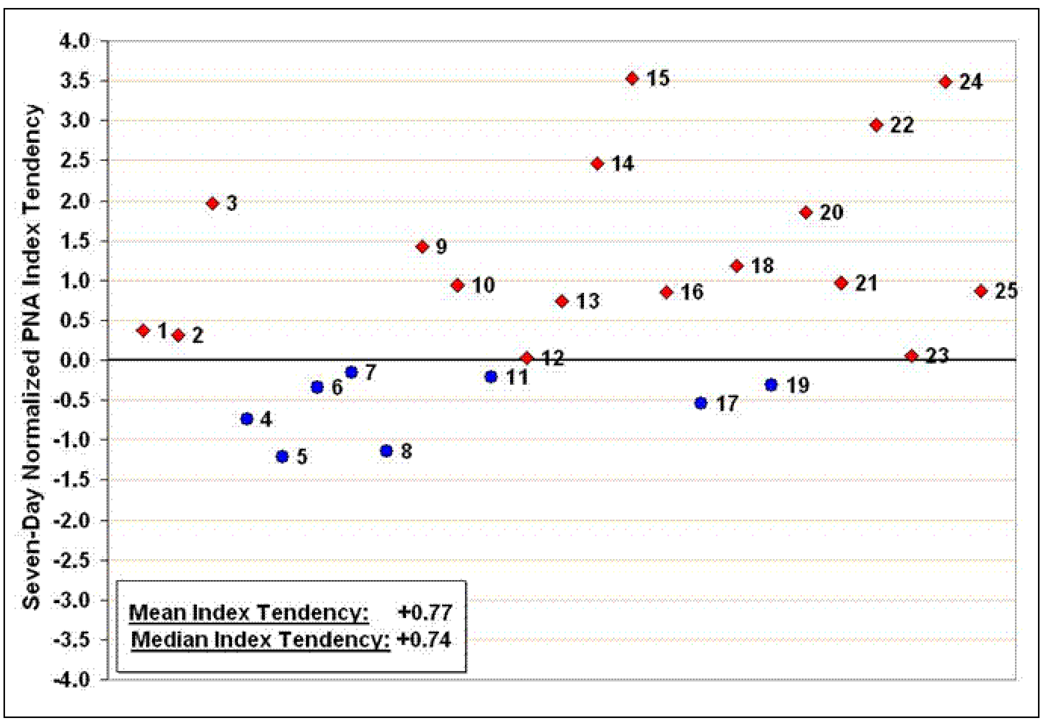

Fig. 4.3b. Same as in Fig. 4.3a, except for seven-day PNA index tendencies.

	Date/*NAO Index* Day 1	Day 7	24-h Northeast Precipitation (mm) 1200 UTC Day 4–1200 UTC Day 5 Mean	Max
1.	11/6/1996/ *+1.1*	11/12/1996/ *−1.2*	30.4	99.0
2.	11/27/1963/ *+1.5*	12/3/1963/ *−1.7*	24.1	70.5
3.	1/16/1996/ *+1.3*	1/22/1996/ *−1.3*	15.6	67.7
4.	4/2/1973/ *+1.1*	4/8/1973/ *−2.0*	14.7	40.6
5.	2/21/1975/ *+1.1*	2/27/1975/ *−1.5*	14.5	48.7

TABLE VI. Dates, mean and maximum Northeast precipitation amounts (mm), and NAO index values for the top five cool-season precipitation events in the Northeast beginning at the midpoint of seven-day positive-to-negative NAO regime transitions.

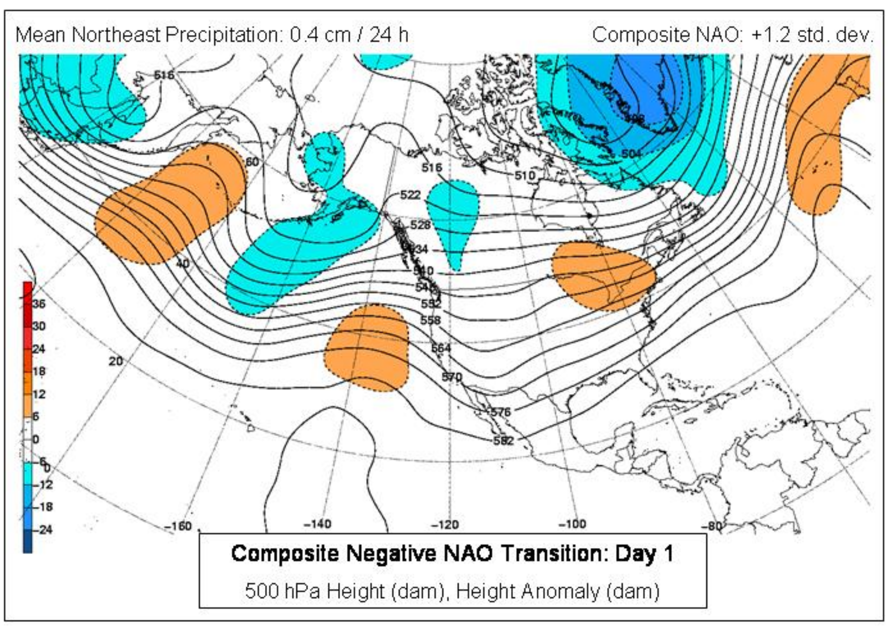

Fig. 4.4a. Composite 500 hPa geopotential heights (dam) and anomalies (dam) corresponding to Day 1 of the top five cool-season precipitation events in the Northeast associated with positive-to-negative NAO regime transitions. Geopotential heights are contoured every 6 dam; anomalies are contoured every 6 dam and are shaded as indicated.

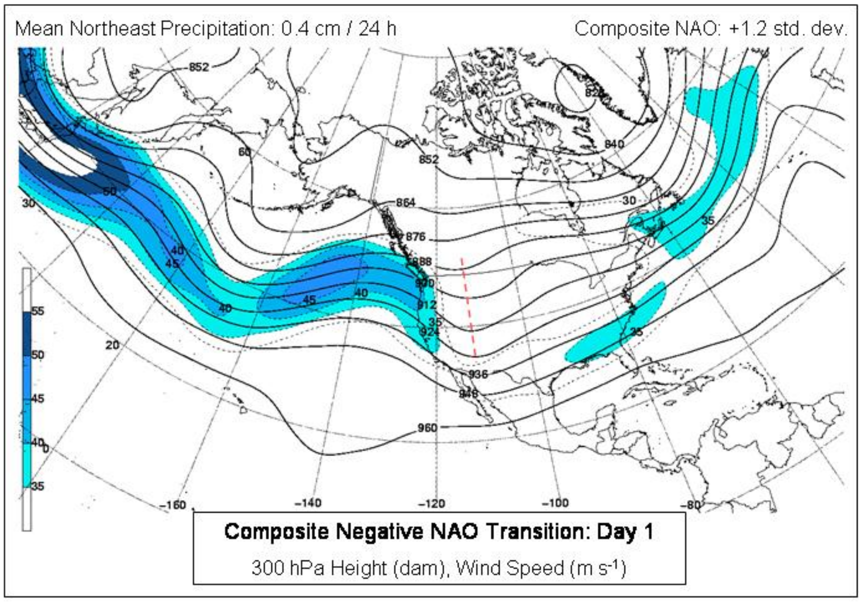

Fig. 4.4b. Composite 300 hPa geopotential heights (dam) and wind speed (m s^{-1}) corresponding to Day 1 of the top five cool-season precipitation events in the Northeast associated with positive-to-negative NAO regime transitions. Geopotential heights are contoured every 12 dam. Wind speed is contoured every 5 m s^{-1} starting at 30 m s^{-1}; shading begins at 35 m s^{-1}.

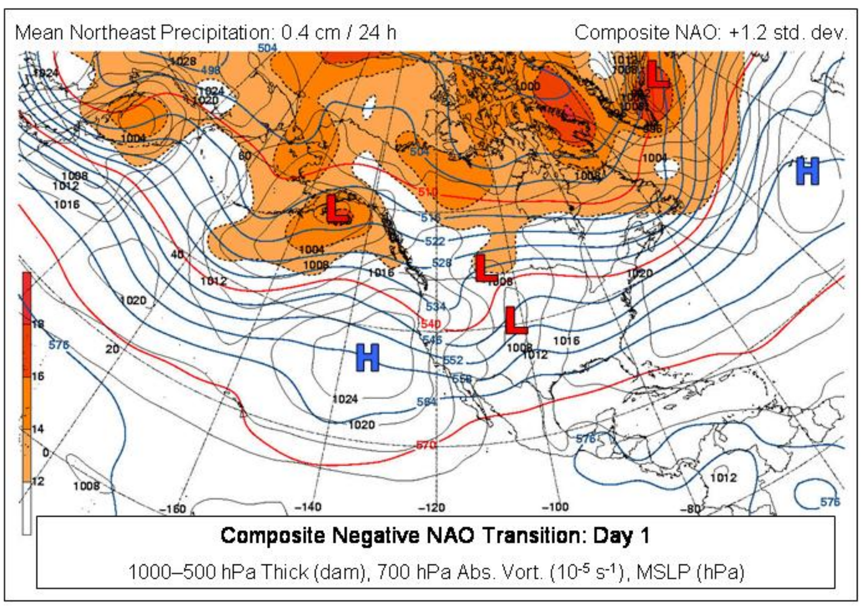

Fig. 4.4c. Composite 1000–500 hPa thickness (dam), 700 hPa absolute vorticity (10^{-5} s^{-1}), and sea level pressure (hPa) corresponding to Day 1 of the top five cool-season precipitation events in the Northeast associated with positive-to-negative NAO regime transitions. Thickness is contoured every 6 dam in blue, except for the 510 dam, 540 dam, and 570 dam thickness contours, which are red. Sea level pressure is contoured every 4 hPa in black. Absolute vorticity is contoured in intervals of 2 x 10^{-5} s^{-1}; shading begins at 12 x 10^{-5} s^{-1}.

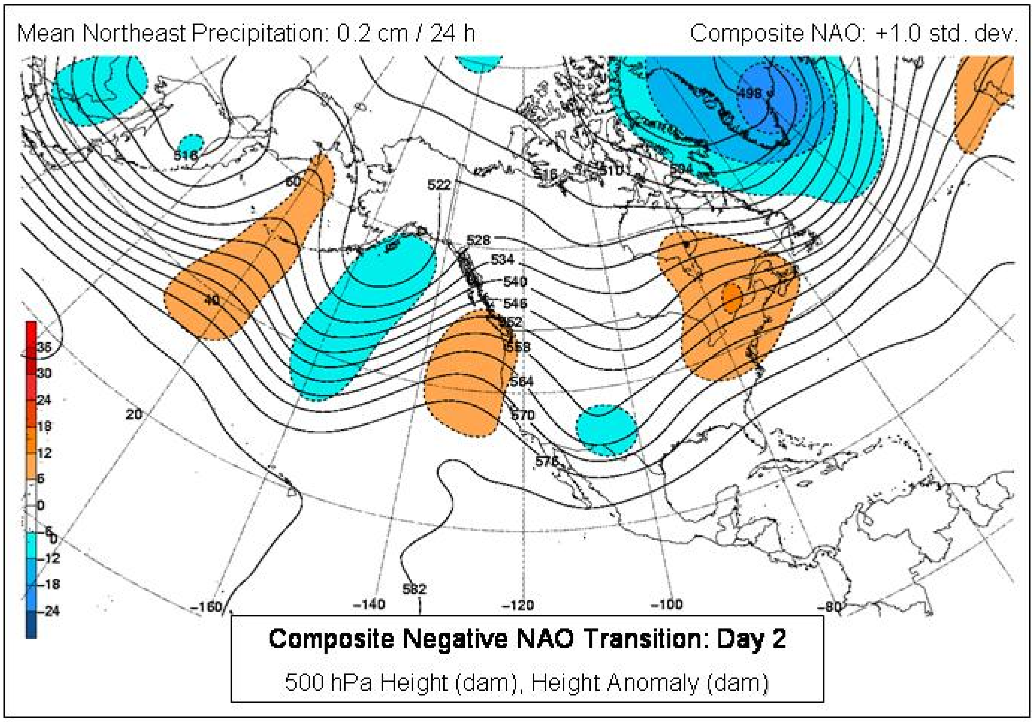

Fig. 4.5a. Same as in Fig. 4.4a, except for Day 2 of a seven-day positive-to-negative NAO regime transition.

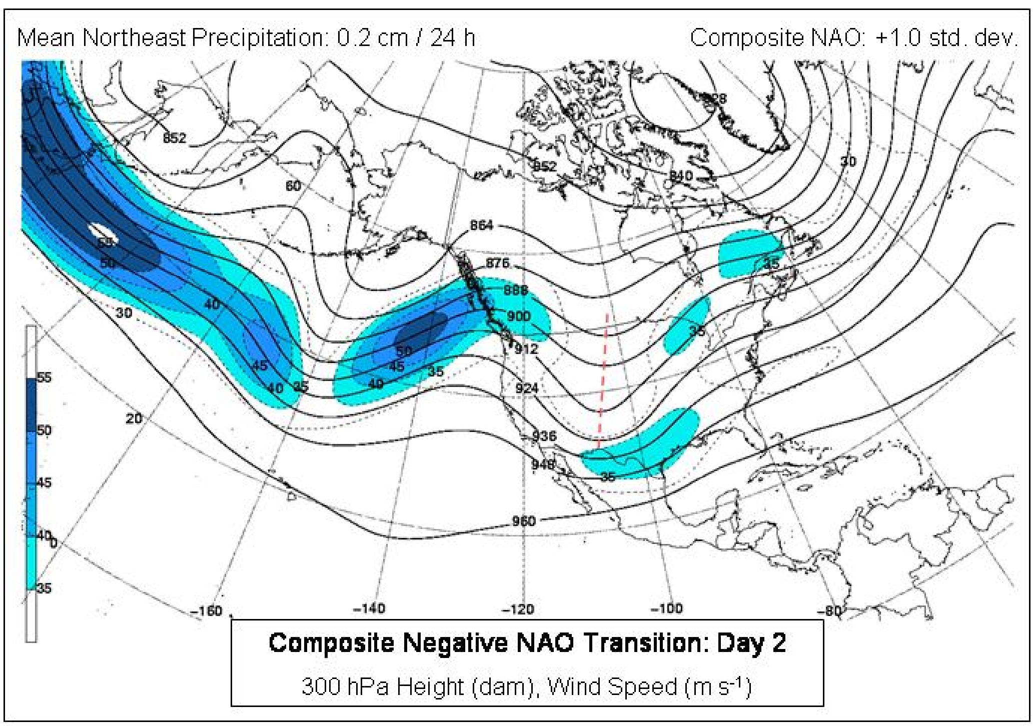

Fig. 4.5b. Same as in Fig. 4.4b, except for Day 2 of a seven-day positive-to-negative NAO regime transition.

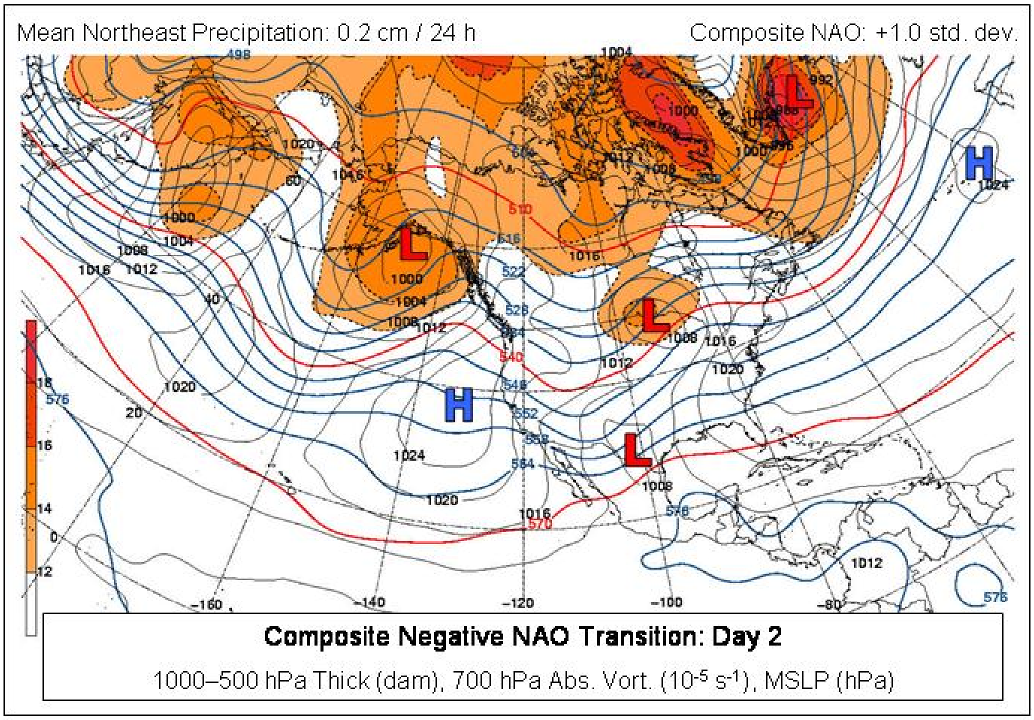

Fig. 4.5c. Same as in Fig. 4.4c, except for Day 2 of a seven-day positive-to-negative NAO regime transition.

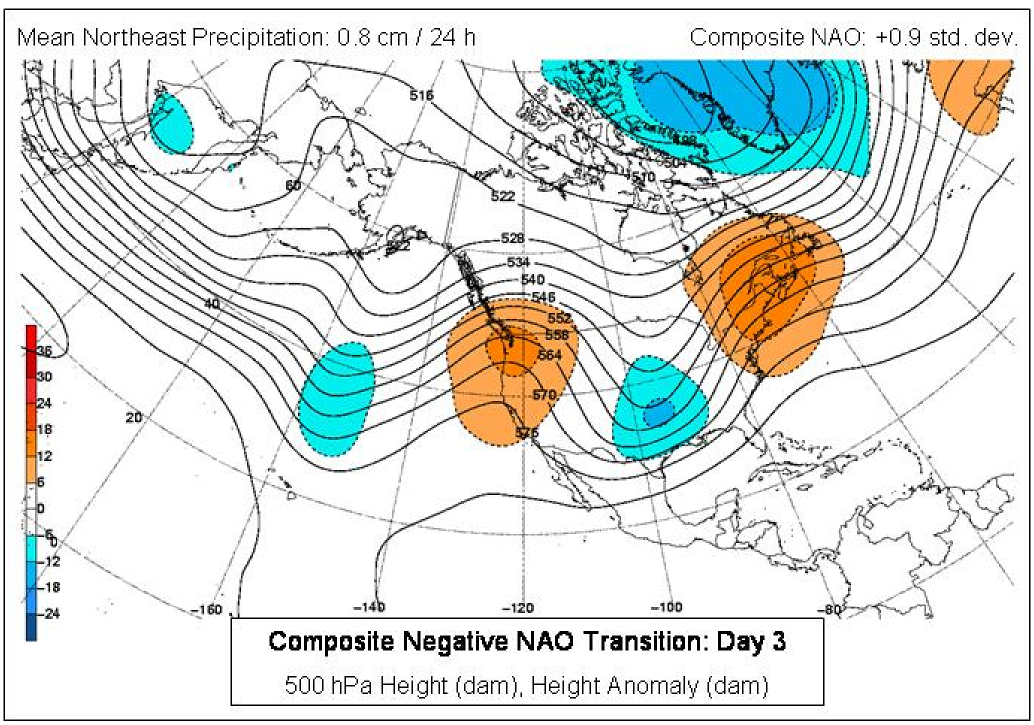

Fig. 4.6a. Same as in Fig. 4.4a, except for Day 3 of a seven-day positive-to-negative NAO regime transition.

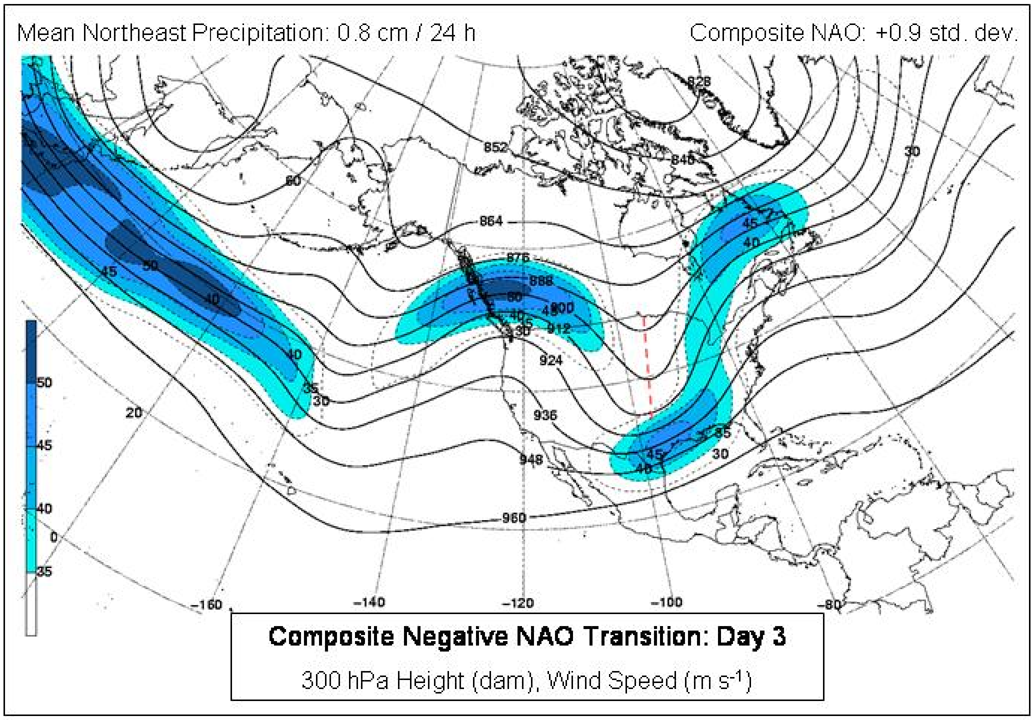

Fig. 4.6b. Same as in Fig. 4.4b, except for Day 3 of a seven-day positive-to-negative NAO regime transition.

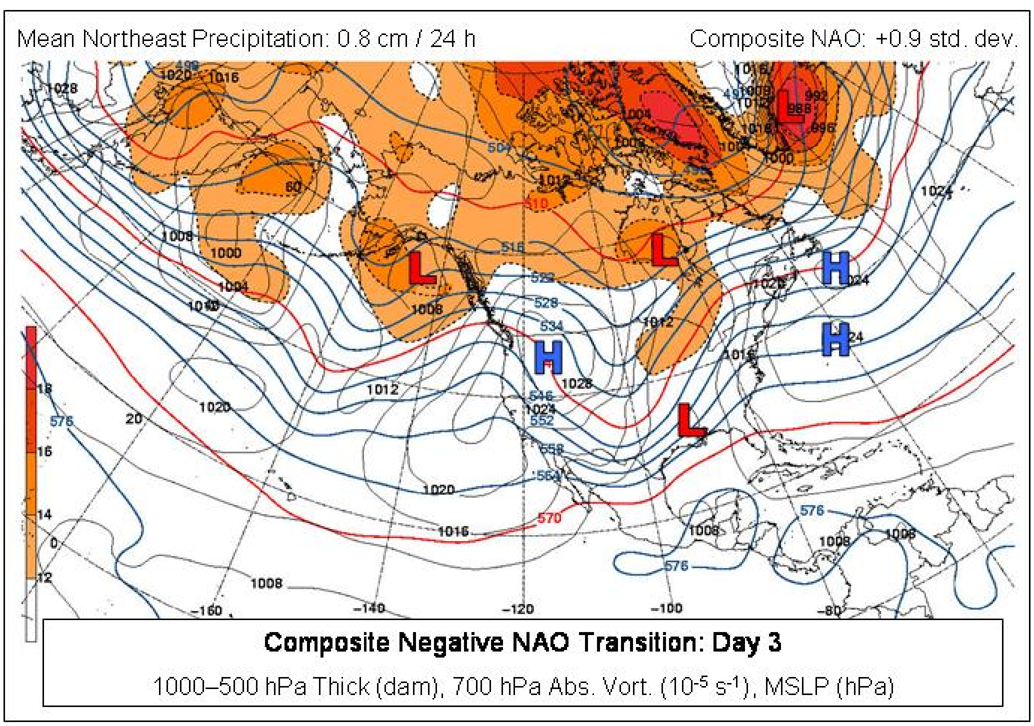

Fig. 4.6c. Same as in Fig. 4.4c, except for Day 3 of a seven-day positive-to-negative NAO regime transition.

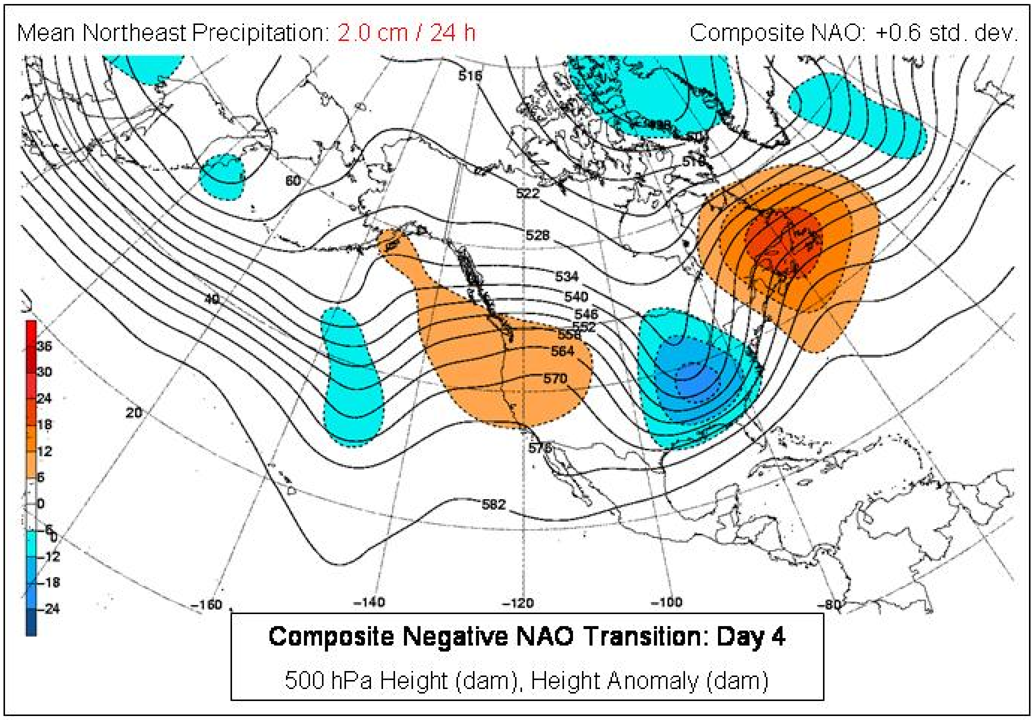

Fig. 4.7a. Same as in Fig. 4.4a, except for Day 4 (day of major Northeast precipitation event) of a seven-day positive-to-negative NAO regime transition.

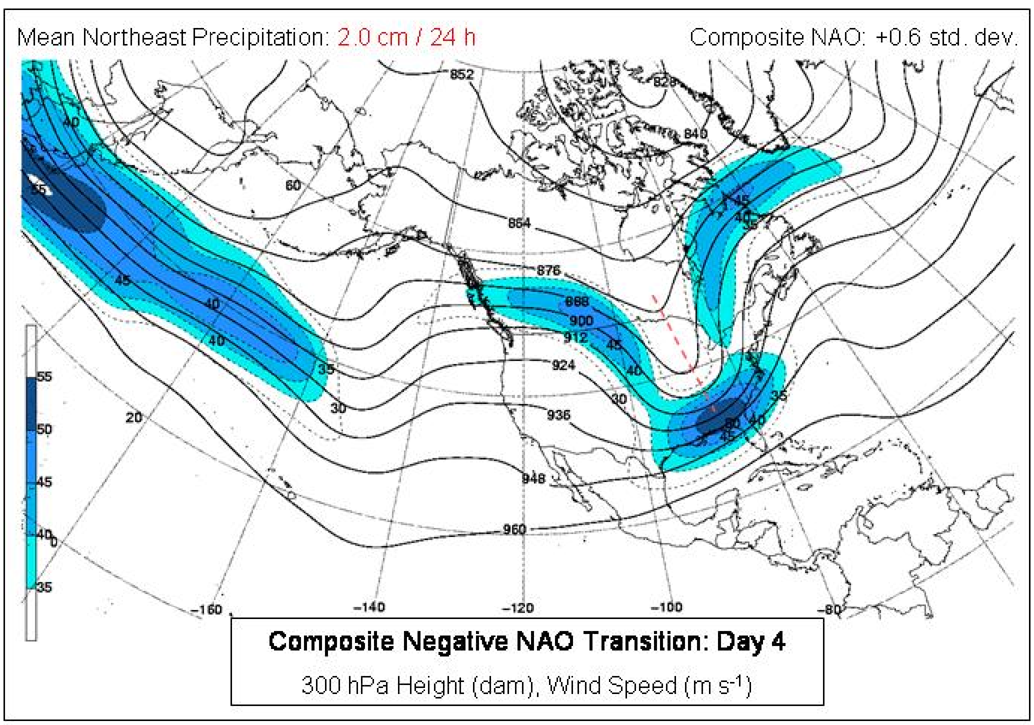

Fig. 4.7b. Same as in Fig. 4.4b, except for Day 4 (day of major Northeast precipitation event) of a seven-day positive-to-negative NAO regime transition.

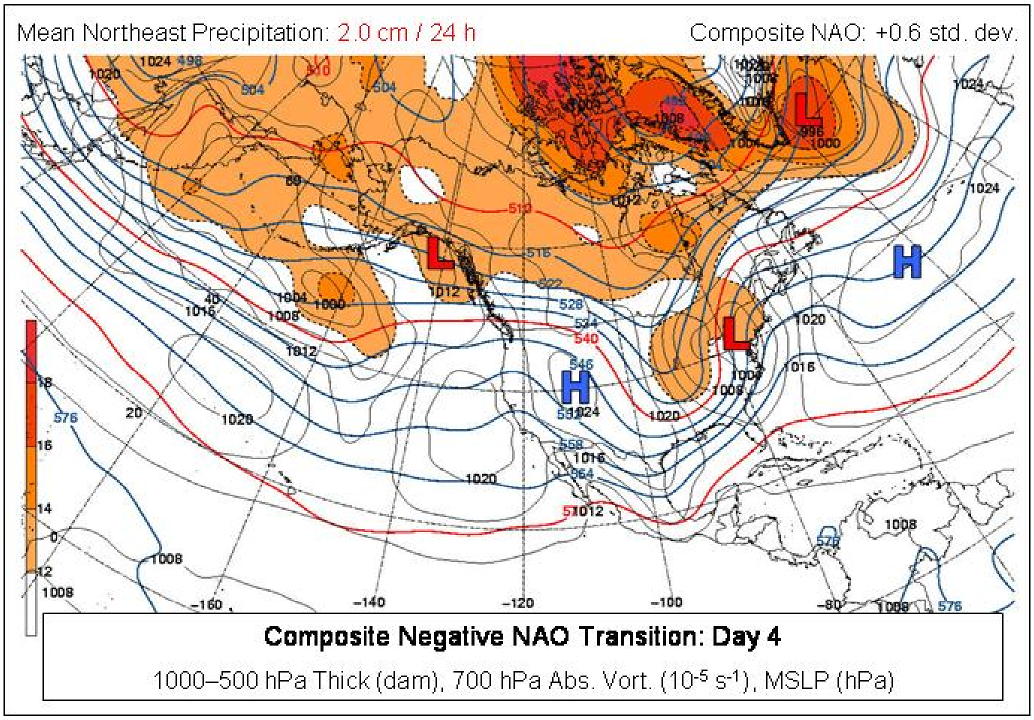

Fig. 4.7c. Same as in Fig. 4.4c, except for Day 4 (day of major Northeast precipitation event) of a seven-day positive-to-negative NAO regime transition.

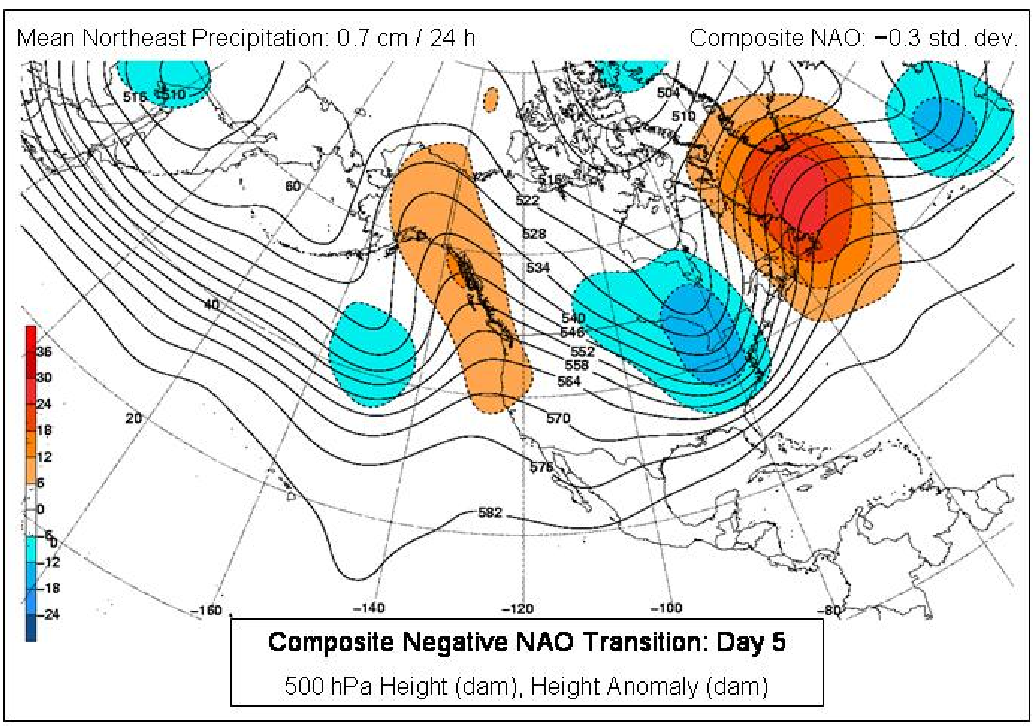

Fig. 4.8a. Same as in Fig. 4.4a, except for Day 5 of a seven-day positive-to-negative NAO regime transition.

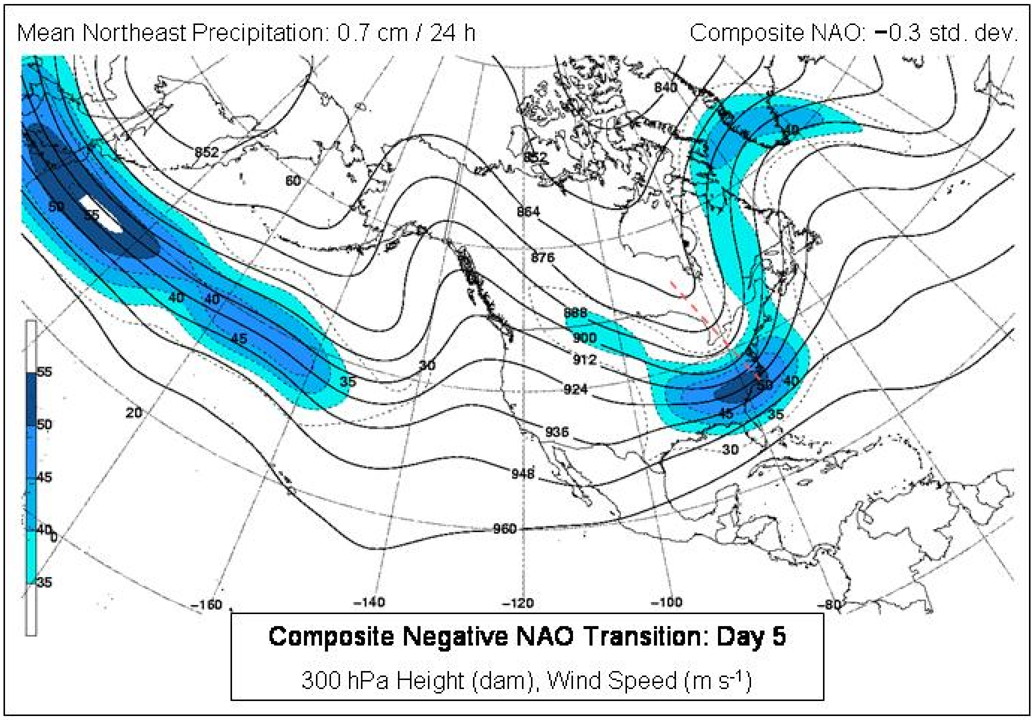

Fig. 4.8b. Same as in Fig. 4.4b, except for Day 5 of a seven-day positive-to-negative NAO regime transition.

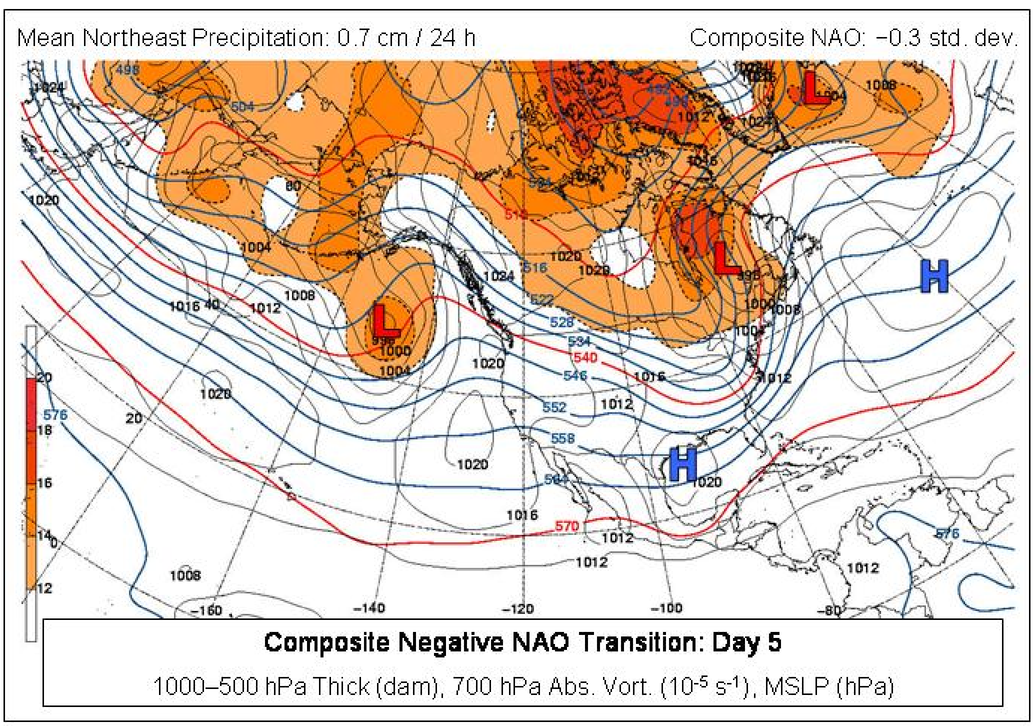

Fig. 4.8c. Same as in Fig. 4.4c, except for Day 5 of a seven-day positive-to-negative NAO regime transition.

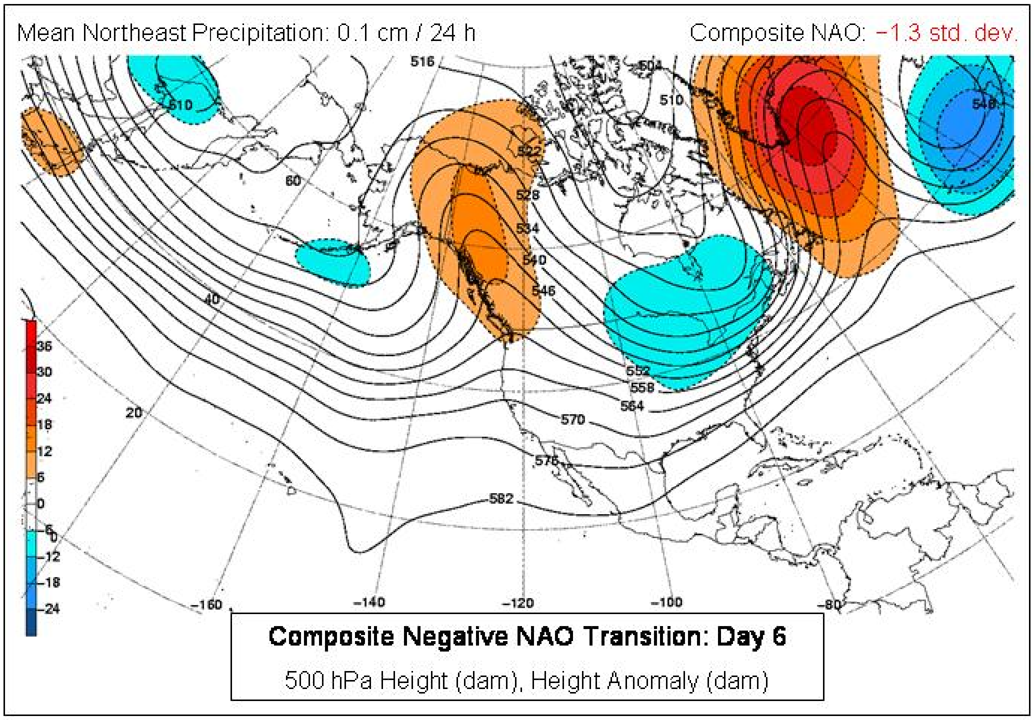

Fig. 4.9a. Same as in Fig. 4.4a, except for Day 6 of a seven-day positive-to-negative NAO regime transition.

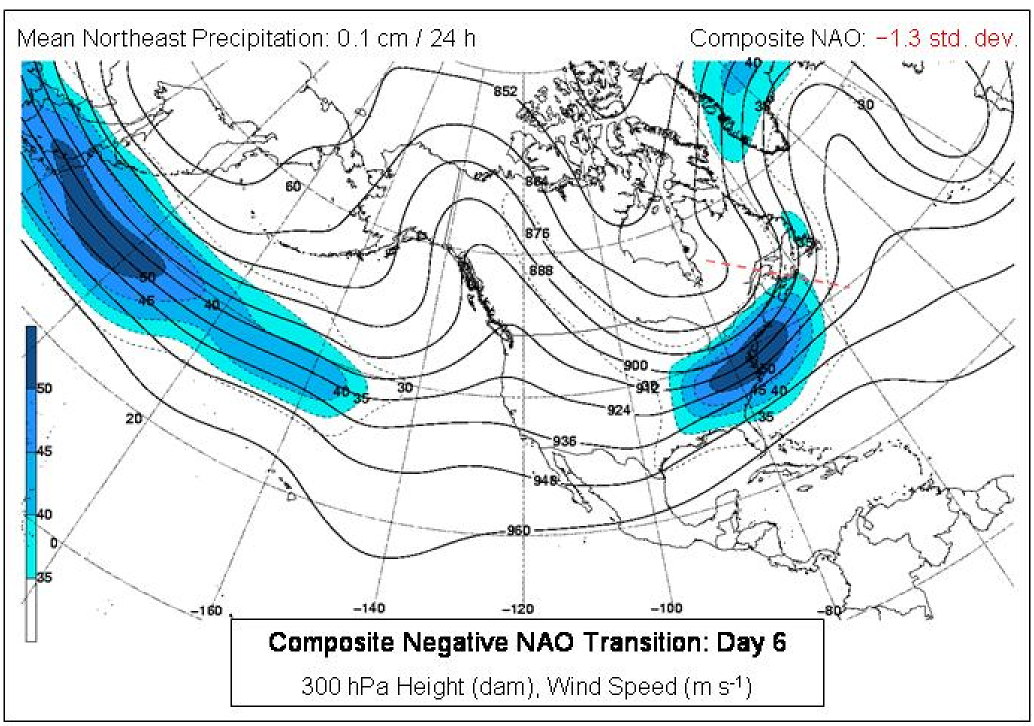

Fig. 4.9b. Same as in Fig. 4.4b, except for Day 6 of a seven-day positive-to-negative NAO regime transition.

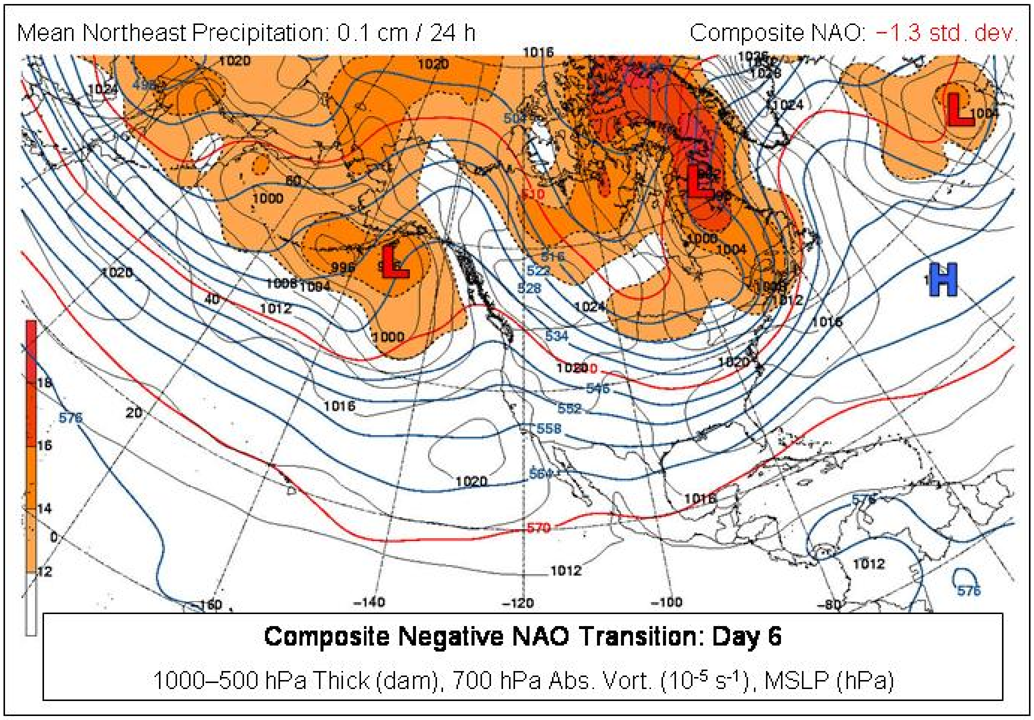

Fig. 4.9c. Same as in Fig. 4.4c, except for Day 6 of a seven-day positive-to-negative NAO regime transition.

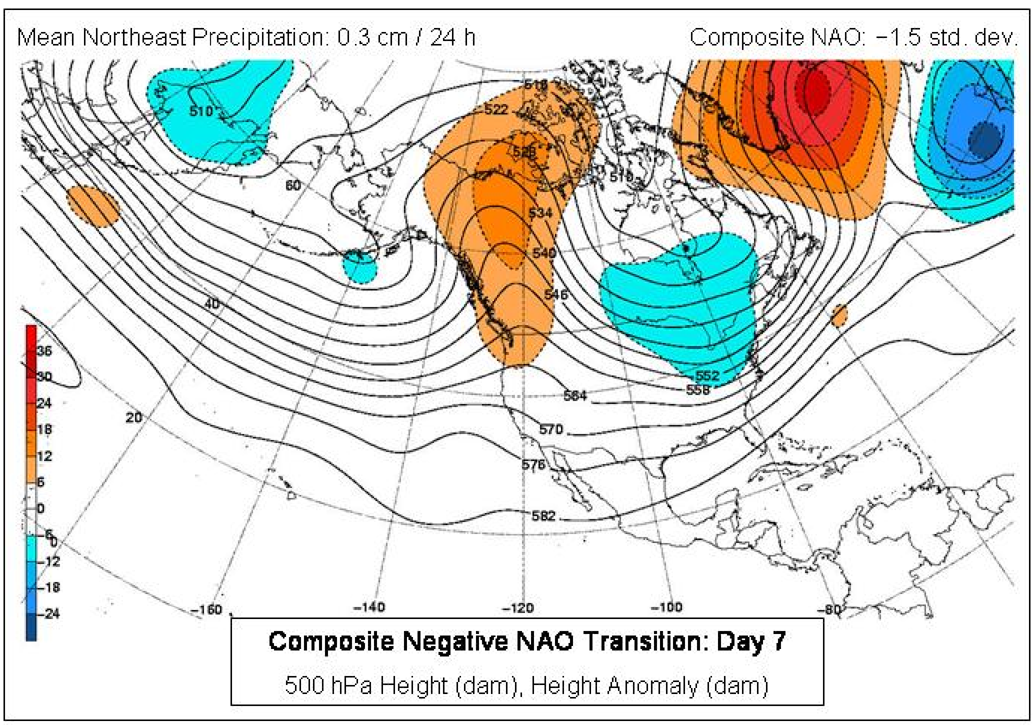

Fig. 4.10a. Same as in Fig. 4.4a, except for Day 7 of a seven-day positive-to-negative NAO regime transition.

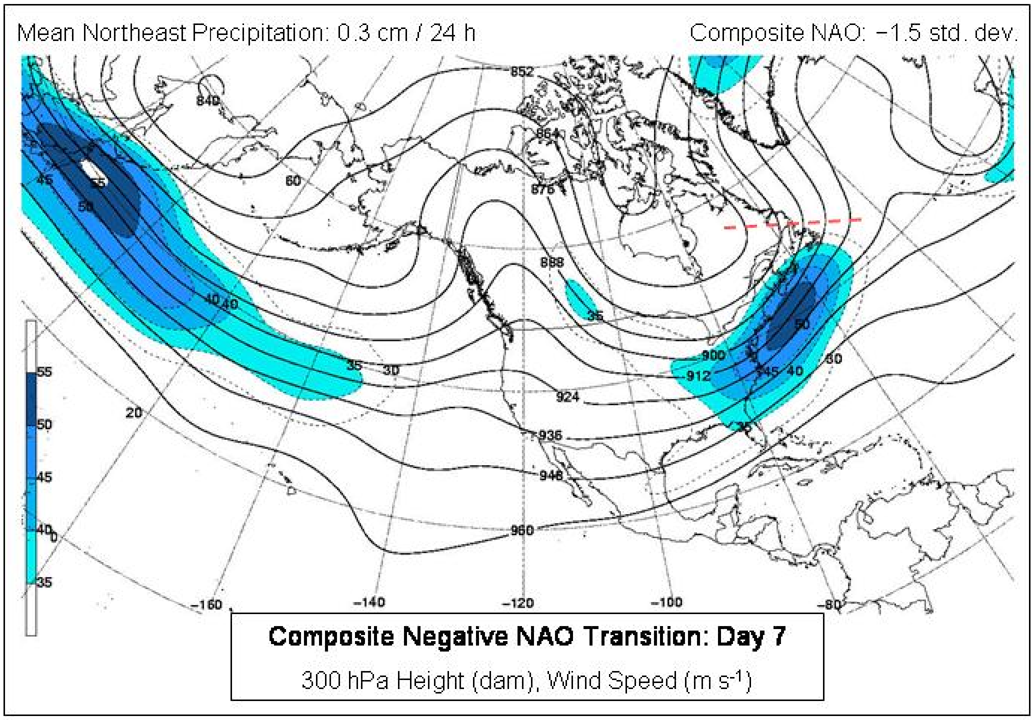

Fig. 4.10b. Same as in Fig. 4.4b, except for Day 7 of a seven-day positive-to-negative NAO regime transition.

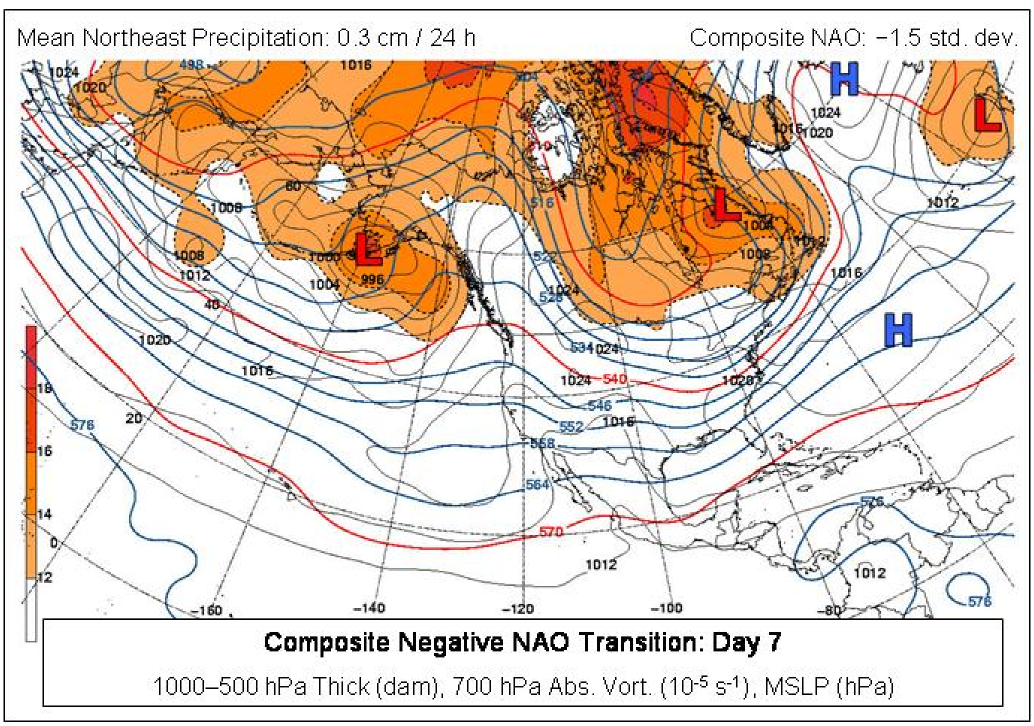

Fig. 4.10c. Same as in Fig. 4.4c, except for Day 7 of a seven-day positive-to-negative NAO regime transition.

	Date/*PNA Index* Day 1	Day 7	Northeast 24-h Precipitation (mm) 1200 UTC Day 4–1200 UTC Day 5 Mean	Max
1.	12/1/1990/ *−1.0*	12/7/1990/ *+1.4*	26.9	77.3
2.	12/14/2000/ *−1.4*	12/20/2000/ *+1.4*	20.2	62.9
3.	2/24/1957/ *−1.3*	3/2/1957/ *+1.5*	12.0	32.1
4.	11 Jan 1976/ *−1.4*	17 Jan 1976/ *+1.2*	11.2	54.3
5.	20 Apr 1977/ *−1.5*	26 Apr 1977/ *+1.6*	11.0	74.1

TABLE VII. Same as in TABLE VI, but for the top five cool-season precipitation events in the Northeast beginning at the midpoint of seven-day negative-to-positive PNA regime transitions.

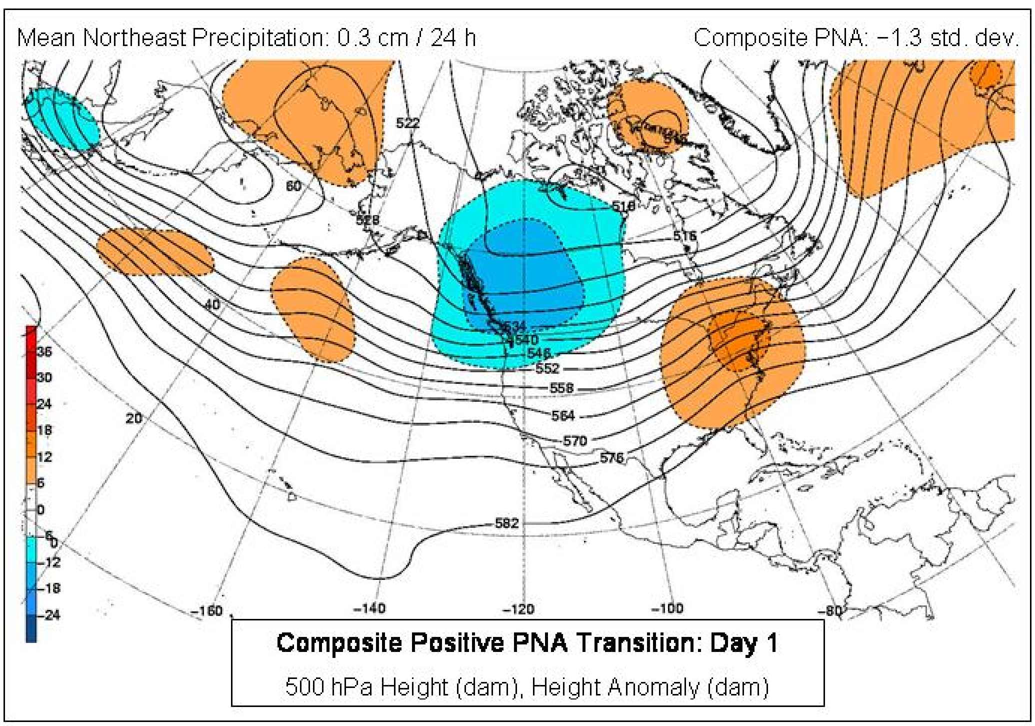

Fig. 4.11a. Same as in Fig. 4.4a, except for Day 1 of a seven-day negative-to-positive PNA regime transition.

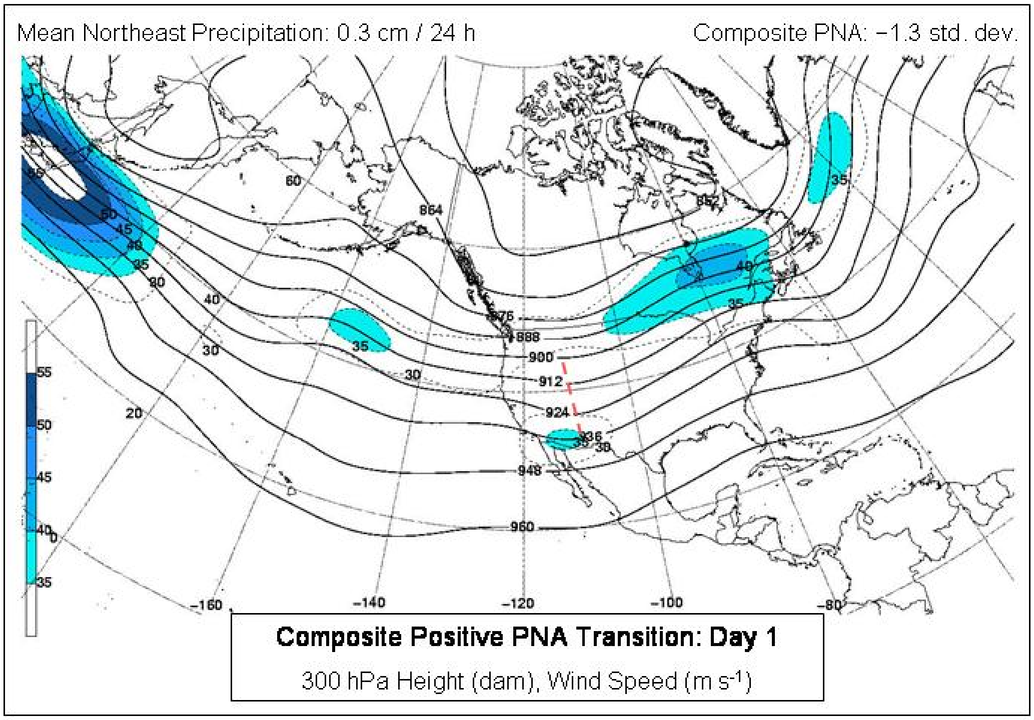

Fig. 4.11b. Same as in Fig. 4.4b, except for Day 1 of a seven-day negative-to-positive PNA regime transition.

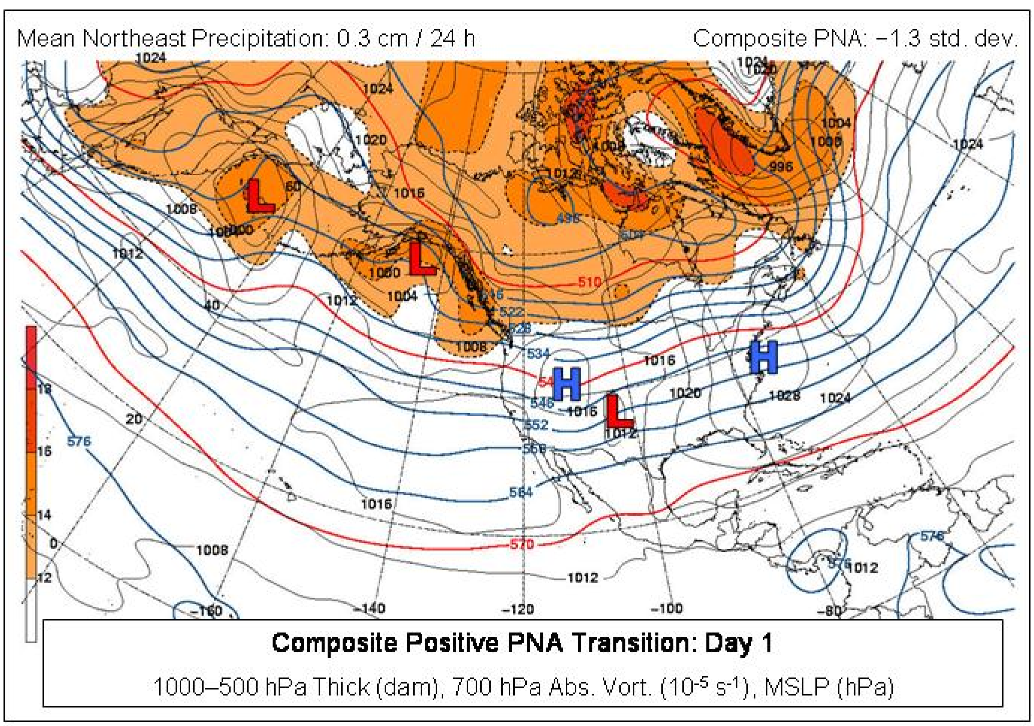

Fig. 4.11c. Same as in Fig. 4.4c, except for Day 1 of a seven-day negative-to-positive PNA regime transition.

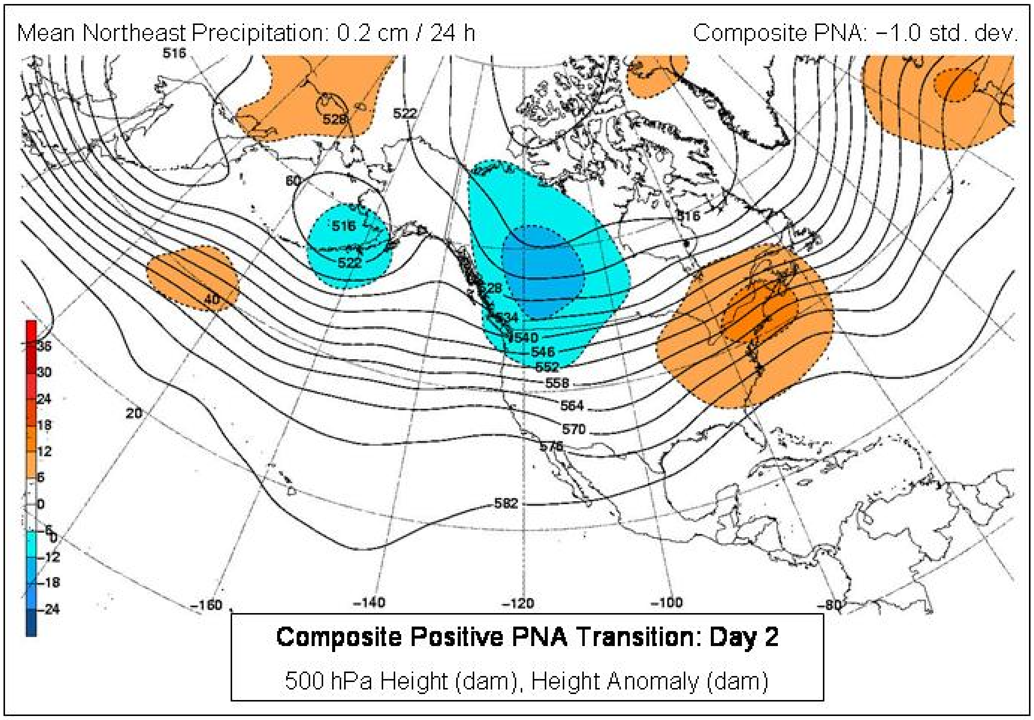

Fig. 4.12a. Same as in Fig. 4.4a, except for Day 2 of a seven-day negative-to-positive PNA regime transition.

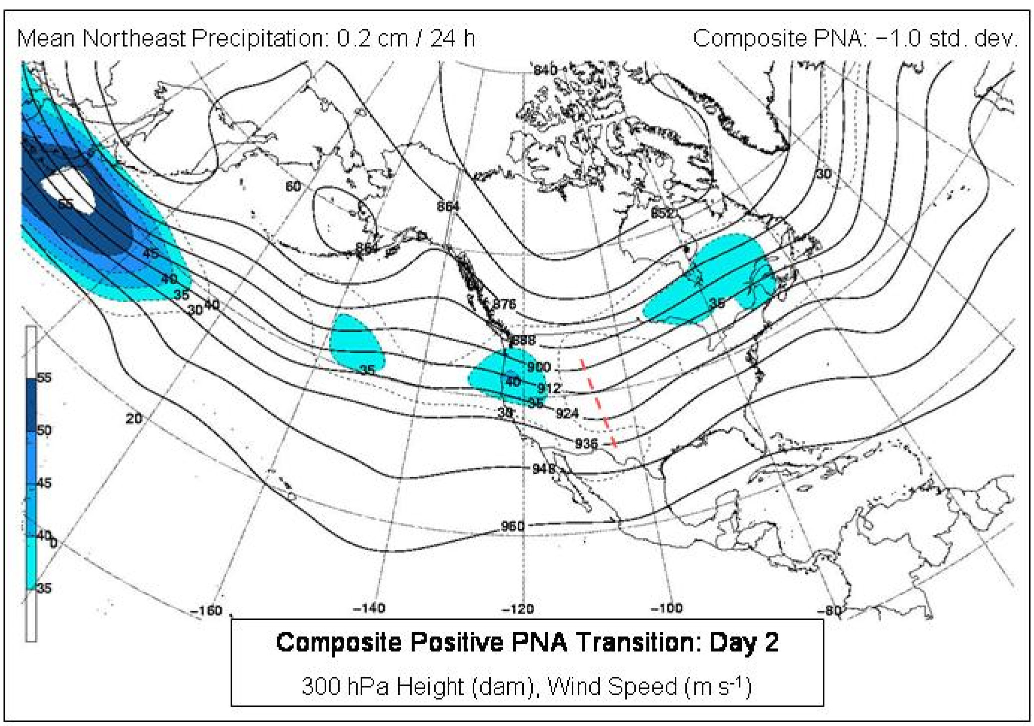

Fig. 4.12b. Same as in Fig. 4.4b, except for Day 2 of a seven-day negative-to-positive PNA regime transition.

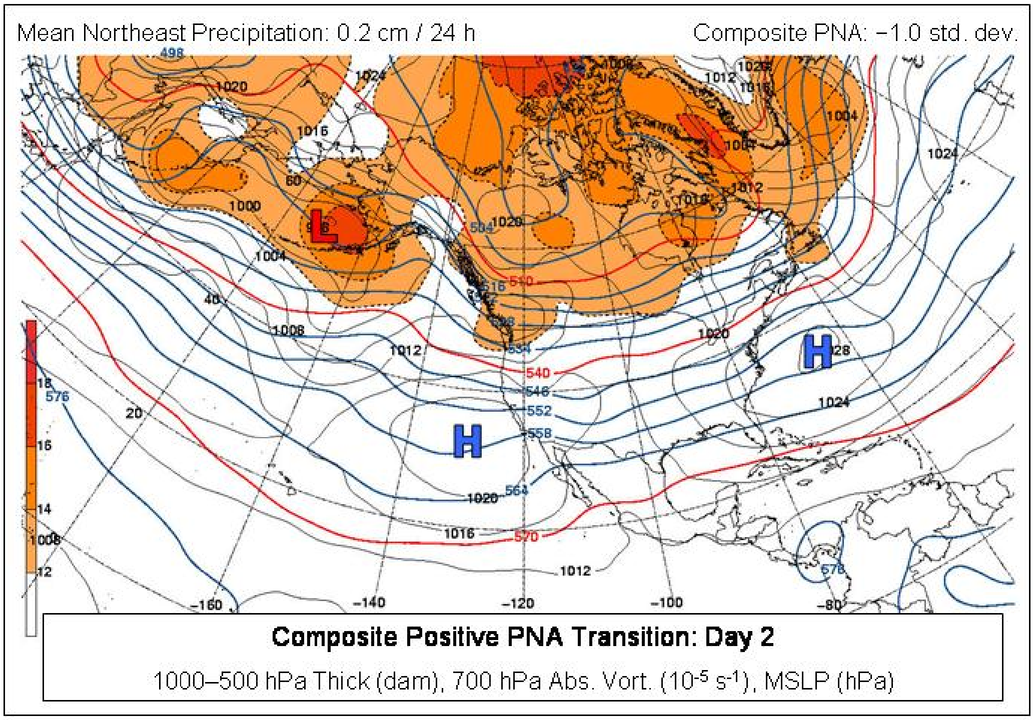

Fig. 4.12c. Same as in Fig. 4.4c, except for Day 2 of a seven-day negative-to-positive PNA regime transition.

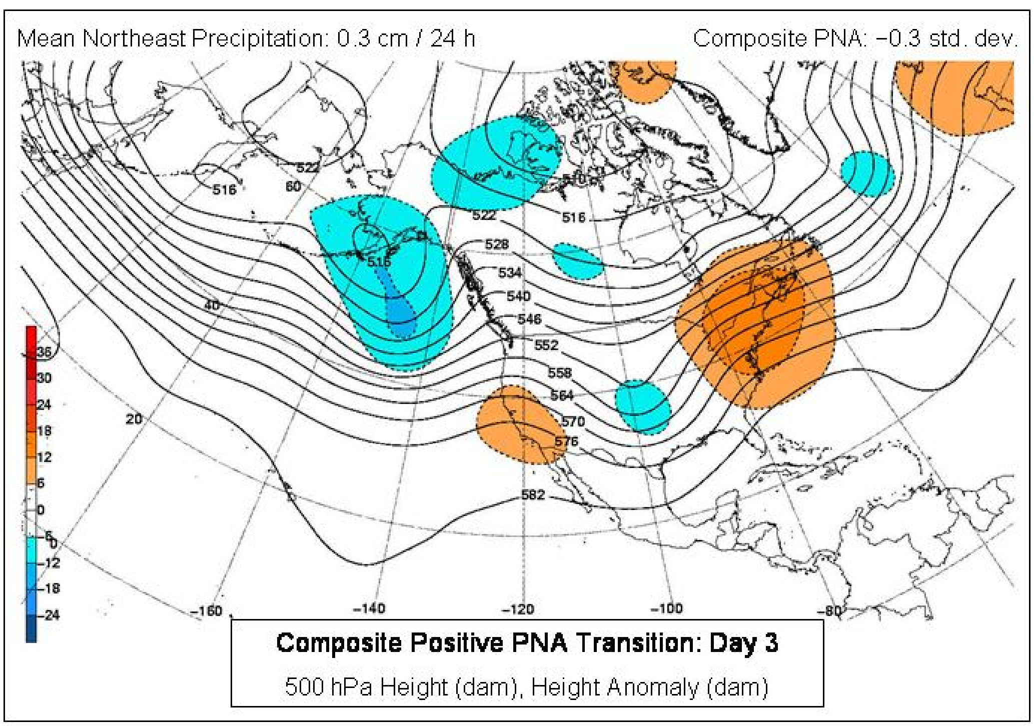

Fig. 4.13a. Same as in Fig. 4.4a, except for Day 3 of a seven-day negative-to-positive PNA regime transition.

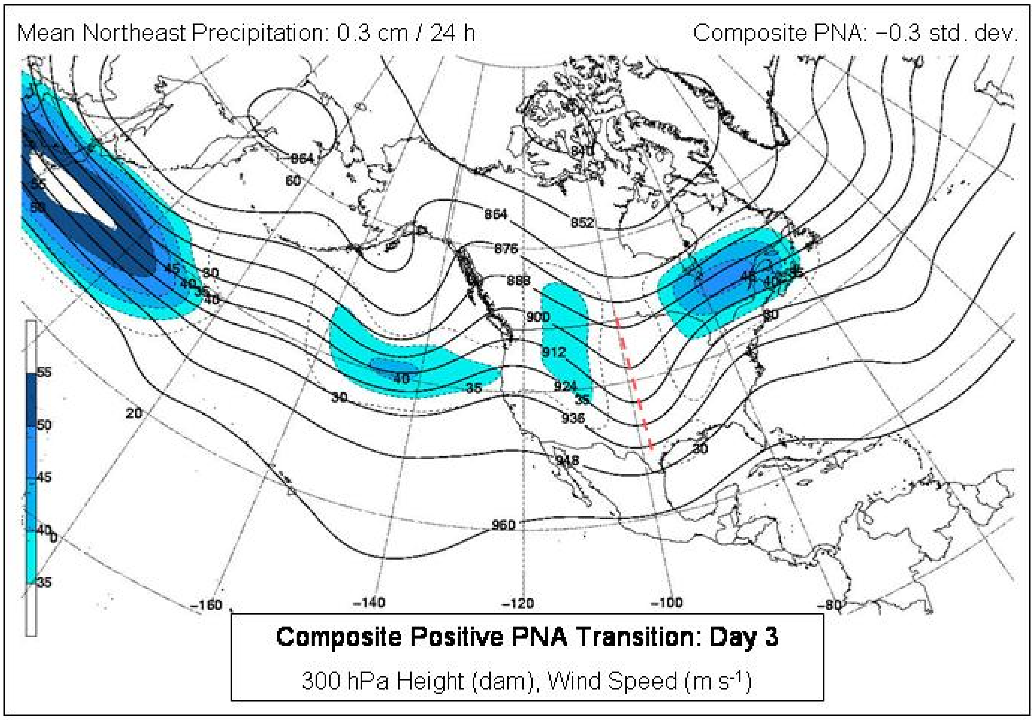

Fig. 4.13b. Same as in Fig. 4.4b, except for Day 3 of a seven-day negative-to-positive PNA regime transition.

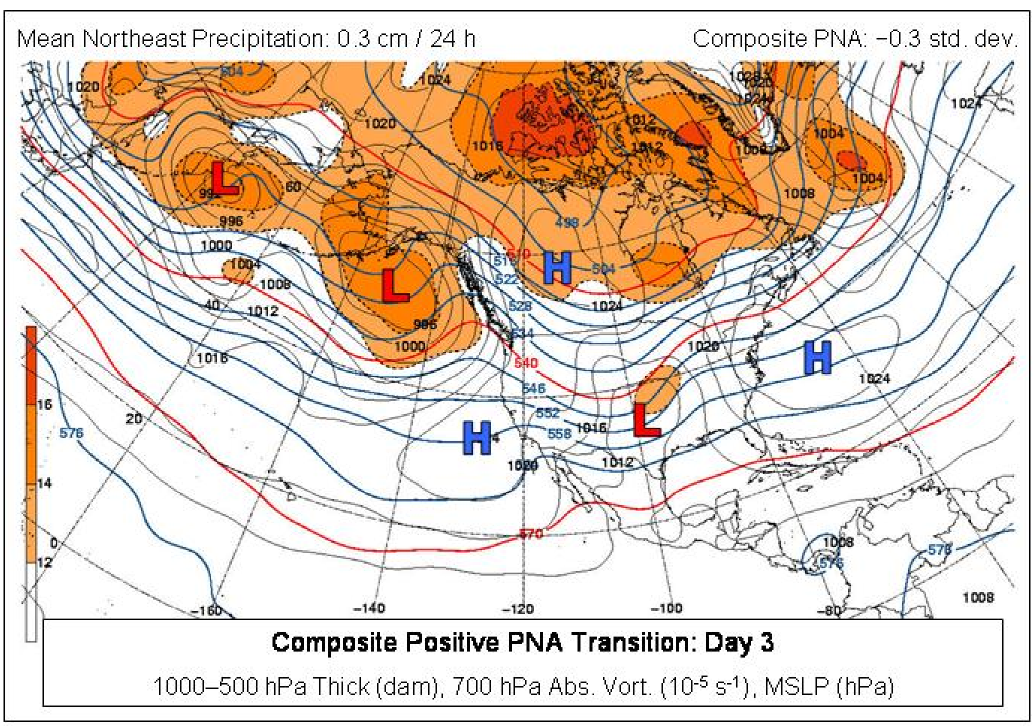

Fig. 4.13c. Same as in Fig. 4.4c, except for Day 3 of a seven-day negative-to-positive PNA regime transition.

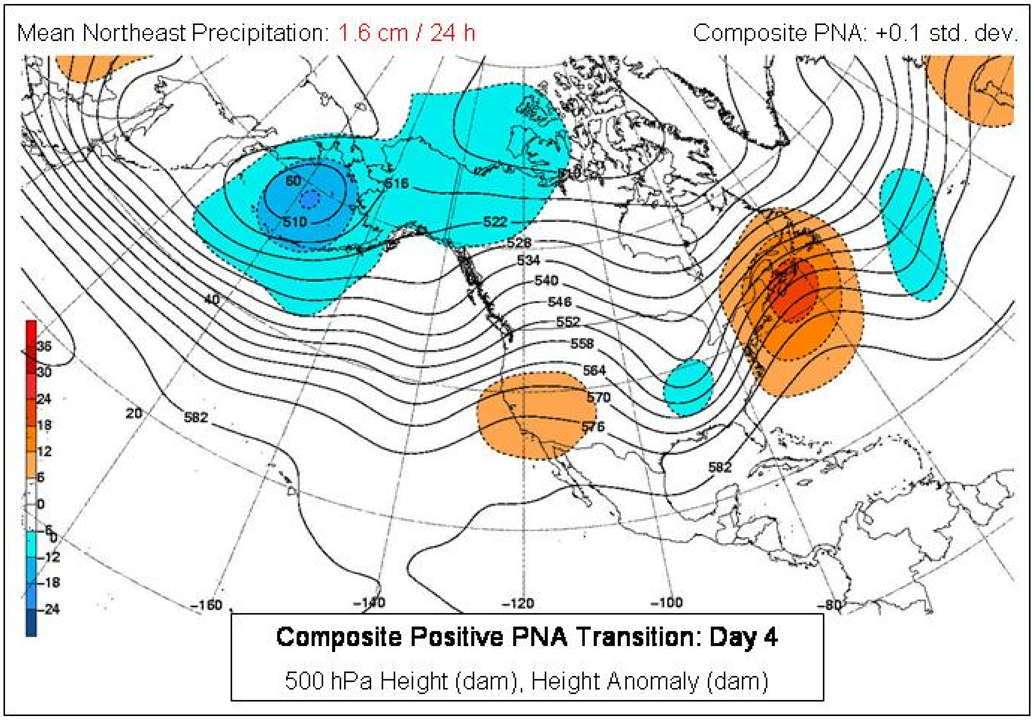

Fig. 4.14a. Same as in Fig. 4.4a, except for Day 3 of a seven-day negative-to-positive PNA regime transition.

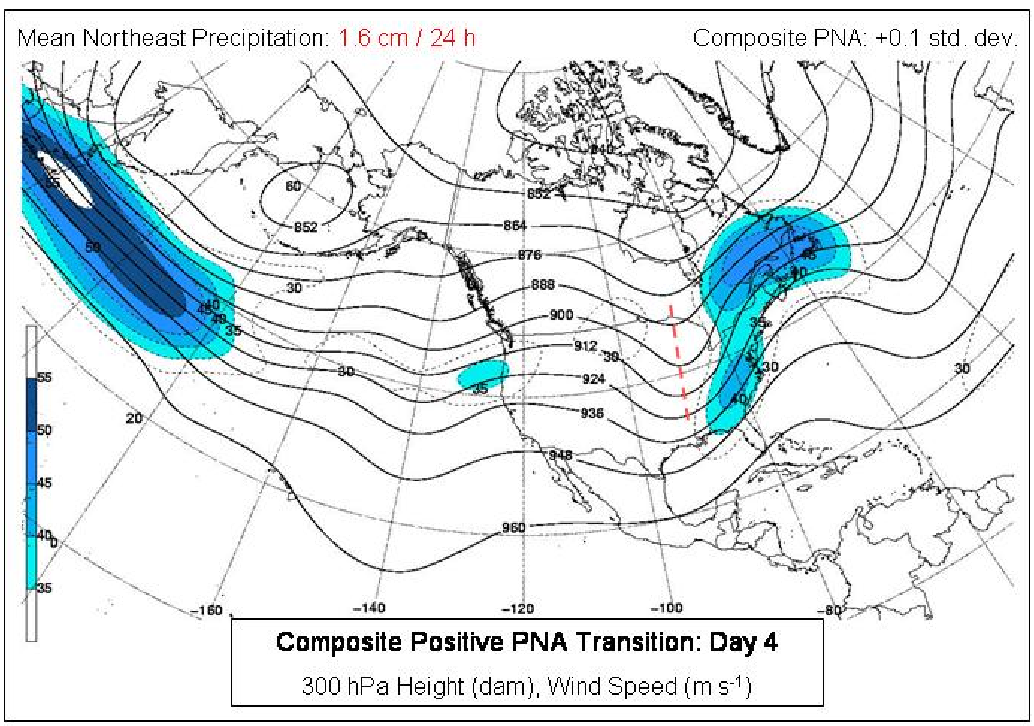

Fig. 4.14b. Same as in Fig. 4.4b, except for Day 4 of a seven-day negative-to-positive PNA regime transition.

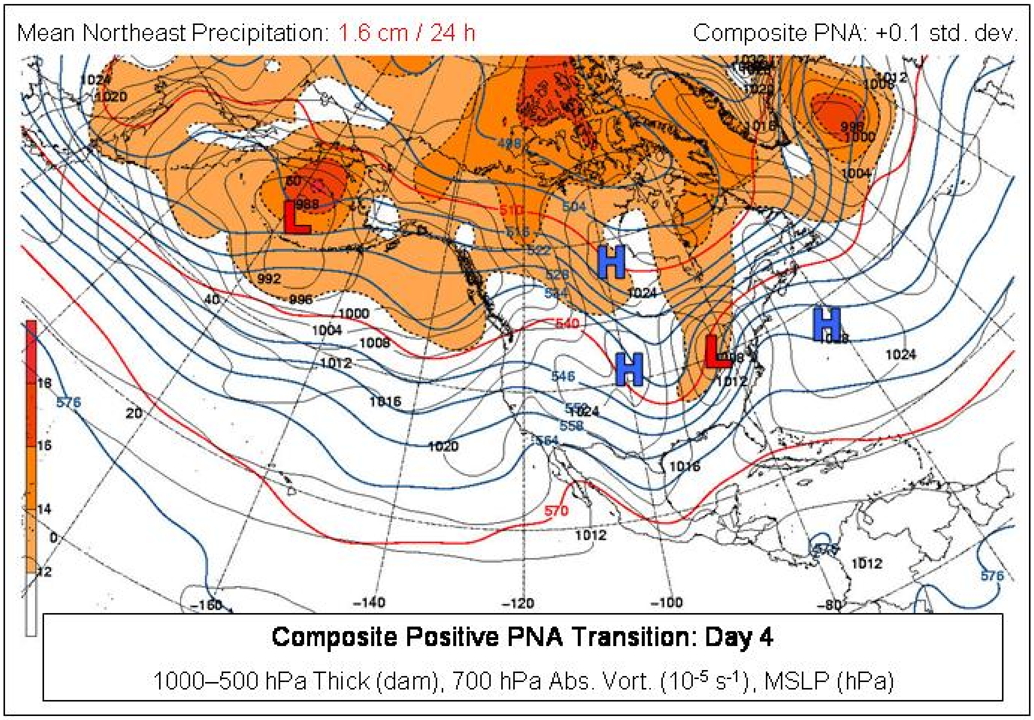

Fig. 4.14c. Same as in Fig. 4.4c, except for Day 4 of a seven-day negative-to-positive PNA regime transition.

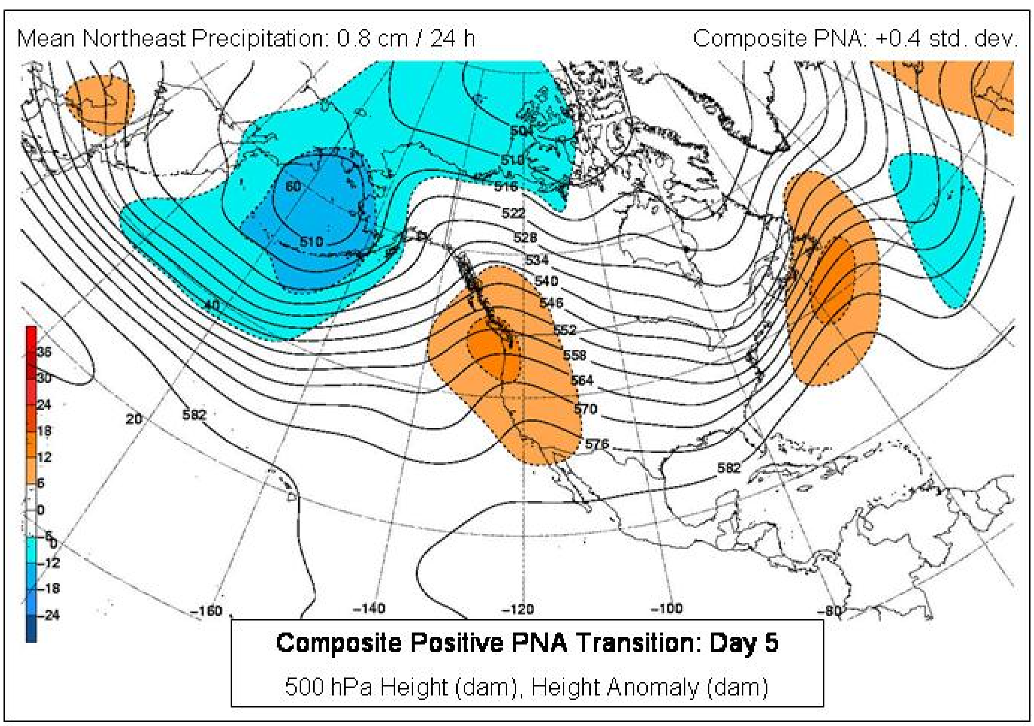

Fig. 4.15a. Same as in Fig. 4.4a, except for Day 5 of a seven-day negative-to-positive PNA regime transition.

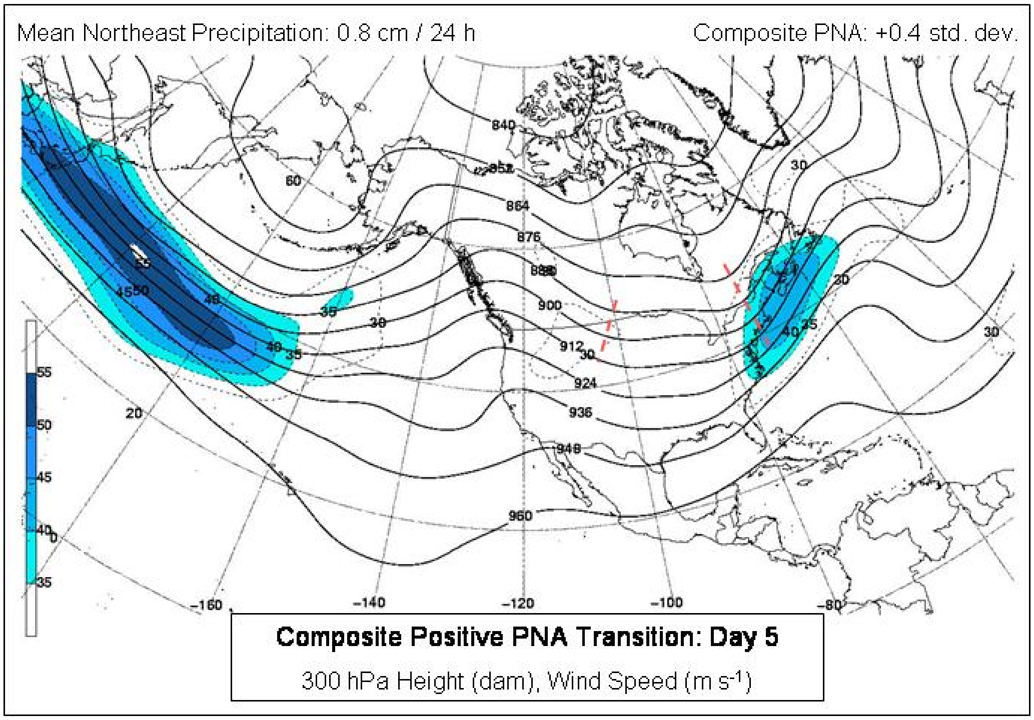

Fig. 4.15b. Same as in Fig. 4.4b, except for Day 5 of a seven-day negative-to-positive PNA regime transition.

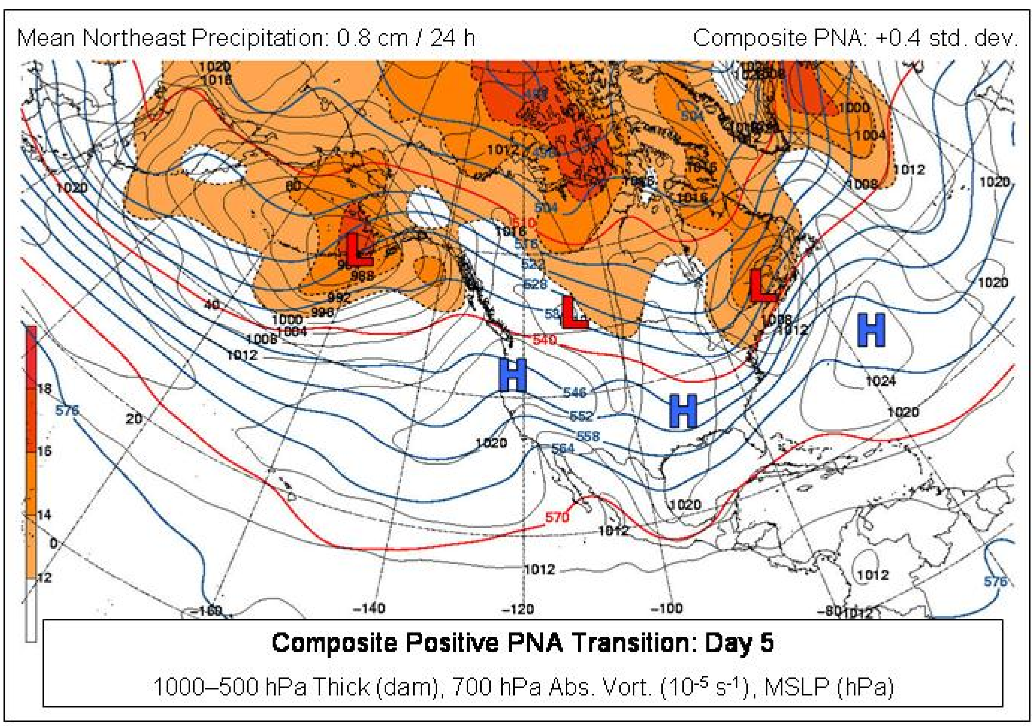

Fig. 4.15c. Same as in Fig. 4.4c, except for Day 5 of a seven-day negative-to-positive PNA regime transition.

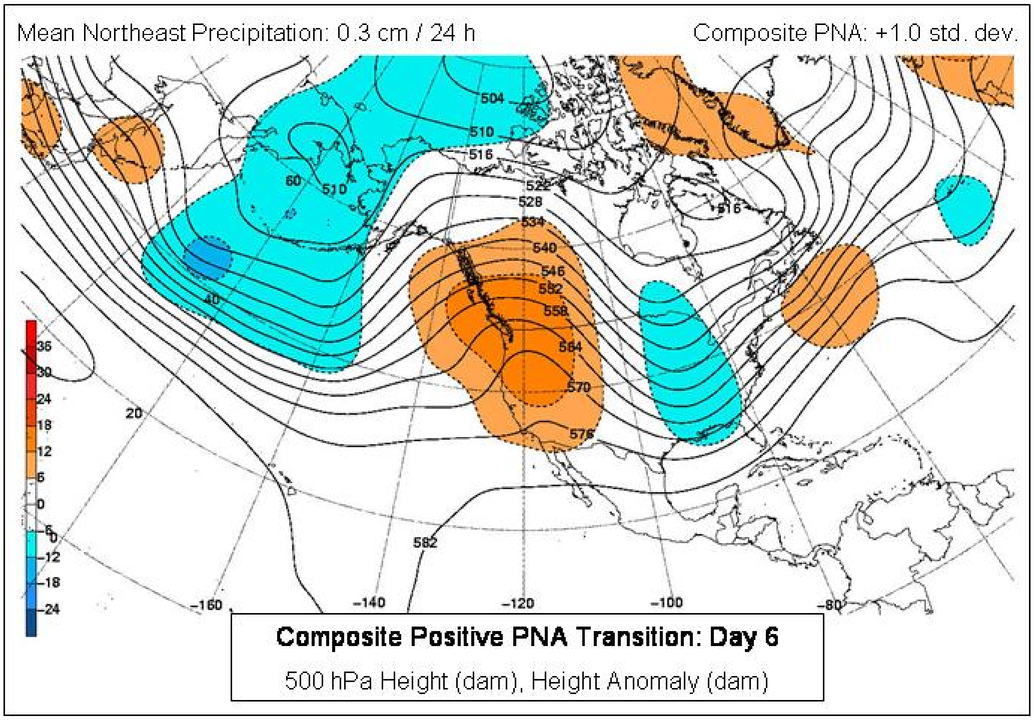

Fig. 4.16a. Same as in Fig. 4.4a, except for Day 6 of a seven-day negative-to-positive PNA regime transition.

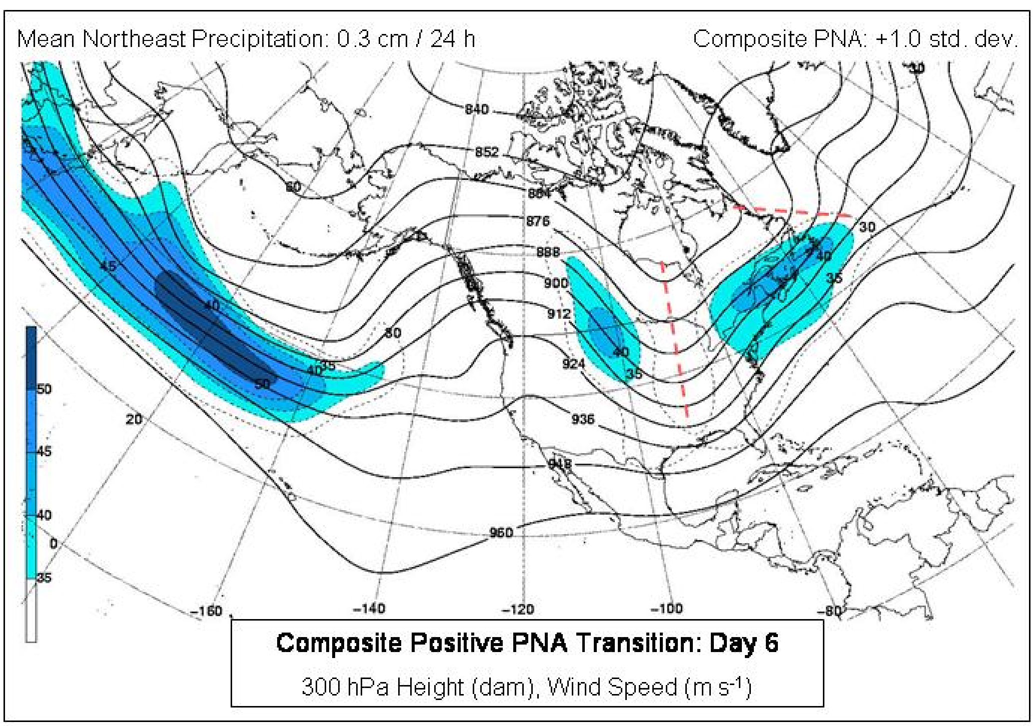

Fig. 4.16b. Same as in Fig. 4.4b, except for Day 6 of a seven-day negative-to-positive PNA regime transition.

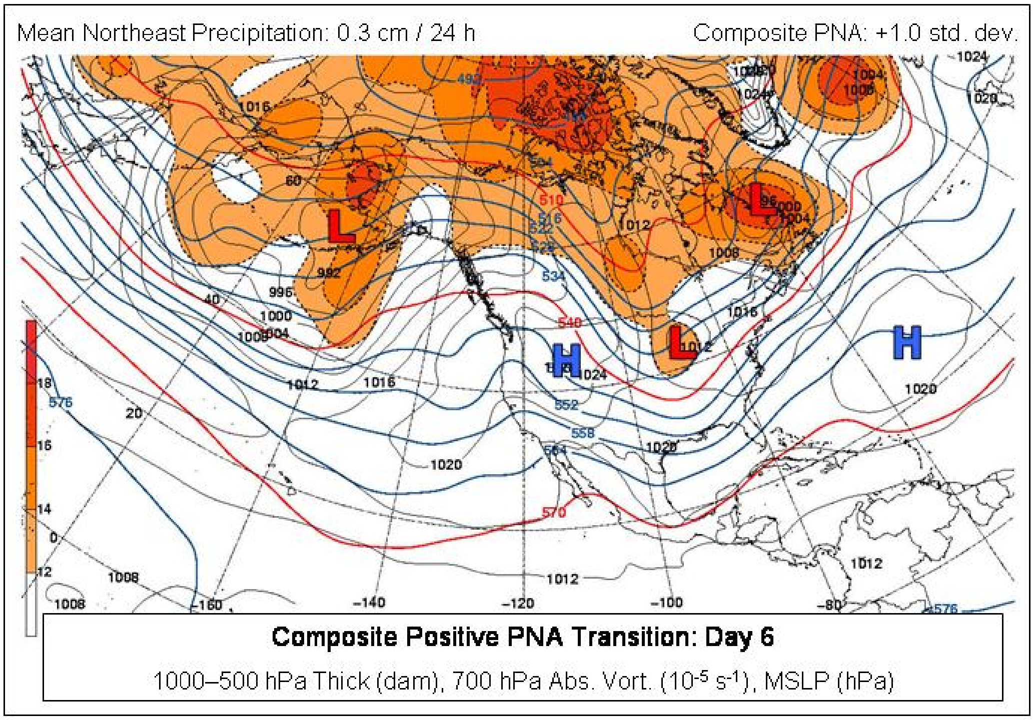

Fig. 4.16c. Same as in Fig. 4.4c, except for Day 6 of a seven-day negative-to-positive PNA regime transition.

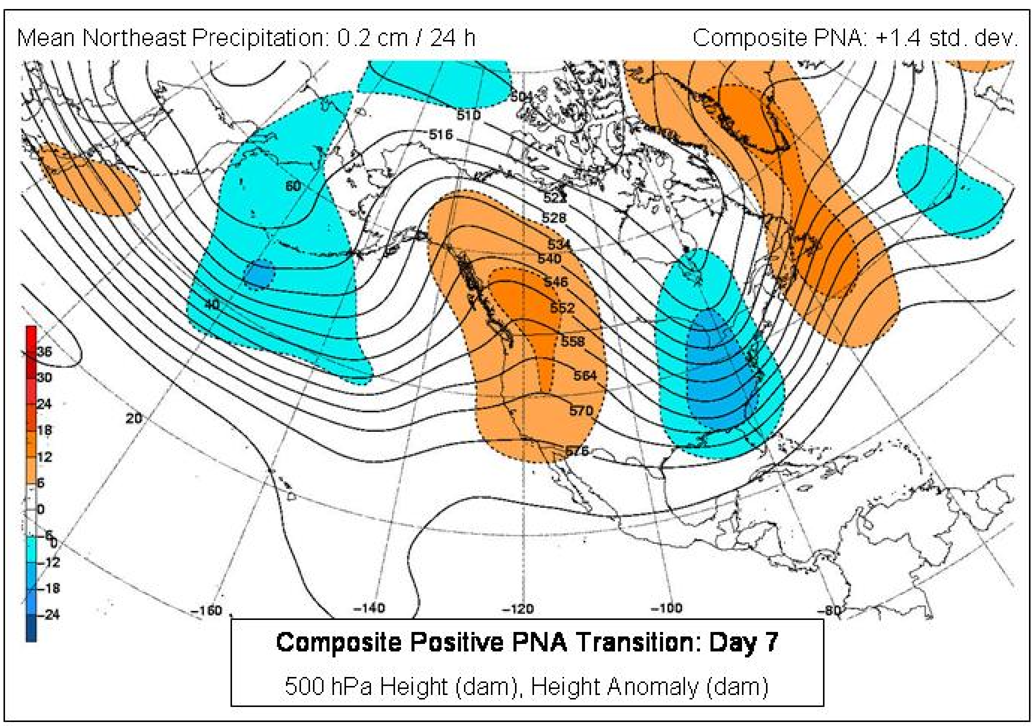

Fig. 4.17a. Same as in Fig. 4.4a, except for Day 7 of a seven-day negative-to-positive PNA regime transition.

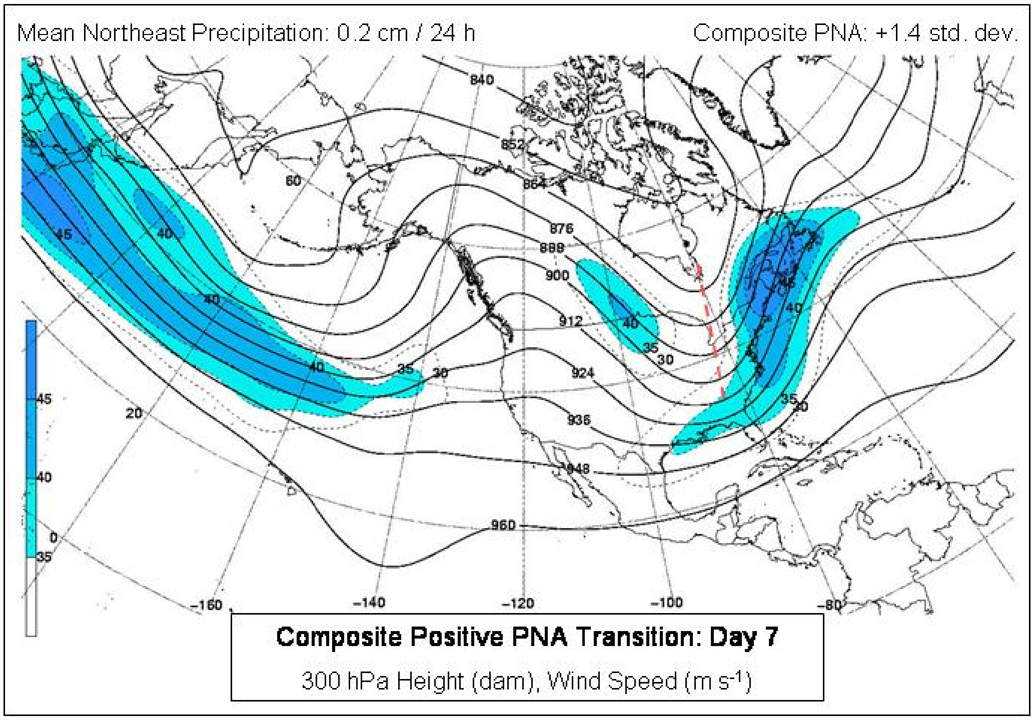

Fig. 4.17b. Same as in Fig. 4.4b, except for Day 7 of a seven-day negative-to-positive PNA regime transition.

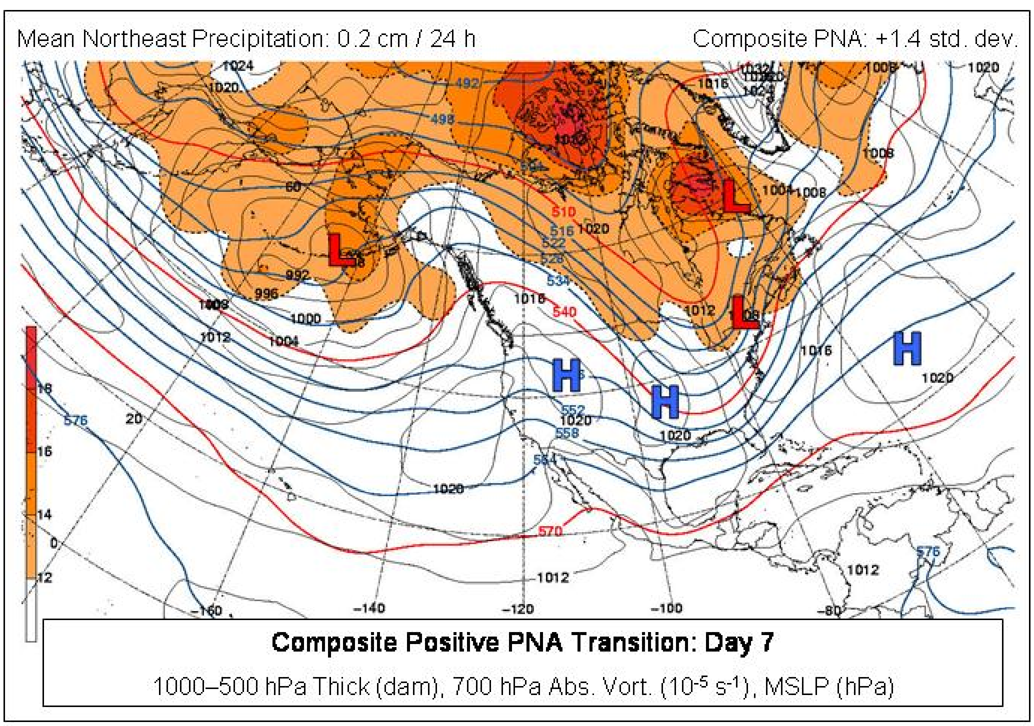

Fig. 4.17c. Same as in Fig. 4.4c, except for Day 7 of a seven-day negative-to-positive PNA regime transition.

5. Discussion

5.1 Relationships between Large-Scale Regimes and Northeast Precipitation in the Cool Season

Statistical relationships shown in Chapter 3 suggest that persistent large-scale regimes influence Northeast precipitation in the cool season. Negative PNA and positive NAO regimes are associated with slightly above-normal precipitation in the Northeast, while positive PNA and negative NAO regimes are linked to slightly suppressed precipitation in the Northeast (Fig. 3.1).

The relationships determined from this research are consistent with prior research indicating that both NAO and PNA regimes modulate Northeast precipitation in the cool season. For example, Hurrell (1995) showed that precipitation is significantly greater than evaporation near the Northeast coast of the U.S. during positive NAO regimes, while evaporation exceeds precipitation in the same region during negative NAO regimes. Leathers et al. (1991) found a weak negative correlation between the phase of the PNA and Northeast precipitation during the latter part of the cool season.

The relatively weak statistical relationships documented in this research are also consistent with past research (e.g., Leathers et al. 1991) indicating that statistical relationships between large-scale regimes and precipitation are not as strong as statistical relationships between large-scale regimes and surface temperature. The relatively tenuous links between large-scale regimes and cool-season precipitation in the Northeast may be explained in the following ways:

First, although past research shows that synoptic-scale systems contribute more substantially to precipitation than do mesoscale systems in the cool season (e.g., Leathers et al. 1991), mesoscale features embedded within synoptic-scale systems have been documented to play an often critical role in the distribution and intensity of cool-season precipitation (e.g., Bosart et al. 1998; Nicosia and Grumm 1999; Novak et al. 2004). Second, precipitation in the cool season is strongly modulated by storm track, suggesting that slight storm track variations associated with a particular large-scale regime may produce markedly different regional precipitation distributions. Thus, the relatively weak relationships between large-scale regimes and Northeast precipitation in the cool season are to be expected since other factors contribute substantially to precipitation variability in the cool season.

A potentially important difference between this research and past research (e.g., Leathers et al. 1991; Hurrell 1995) is that this research documents relationships between large-scale regimes and precipitation for time scales on the order of days rather than on the order of months or years. Despite this difference, the relationships are similar to prior results. That these results are consistent with results from previous studies suggests that despite the relative weakness of the relationships between large-scale regimes and Northeast precipitation in the cool season, these relationships are verifiable.

As discussed above, cool-season precipitation in the Northeast is shown to be enhanced during certain phases of the NAO and PNA pattern (Fig. 3.1). An alternative approach to exploring cool-season relationships between teleconnection patterns and Northeast precipitation is to determine whether certain phases of the NAO and PNA are favored during major cool-season precipitation events in the Northeast. To explore these relationships, daily NAO and PNA index values were calculated for the top 25 24-h cool-season precipitation events in the Northeast.

Results indicate that the NAO shows a slight tendency to be in a positive phase during major cool-season precipitation events in the Northeast (Fig. 3.2a). Initially, this result might seem to conflict with the observation by Kocin and Uccellini (2004, p. 32) that the NAO is often negative during major snowstorms in the Northeast. However, this discrepancy is likely related to Kocin and Uccellini's (2004) comparatively narrow focus on Northeast snowstorms in contrast to this work's relatively broader study of major Northeast precipitation events in the cool season. The apparent cool-season relationship between major Northeast precipitation events and the positive phase of the NAO documented in section 3.2 does not necessarily contradict the relationship between Northeast snowstorms and the negative phase of the NAO documented by Kocin and Uccellini (2004); in contrast to the events studied in this research, Northeast snowstorms do not necessarily produce high liquid-water totals over a large area.

That the NAO shows a slight tendency to be positive during major precipitation events (Fig. 3.2a) appears to be consistent with results suggesting that persistent positive NAO regimes are associated with enhanced Northeast precipitation in the cool season (Fig. 3.1). These statistical results suggest that a stronger-than-average North Atlantic jet is weakly linked to above-normal precipitation in the Northeast, and may also be slightly more conducive than a weaker-than-average North Atlantic jet to the development of a significant precipitation event in the Northeast in the cool season.

Results documented in section 3.2 indicate that the PNA tends to be in a positive phase during major cool-season Northeast precipitation events (Fig. 3.2b) and suggest that the phase of the PNA is more strongly related to major Northeast precipitation events than is the phase of the NAO (compare Fig. 3.2b to Fig. 3.2a). A physical interpretation of this statistical result is that an anomalous trough is often situated over the eastern U.S. and an anomalous ridge is situated over the western U.S. during major Northeast precipitation events in the cool season. This interpretation, when related to the apparent link between persistent positive PNA regimes and suppressed Northeast precipitation discussed in Chapter 3, suggests that a large-scale regime characterized by a trough in the East and a ridge in the West is often observed during major Northeast precipitation events, yet is not typically favorable for above-normal precipitation in the Northeast when it persists over several days. Conversely, a large-scale regime characterized by a trough in the West and a ridge in the East rarely is observed during major Northeast precipitation events, but is typically favorable for above-normal Northeast precipitation when it persists for several days.

Based upon composite analyses displayed in section 3.3 (Figs. 3.3–3.6), important synoptic-scale features of major Northeast precipitation events associated with positive NAO, negative NAO, positive PNA, and negative PNA regimes are shown in Figs. 5.1a–d, respectively. Figure 5.1a shows that in addition to the characteristic positive NAO structure located over the North Atlantic as described by Wallace and Gutzler (1981) and Barnston and Livezey (1987), another north–south dipole is located over western North America. This feature is characterized by lower-than-average 500 hPa geopotential heights centered over western Canada and higher-than-average 500 hPa geopotential heights centered near the southwestern U.S.. The characteristic pattern associated with positive NAO precipitation events suggests that the atmospheric structure during these events is conducive to faster-than-average westerlies not only across the North Atlantic, but also farther west across the U.S..

As illustrated by Fig. 5.1a, during a major positive NAO precipitation event in the Northeast, a surface low typically is located beneath the right-entrance region of the North Atlantic jet at 300 hPa (also see Figs. 3.3b,c). The position of the surface low relative to the North Atlantic jet suggests that during a typical major positive NAO precipitation event in the Northeast, the upward branch of a secondary circulation induced by transverse ageostrophic flow in the jet-entrance region may favor a surface cyclone over the Northeast (e.g., Namias and Clapp 1949).

Inspection of Fig. 5.1a and Figs. 3.3a,b suggests that major Northeast precipitation events in the cool season that occur during positive NAO regimes often may be associated with weakening upper-level troughs. Based upon the characteristic location of the upper-level trough in the entrance region of the North Atlantic jet during this type of precipitation event, the upper-level trough can be expected to encounter deformation and weaken with time as it is sheared by the jet-stream flow.

Inspection of significant synoptic-scale features associated with major Northeast precipitation events that occur during negative NAO regimes (Fig. 5.1b) finds a 500 hPa geopotential height anomaly dipole over the North Atlantic characteristic of a negative NAO pattern (Wallace and Gutzler 1981; Barnston and Livezey 1987). Farther west, a separate negative geopotential height anomaly centered over the Southeast is associated with a deep 500 hPa trough that supports a significant surface cyclone in the Northeast. Although the negative NAO pattern is associated with a deeper 500 hPa trough and seems more dynamically favorable for a Northeast precipitation event than the positive NAO pattern (compare Fig. 5.1b to Fig. 5.1a), the mean domain-average Northeast precipitation amount associated with a major negative NAO precipitation event is comparable to the amount associated with a major positive NAO precipitation event (compare Table III to Table II). The similarity in mean precipitation amounts despite an apparent difference in the strength of the dynamics in each case may suggest that surface lows associated with negative NAO regimes are often stronger but are more likely to track offshore than those associated with positive NAO regimes.

In addition to the negative geopotential height anomaly over the southeastern U.S., two other negative 500 hPa geopotential height anomalies are evident for a composite major negative NAO precipitation event in the Northeast; one anomaly is located over the southwestern U.S., and the other is centered over the North Pacific (Fig. 5.1b). With the exception of the latter negative height anomaly, in general, negative geopotential height anomalies associated with a negative NAO precipitation event are located mainly in the midlatitudes, while a positive geopotential height anomaly is located in high latitudes. This pattern supports weaker-than-average westerlies in the middle troposphere across North America in addition to weaker-than-average westerlies over the North Atlantic characteristic of a negative NAO regime. The blocked nature of the large-scale pattern during major negative NAO precipitation events is consistent with research by Shabar et al. (2001) that shows a strong relationship between the negative phase of the NAO and North Atlantic blocking.

In contrast to the composite position of the surface low associated with a major positive NAO precipitation event, the surface low associated with a major negative NAO precipitation event seems to be coupled to the left-exit region rather than the right-entrance region of a jet streak (compare Fig. 5.1b to Fig. 5.1a). This configuration suggests that, in addition to the relatively deep 500 hPa trough associated with negative NAO regimes, the forcing associated with the left-exit region of a jet streak helps create a favorable environment for a major Northeast precipitation event. This statement is supported by past research by Uccellini and Kocin (1987), who showed that the surface low pressure center associated with major Northeast snowstorms is typically located beneath the left-exit region of a jet streak.

Salient features associated with major positive PNA precipitation events are shown in Fig. 5.1c. Inspection of Fig. 5.1c shows negative 500 hPa geopotential height anomalies over the North Pacific and the southeastern U.S. and a positive 500 hPa geopotential height anomaly over western North America. This pattern resembles the positive PNA pattern identified by Wallace and Gutzler (1981) and Barnston and Livezey (1987). A closed 500 hPa low located over the northeastern U.S. (Fig. 5.1c) during these types of Northeast precipitation events is also commonly observed during cyclogenesis associated with a major Northeast snowstorm (Kocin and Uccellini 2004, p. 101)

An additional positive 500 hPa geopotential height anomaly typically not considered part of the positive PNA pattern is located over the western North Atlantic (Fig. 5.1c). This additional positive geopotential height anomaly appears to be the result of warm air advection occurring downstream of a surface low over the Northeast (see Fig. 3.5a). The configuration of the midtropospheric geopotential height anomalies associated with positive PNA precipitation events in the Northeast is reminiscent of a Rossby wave-train pattern and suggests that downstream development may be an important factor in the formation of a major precipitation event in the Northeast during a positive PNA regime.

As in negative NAO precipitation events (Fig. 5.1b), the surface low associated with a positive PNA precipitation event in the Northeast appears to be located beneath the left-exit region of an upper-tropospheric jet (Fig. 5.1c). In addition, a typical major positive PNA precipitation event seems to be supported by a deep midtropospheric trough over the eastern U.S (Figs. 5.1c and 3.5a).

The highly amplified flow pattern across North America appears to indicate that a major precipitation event in the Northeast occurring during a positive PNA regime is associated with strong dynamics.

The key synoptic features associated with a typical negative PNA precipitation event in the Northeast are shown in Fig. 5.1d and suggest that the flow pattern is considerably more zonal during this type of precipitation event than during a positive PNA precipitation event (Fig. 5.1c) or a negative NAO precipitation event (Fig. 5.1b); only a weak trough is present at 500 hPa during a typical negative PNA precipitation event. In addition, the surface low accompanying this type of precipitation event does not appear to be related to a secondary vertical circulation associated with an upper-tropospheric jet streak. Rather, this type of precipitation event in the Northeast appears to be associated with a strong midtropospheric moisture feed from the western Gulf of Mexico, perhaps suggesting that this type of precipitation event in the Northeast is driven primarily by warm air advection. The critical role of moist air originating over the Gulf of Mexico in fueling a major Northeast precipitation event during a positive PNA regime has been documented by Gyakum and Roebber (2001) in their analysis of the 5–9 January 1998 ice storm that affected eastern Canada and northern sections of the Northeast. The dramatic synoptic-scale differences between negative PNA and positive PNA precipitation events in the Northeast help support the assertion made earlier that a persistent positive PNA pattern is usually favorable for infrequent but major Northeast precipitation events, while a negative PNA pattern is usually favorable for more frequent but relatively minor Northeast precipitation events.

5.2 Relationships between Large-Scale Regime Transitions and Northeast Precipitation in the Cool Season

Results documented in section 4.2 indicate a statistically significant relationship between transitions from positive to negative NAO regimes and enhanced precipitation in the Northeast (Fig. 4.1). Conversely, results suggest that a relationship exists between transitions from negative to positive NAO regimes and suppressed precipitation in the Northeast, though this relationship was not verified to be statistically significant (Fig. 4.1). Like NAO regime transitions, PNA regime transitions influence Northeast precipitation; a transition from a positive to negative PNA regime is associated with a statistically significant composite negative precipitation anomaly in the Northeast, while a transition from a negative to positive PNA regime is associated with a non-statistically significant composite positive precipitation anomaly (Fig. 4.1).

Statistical relationships documented in this study show that, on average, Northeast precipitation anomalies associated with regime transitions are slightly greater in magnitude than precipitation anomalies associated with persistent weather regimes (compare Fig. 4.1 to Fig. 3.1). These results suggest that a rapid change in the large-scale pattern may be more conducive to anomalous precipitation in the Northeast than a persistent large-scale pattern.

As discussed above, cool-season precipitation in the Northeast appears to be influenced by certain types of large-scale flow reconfigurations. To determine whether large-scale flow changes are associated with anomalous precipitation events, the seven-day tendencies of the NAO and PNA were calculated for the top 25 24-h cool-season precipitation periods in the Northeast. Calculations indicate that, on average, the NAO index tends to decrease during major precipitation events in the Northeast (Fig. 4.3a). This result seems to contradict research results by Kocin and Uccellini (2004, p. 34) indicating that the NAO index tends to increase surrounding a major winter storm in the Northeast. However, this apparently discrepancy may be due to Kocin and Uccellini's specific focus on Northeast snowstorms discussed in section 5.1.

The tendency for the large-scale pattern to trend toward the negative phase of the NAO during major Northeast precipitation events in the cool season (Fig. 4.3a) appears to be consistent with the previously discussed result that transitions from positive to negative NAO regimes are associated with above-normal precipitation in the Northeast (Fig. 4.1). A physical interpretation of this result is that a weakening North Atlantic jet is conducive to above-normal Northeast precipitation, and that the North Atlantic jet typically weakens during the period surrounding a major precipitation event in the Northeast.

Similar to the tendency of the NAO index, the tendency of the PNA index also shows a strong signal surrounding a major precipitation event in the Northeast during the cool season. In contrast to the NAO index, the PNA index tends to increase in association with major Northeast precipitation events (Fig.

4.3b). The tendency for the PNA index to increase surrounding major Northeast precipitation events is consistent with the observation of NWS forecasters that the PNA index often shows a positive tendency surrounding major winter storms in New England (W. Drag, personal communication). Since negative-to-positive PNA regime transitions tend to be associated with above-average precipitation in the Northeast (Fig. 4.1), the above results can be interpreted as suggesting that an amplifying trough (ridge) over eastern (western) North America is conducive to above-normal Northeast precipitation and is more common in the period surrounding a major precipitation event in the Northeast than is an amplifying ridge (trough) over eastern (western) North America.

Important synoptic-scale features associated with two types of regime transitions with major precipitation events at their midpoints are shown in Figs. 5.2a–c and 5.3a–c. Figures 5.2a–c show important features present at the onset, midpoint, and termination, respectively, of a typical positive-to-negative NAO regime transition associated with a midpoint precipitation event. Figures 5.3a–c show important features present at the beginning, midpoint, and termination, respectively, of a typical negative-to-positive PNA regime transition associated with a midpoint precipitation event in the Northeast.

Inspection of Figs. 5.2a–c and Figs. 4.4–4.10 shows that the evolution of from a low-amplitude wave pattern characteristic of a positive NAO regime to a high-amplitude wave pattern characteristic of a negative NAO regime appears to be associated with downstream development. At the onset of the positive-to-negative NAO regime transition, a Rossby wave train is found across the North

Pacific but has not yet reached the west coast of North America (Fig. 5.2a). At the midpoint of the transition, a wave train extends from the central North Pacific eastward to the eastern North Atlantic (Fig. 5.2b). By the conclusion of the regime transition, the pattern is highly amplified, with positive 500 hPa geopotential height anomalies located in high latitudes (Fig. 5.2c). The development of a western North Atlantic ridge by the end of the transition (Fig. 5.2c) is consistent with past research suggesting that western North Atlantic ridge development is associated with explosive cyclogenesis along the East Coast (Lackmann et al. 1996). By the end of the transition, the surface low associated with heavy precipitation at the midpoint of the transition (Fig. 5.2b) has moved northward and weakened, possibly as a result of the energy of the wave packet having propagated to the east to the North Atlantic (Fig. 5.2c).

As discussed in section 4.3.1, the surface low associated with a major precipitation event in the Northeast at the midpoint of the positive-to-negative NAO transition appears to play a critical role in this large-scale regime transition. Strong warm air advection ahead of the system appears to build a high-latitude ridge over the North Atlantic (see Figs. 4.7 and 4.8), a finding consistent with research by Lackmann et al. (1996), who noted that a positive midtropospheric height anomaly typically forms downstream of a major cyclogenesis event near the east coast of the U.S. and tends to persist for several days.

The pattern that develops during a positive-to-negative NAO transition is consistent with a cyclonic wave-breaking event (Thorncroft et al. 1993) that is found to commonly precede the development of a negative NAO regime

(Franzke et al. 2003; Benedict et al. 2004). According to Franzke et al. (2003) and Benedict et al. (2004), cyclonic wave breaking occurs when the latitudinal potential temperature gradient on the DT reverses sign. Cyclonic wave breaking can be interpreted synoptically as occurring when a synoptic-scale disturbance becomes negatively tilted (Franzke et al. 2003; Benedict et al. 2004). The studies by Franzke et al. (2003) and Benedict et al. (2004) note that negatively tilted disturbances tend to be present over the middle- and high-latitude North Atlantic prior to the development of a negative NAO pattern. Although the current research does not address the evolution of potential temperature gradients on the DT, the northern portion of the upper-level ridge that develops downstream of the Northeast surface low during a positive-to-negative NAO transition displays a negative tilt at both 500 hPa and 300 hPa (Figs. 4.7a,b, respectively). This observation suggests that an analysis of potential temperature on the DT during positive-to-negative NAO regime transitions would show cyclonic wave breaking as defined by Franzke et al. (2003) and Benedict et al. (2004).

As was the case for Northeast precipitation events associated with certain large-scale regimes discussed in sections 3.3 and 5.1, a typical Northeast precipitation event occurring at the midpoint of a positive-to-negative NAO transition appears to be associated with entrance and exit regions of upper-level jet streaks (Fig. 5.2). Figure 5.2b shows that the surface low associated with a heavy precipitation event at the midpoint of a positive-to-negative NAO transition is located below the left-exit region of a 300 hPa jet streak across the Southeast and the right-entrance region of a second 300 hPa jet streak across eastern Canada. This pattern suggests that the surface low may be related to the upward branches of vertical circulations in the entrance and exit regions of the two jets, a phenomenon found to be associated with heavy snow along the East Coast (e.g., Uccellini and Kocin 1987; Kocin and Uccellini 2004, p. 117).

Similar to a transition from a positive to a negative NAO regime associated with a midtransition precipitation event in the Northeast, the transition from a negative to a positive PNA regime (Figs. 5.3a–c) is found to be associated with an overall pattern amplification. Also similar to the positive-to-negative NAO transition discussed above, a negative-to-positive PNA transition associated with a midtransition precipitation event in the Northeast is linked to the development of blocking across the western North Atlantic (Fig. 5.3c), though the blocking is not as strong as in the positive-to-negative NAO transition case.

As during positive-to-negative NAO regimes associated with mid-transition precipitation events, synoptic-scale features appear to play a critical role in the transition of the pattern from a negative to a positive PNA regime. One important synoptic-scale feature is the relatively weak 500 hPa trough associated with the Northeast precipitation event at the midpoint of the transition (Fig. 5.3b). The surface low associated with the relatively weak 500 hPa trough is denoted by L1. The development of this trough at 500 hPa appears to precondition the atmosphere for the development of a second, stronger 500 hPa trough over the eastern U.S. by the end of the transition period (Fig. 5.3c). The surface low associated with the relatively strong 500 hPa trough is denoted by

L2. The second synoptic-scale feature associated with the transition from a negative to a positive PNA regime is a persistent surface low located near the Aleutians during the second half of the transition period (see Figs. 4.15c–4.17c). Persistent warm air advection in the Gulf of Alaska associated with this surface low appears to contribute to the amplification of the mid and upper-tropospheric ridge over western North America during the regime transition (see Figs. 4.15a,b–4.17a,b). Once this ridge builds, the mid and upper-tropospheric trough over the eastern U.S. deepens, possibly in association with downstream development (see Figs. 4.15a,b–4.17a,b).

The transition from a negative to positive PNA pattern seems to be linked to extratropical synoptic-scale features, a result that is consistent with research suggesting that the PNA pattern could be excited either by anomalous heating in the tropical Pacific or by extratropical high-frequency eddies (e.g., Cash and Lee 2001). However, the influence of the tropical Pacific is not addressed in this study and could prove to be equally important in transitions from negative to positive PNA regimes.

As was the case for a typical Northeast precipitation event associated with a positive-to-negative NAO regime transition, the characteristic Northeast precipitation event occurring at the midpoint of a negative-to-positive PNA transition also appears to be related to the entrance and exit regions of upper-level jets. Figure 5.3b shows that the surface low associated with a heavy precipitation event at the midpoint of a negative-to-positive PNA transition is located below the left exit region of a jet streak over the Southeast and the right entrance region of a second jet located across eastern Canada.

The overall pattern amplification seen in a composite negative-to-positive PNA transition (Fig. 5.3) and a composite positive-to-negative NAO transition (Fig. 5.2) is consistent with past research results such as those by Kocin and Uccellini (2004, p. 105) indicating that the 500 hPa flow typically amplifies preceding major Northeast snowstorms. The apparent relationship between pattern amplification and the development of a surface cyclone can be explained by the fact that flow amplification causes an increase in gradients of absolute vorticity along the flow, and thus an increase in upper-level divergence and subsequent cyclone intensification (e.g., Palmén and Newton 1969, p. 325).

5.3 Planetary-/Synoptic-Scale Interactions during Large-Scale Regime Transitions

In addition to examining how Northeast precipitation in the cool season is modified by large-scale regimes and their transitions, this research sought to explore interactions between synoptic-scale features and the planetary-scale flow pattern during large-scale regime transitions. Results from this research suggest that certain regime transitions can produce favorable conditions for surface lows to affect the Northeast. For example, the change from a low-amplitude wave pattern to a high-amplitude wave pattern that appears to be associated with heavy precipitation events in the Northeast may allow synoptic-scale systems to move more northward than eastward, allowing them to track along the East Coast rather than sending them out to sea. In support of this statement, inspection of Figs. 5.2 and 5.3 shows that mid-transition Northeast surface lows associated with positive-to-negative NAO regime transitions and negative-to-positive PNA regime transitions, respectively, tend to track northward upon exiting the Northeast.

In addition to affecting the track of synoptic-scale systems, a transition to a high-amplitude wave pattern might allow systems to strengthen rather than be "sheared out" as open waves. An example of the influence of the large-scale pattern on the strength of synoptic-scale systems can be seen when comparing the composites of a positive PNA precipitation event in the Northeast (Figs. 3.5a–c) to composites of a negative PNA precipitation event (Figs. 3.6a–c). In the case of the negative PNA precipitation event, the surface circulation associated with the East Coast precipitation event is relatively weak (Fig. 3.6c) and is located well to the east of a weak 500 hPa trough (Fig. 3.6a). On the other hand, the surface circulation associated with a positive PNA precipitation event (Fig. 3.5c) is relatively strong and is located just east of a strong 500 hPa trough (Fig. 3.5a). Thus, the low-amplitude flow pattern associated with a negative PNA or positive NAO regime may not be conducive for the strengthening of a surface cyclone.

Past research indicates that synoptic-scale systems are governed extensively by the large-scale flow regime. For instance, Dole (1986) and Branstator (1995) found that storm tracks vary substantially depending upon the governing large-scale weather regime. Hurrell (1995) also noted that changes in the large-scale circulation are accompanied by pronounced shifts in storm track and associated eddy transports.

In addition to demonstrating the apparent influence of large-scale flow changes on synoptic-scale features, this research shows that synoptic-scale systems can influence the planetary-scale flow. For example, this research demonstrates that surface cyclones such as those that bring significant precipitation to the Northeast during the midpoints of positive-to-negative NAO transitions can cause downstream ridge amplification that is linked to the establishment of blocking regimes. In a typical positive-to-negative NAO regime transition, a ridge at 500 hPa develops in advance of the surface low pressure system affecting the Northeast, and as the cyclone eventually moves north, the 500 hPa ridge builds northward and weakens the North Atlantic jet (Fig. 5.2). However, downstream ridge amplification associated with East Coast cyclones does not always result in a blocking regime. The 12–14 March 1993 "Superstorm" is a well-documented example of how downstream ridge building can lead to the *strengthening* of the North Atlantic westerlies. In this case, diabatically induced outflow associated with downstream ridge development appeared to generate strong westerlies over the western North Atlantic in conjunction with the development of a deep mid and upper-tropospheric tropospheric trough over the East Coast and western North Atlantic (Bosart et al. 1996; Dickinson et al. 1997).

Results from this research indicate that a weak cold surge associated with a midtropospheric trough in the wake of the Northeast precipitation event at the midpoint of negative-to-positive PNA transitions can act to precondition the atmosphere for the development of a second, stronger cold surge and a deeper midtropospheric trough in the Northeast (see Figs. 4.15–4.17 and Fig. 5.3). Other cases where the passage of a transient trough precedes the development of a more significant trough in the Northeast are documented by Lackmann et al. (1996), who found that one or more weak upper-level troughs tend to cross the eastern U.S. preceding the rapid deepening of an upper-level trough over the East Coast. They suggested that an initial trough preconditions the atmosphere for cyclogenesis and the development of an associated deeper second trough, perhaps by establishing a strong baroclinic zone through cold air advection in its wake. This result is also consistent with research by Konrad and Colucci (1989), who found that a cold surge in the wake of a developing cyclone preceded a major cold air outbreak in the eastern U.S.

Other studies have shown that synoptic-scale systems often influence the reconfiguration of the planetary-scale flow. For example, Reinhold and Pierrehumbert (1982) found that synoptic-scale forcing is responsible for both the disruption and the stabilization of weather regimes. Colucci (1985) demonstrated through case studies that surface cyclones act as “agents of change” of the large-scale flow pattern, and Colucci (1987) showed that rapid cyclogenesis occurring upstream of a large-scale ridge favors the establishment of a blocking anticyclone.

Research results from the current study seem to suggest that regime transitions linked to the development of blocking might be associated with a positive feedback mechanism between the planetary scale and the synoptic scale. This feedback mechanism begins with areas of warm and cold air advection associated with a surface cyclone helping to build a downstream ridge and an upstream trough. The development of the downstream ridge and upstream trough allows the large-scale pattern to become more amplified, which implies that the cyclone track becomes more northerly (Figs. 5.2b and 5.3b). Subsequently, warm (cold) air advection occurs to the north (south) of surface cyclones rather than to the east (west) of the cyclones (Figs. 4.7c and 4.8c, Figs. 4.13c–4.15c; e.g., Mullen 1987, Pelly and Hoskins 2003a). Finally, the north–south orientation of the thermal advection associated with the surface cyclones helps to reinforce the relatively amplified flow pattern (Figs. 5.2c and 5.3c).

Evidence of positive feedback mechanisms between the synoptic-scale and the planetary-scale flow is extensively documented in past research. For example, Colucci (1987) recognized that a positive feedback between the synoptic-scale and the planetary-scale flow seems to occur preferentially during blocking events. He found that the planetary-scale response to a synoptic-scale cyclone is in part dependent upon the location of the cyclone with respect to the large-scale ridge or trough. Colucci (1987) also suggested that a positive feedback process can only occur when PV fluxes associated with synoptic-scale disturbances persist in both time and space. Colucci's (1987) suggestion that persistent fluxes are critical for generating a positive feedback is consistent with our results suggesting that persistent warm air advection over western North America is an important factor in the transition of the large-scale pattern from a negative to a positive PNA regime (see section 4.3.2 and section 5.2). Cai and Mak (1990) showed that planetary and synoptic-scale waves are “symbiotically” related, and Cash and Lee (2001) demonstrated that two-way interactions between high- and low-frequency disturbances are important in the formation of positive and negative streamfunction anomalies associated with the PNA pattern.

5.4 Forecasting Implications

Results of this research suggest that model forecasts of NAO and PNA indices could be useful for making medium-range precipitation forecasts. Forecasts of NAO and PNA indices have improved substantially over the past few years; the Global Forecast System (GFS; Kanamitsu et al. 1991) seven- and ten-day ensembles consistently generate PNA and NAO index forecasts that correlate well with observed indices. Thus, NAO and PNA index forecasts may serve to alert forecasters to periods when enhanced precipitation is favored in the Northeast, such as during persistent negative PNA regimes and transitions from positive NAO to negative NAO regimes.

Results of this research may also be used to improve forecaster awareness of when the large-scale pattern is favorable or unfavorable for the development of a significant precipitation event in the Northeast. For example, a model prediction of a negative trend in the NAO index concurrent with a positive trend in the PNA index would suggest that the large-scale environment is favorable for a major precipitation event in the Northeast, although these conditions are not *sufficient* for the development of such an event.

In addition to improving medium-range precipitation forecasting in the Northeast, results from this research may help improve the prediction of a shift in the large-scale flow pattern. Specifically, recognizing synoptic precursors for the onset of blocking, such as in a strong negative NAO regime, is a critical problem in operational forecasting since model forecast skill has been shown to significantly decline with the onset of blocking (e.g., Tracton et al. 1989; Tracton 1990; Tibaldi and Molteni 1990; Kimoto et al. 1992; Tibaldi et al. 1997; Oortwijn 1998; Pelly and Hoskins 2003b). Research results discussed above indicate that a major precipitation event in the Northeast during the cool season may be accompanied by a significant shift in the large-scale pattern such as a weakening North Atlantic jet or an amplifying trough in the East and ridge in the West.

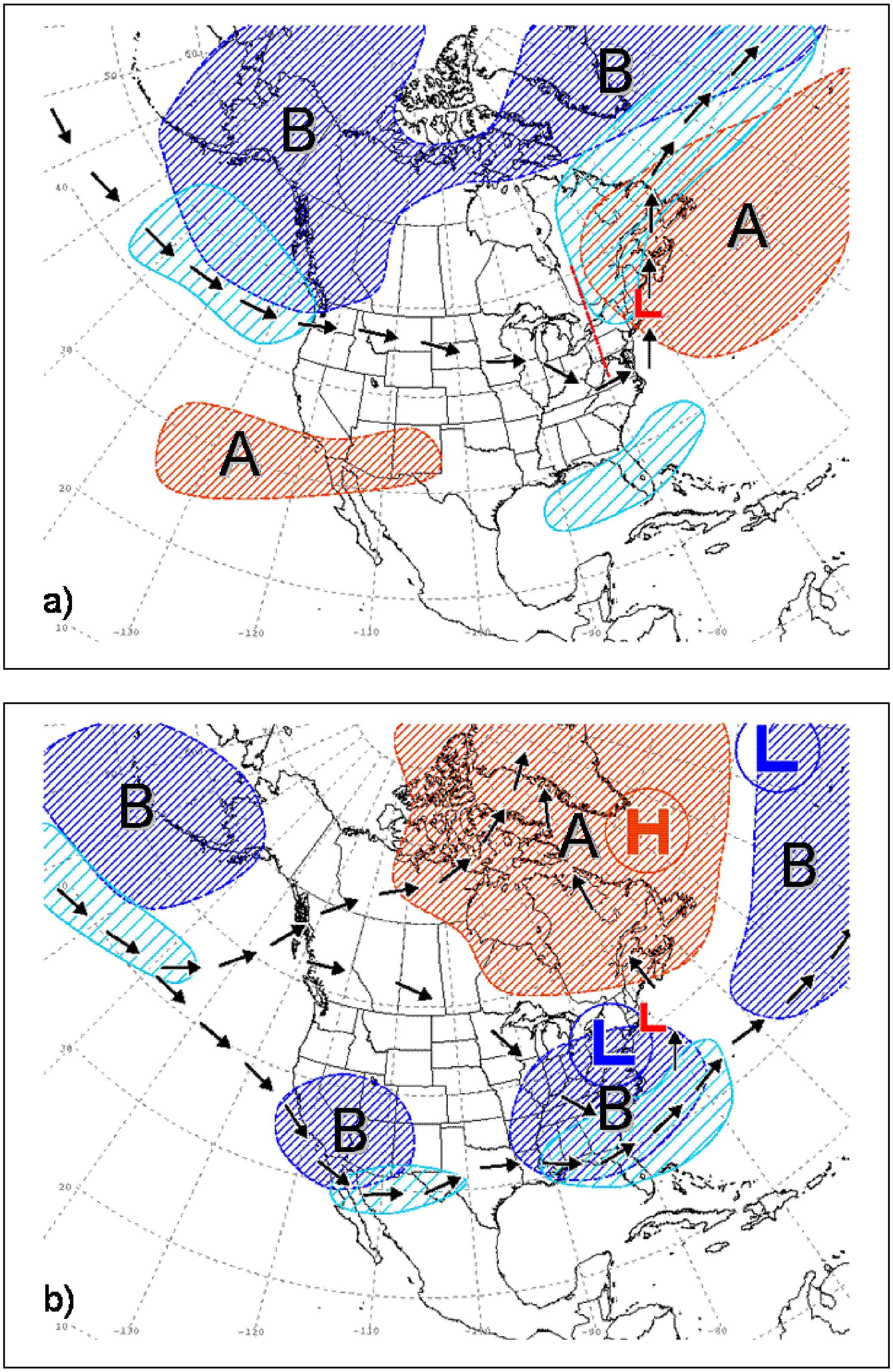

Figure 5.1

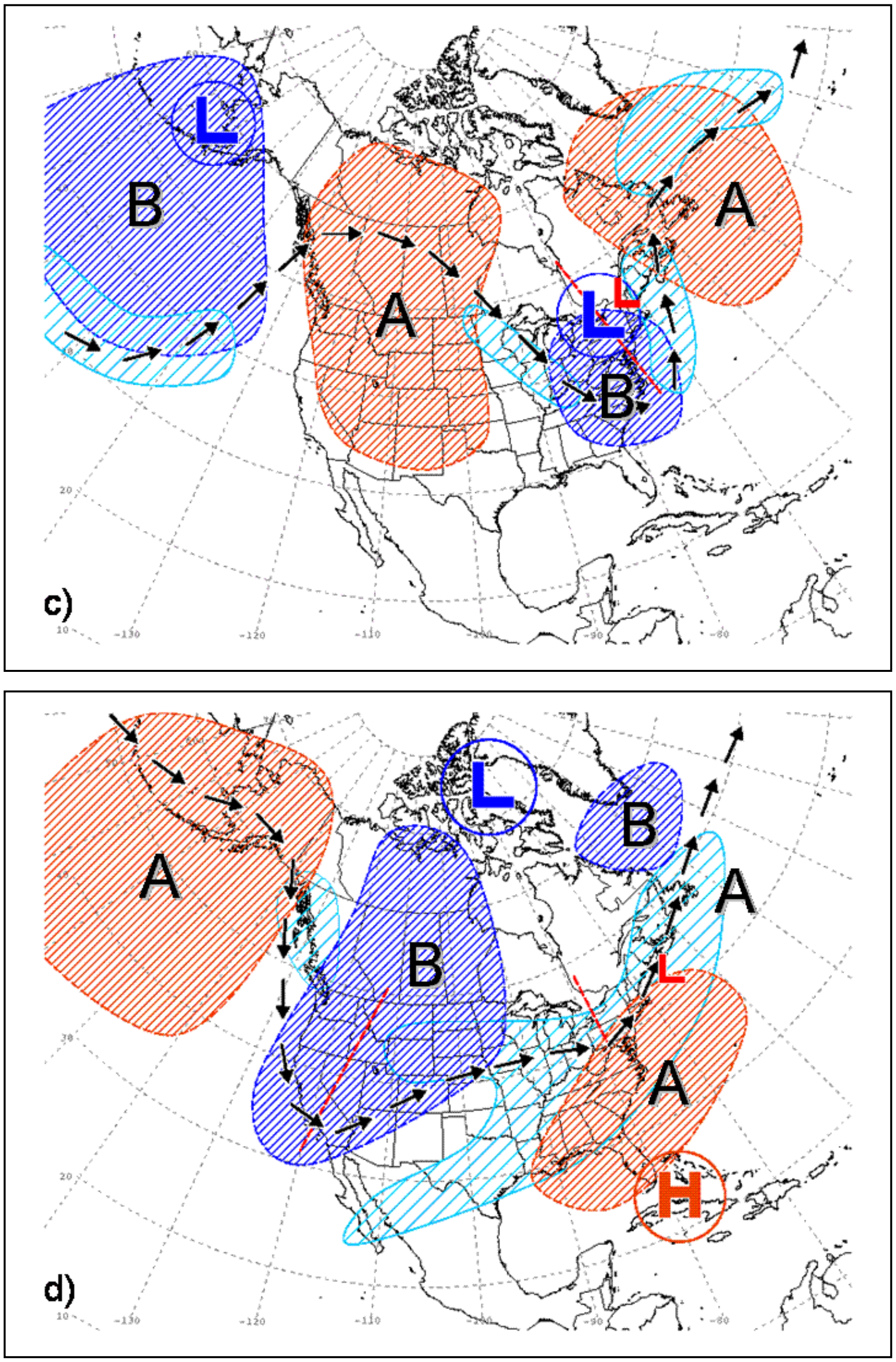

Fig. 5.1. Key synoptic-scale features associated with a major cool-season precipitation event in the Northeast occurring during a (a) positive NAO regime, (b) negative NAO regime, (c) positive PNA regime, and (d) negative PNA regime. The light blue hatched areas are jet maxima at 300 hPa. The red (dark blue) hatched areas represent above normal (below normal) 500 hPa geopotential heights. The encircled L's (H's) indicate closed lows (highs) at 500 hPa. The black arrows indicate the direction of the flow at 500 hPa, while the dashed red lines show trough axes at 500 hPa.

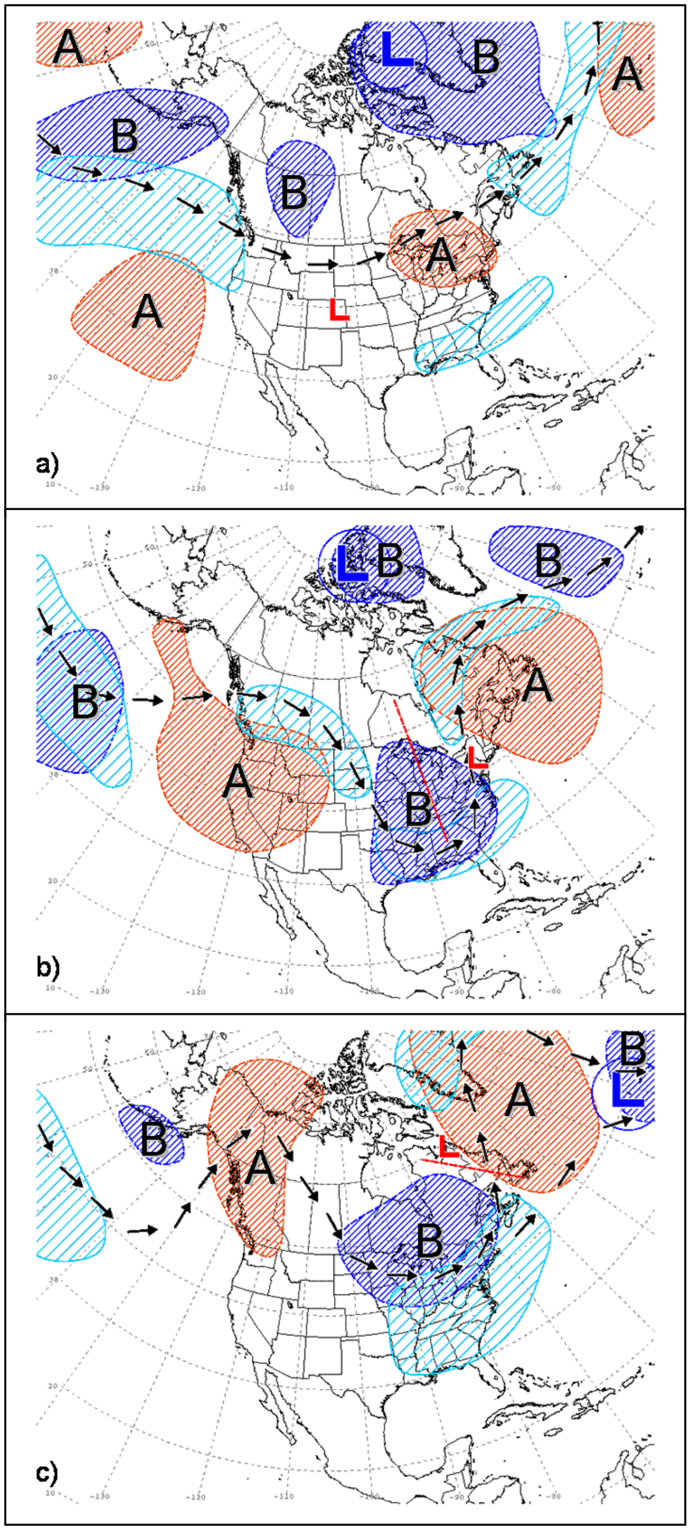

Fig. 5.2. Same as in Fig. 5.1, except for (a) the onset, (b) the midpoint, and (c) the conclusion of a positive-to-negative NAO regime transition with a major Northeast precipitation event occurring at the transition midpoint.

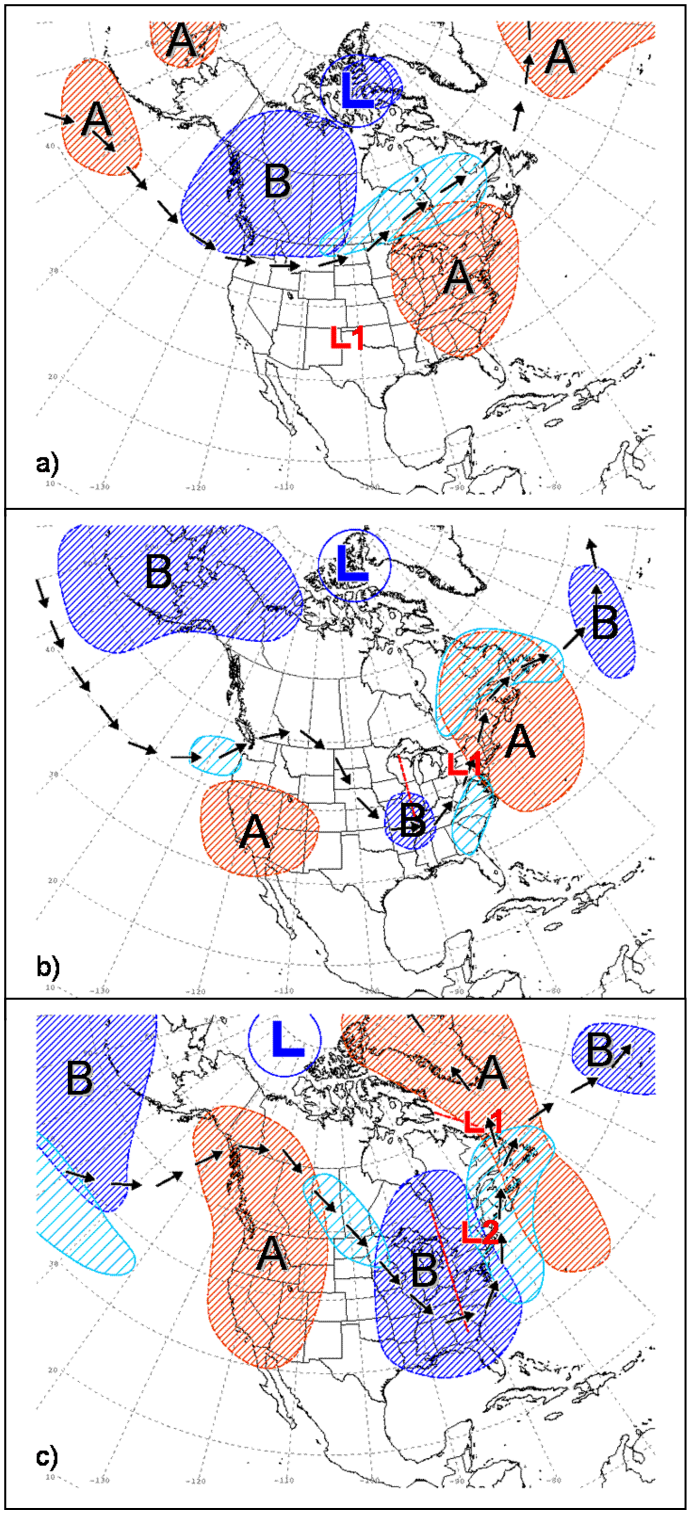

Fig. 5.3. Same as in Fig. 5.2, except for (a) the onset, (b) the midpoint, and (c) the conclusion of a negative-to-positive PNA regime transition with a major Northeast precipitation event occurring at the transition midpoint. L1 and L2 indicate surface lows associated with Northeast precipitation events at the midpoint and end of the transition, respectively.

6. Summary and Suggestions for Future Work

6.1 Summary

Past research indicates that reconfigurations of the large-scale flow can alter regional weather patterns due to storm track shifts and associated eddy transports of heat, vorticity, and momentum (e.g., Dole 1986; Leathers et al. 1991; Branstator 1995; Hurrell 1995). Previous research also documents the critical role of synoptic-scale disturbances in certain large-scale regime transitions (Reinhold and Pierrehumbert 1982; Colucci 1985, 1987; Konrad and Colucci 1989). Motivated by this research, this thesis investigates how large-scale regimes and regime transitions are related to Northeast precipitation in the cool season (November–April). This problem is examined by exploring how the planetary-scale flow influences Northeast precipitation, as well as how Northeast precipitation events influence the planetary-scale flow.

The first part of this thesis specifically seeks to determine how persistent large-scale regimes influence Northeast precipitation in the cool season. A persistent large-scale regime was defined to be a greater than one-standard deviation anomaly in the magnitude of the NAO or PNA index persisting for seven days. Using this definition, composite precipitation anomalies based upon daily domain-average Northeast precipitation amounts were calculated for persistent large-scale regimes.

Research results suggest that relationships exist between persistent large-scale weather regimes and Northeast precipitation in the cool season. Persistent positive NAO and negative PNA regimes are found to be associated with enhanced precipitation in the Northeast, while persistent positive PNA and negative NAO regimes are found to be associated with suppressed precipitation in the Northeast.

In addition to exploring how persistent large-scale regimes influence Northeast precipitation in the cool season, this work investigates characteristic large-scale flow patterns associated with major cool-season precipitation events in the Northeast. To investigate the characteristic flow patterns, NAO and PNA indices during each of the top 25 24-h cool-season precipitation events in the Northeast were calculated. Results suggest that the NAO shows a slight tendency to be in a positive phase during these events, while the PNA shows a greater tendency to be in a positive phase during these events. In order to determine the synoptic signatures of Northeast precipitation events associated with different large-scale regimes, composite analyses were created of the top five 24-h precipitation events associated with strong large-scale regimes (large-scale flow patterns associated with at least a two-standard deviation teleconnection index anomaly). These composite analyses suggest that large-scale regimes strongly modulate the synoptic-scale features associated with major Northeast precipitation events in the cool season. For example, the strength of the surface low and upper-level trough and the influence of upper-level jet streaks seem to depend on the governing large-scale regime.

The second part of this thesis explores relationships between large-scale regime transitions and Northeast precipitation in the cool season. A regime transition was defined as at least a two-standard deviation NAO or PNA index change centered on zero occurring over seven days. Using this definition, composite precipitation anomalies based upon daily domain-average Northeast precipitation amounts were calculated for large-scale regime transitions. Research results show that positive-to-negative NAO regime transitions and negative-to-positive PNA regime transitions are associated with slightly above-normal precipitation in the Northeast, while positive-to-negative PNA transitions and negative-to-positive NAO regime transitions are associated with slightly below-normal precipitation in the Northeast.

In addition to investigating how large-scale regime changes influence precipitation in the Northeast, this research investigates the evolution of the large-scale flow during periods surrounding major Northeast precipitation events. To explore the evolution of the large-scale pattern, seven-day NAO and PNA index tendencies were calculated for the top 25 24-h cool-season precipitation events in the Northeast. These calculations showed that the NAO index typically decreases and the PNA index typically increases in the periods surrounding major precipitation events in the Northeast

To explore the evolution of the synoptic-scale pattern during large-scale regime transitions typically associated with enhanced Northeast precipitation, composite analyses were created of positive-to-negative NAO and negative-to-positive PNA regime transitions with midtransition precipitation events in the Northeast. Composite analyses show that a positive-to-negative NAO regime transition is typically associated with an overall amplification of the flow pattern across North America and the North Atlantic that may be associated with the eastward dispersion of a Rossby wave packet. Interactions between synoptic-scale disturbances and the planetary-scale flow appear to be important in this type of regime transition; strong warm air advection associated with midtransition cyclogenesis over the Northeast appears to build a downstream ridge and lead to a blocking regime over the North Atlantic.

Similar to a positive-to-negative NAO regime transition, a negative-to-positive PNA regime transition is typically associated with an amplification of the large-scale flow pattern across North America and the North Atlantic. Interactions between synoptic-scale features and the large-scale flow also appear to be important in negative-to-positive PNA regime transitions. Two main mechanisms appear to contribute to this kind of regime transition. The first mechanism is the strong, persistent warm air advection that helps build an upper-level ridge over western Canada and perhaps leads to the formation of an upper-level trough over the eastern U.S. through downstream development. Second, midtropospheric geopotential height falls associated with an initial cold surge in the wake of a midtransition Northeast precipitation event appear to precondition the atmosphere for the subsequent formation of a deep upper-level trough over the eastern U.S.

A unique outcome of this research is that Northeast precipitation in the cool season is found to be enhanced during certain large-scale regime transitions. Further, this research suggests that synoptic-scale precursors play an important role in such large-scale regime transitions while also influencing Northeast precipitation.

6.2 Suggestions for Future Work

Composite analyses shown in this thesis suggest that surface lows associated with major Northeast precipitation events in the cool season tend to be located in right-entrance or left-exit regions of upper-level jet streaks, regions dynamically favored for QG ascent. Thus, future work should attempt to quantify the role of upper-level jet streaks in forcing QG ascent over the Northeast during major precipitation events by comparing 700 hPa vertical motion attributable to jet streak secondary circulations to the observed 700 hPa vertical motion.

Another opportunity to expand upon this research may be to study the evolution of potential temperature on the DT during large-scale regime transitions. Recent work on the evolution of large-scale regimes shows that this type of analysis is useful in identifying Rossby wave breaking (Franzke et al. 2003, Benedict et al. 2004) and blocking (Pelly and Hoskins 2003a), phenomena found to be relevant to the understanding of large-scale regime transitions.

Results documented in this thesis suggest that downstream development associated with a Rossby wave train may be an important aspect of the transition from a positive to negative NAO regime. Future work will be to determine the validity of this observation by calculating from a Hovmöller diagram the approximate group velocity of the Rossby waves associated with the composite positive-to-negative NAO transition.

The final suggestion for future work is to assess the predictability of large-scale regime transitions by comparing model skill scores (e.g., anomaly correlation coefficients) during different types of regime transitions. The onset of blocking has been linked to reduced predictability (e.g., Tracton et al. 1989; Tracton 1990; Tibaldi and Molteni 1990; Kimoto et al. 1992; Tibaldi et al. 1997; Oortwijn 1998; Pelly and Hoskins 2003b), suggesting that positive-to-negative NAO regime transitions may be relatively challenging to forecast.

List of Figures

Fig. 4.2a. Composite standardized cool-season Northeast precipitation anomalies during large-scale NAO regime transitions by month. The number of independent events occurring in each month is shown above and below the bars.

Fig. 4.2b. Same as in Fig. 4.2a, except for PNA regime transitions.

Fig. 4.3a. Normalized seven-day NAO index tendencies centered on the top 25 24-h cool-season precipitation events in the Northeast. Numbers to the right of the points indicate the rank of the precipitation events.

Fig. 4.3b. Same as in Fig. 4.3a, except for seven-day PNA index tendencies.

Fig. 4.4a. Composite 500 hPa geopotential heights (dam) and anomalies (dam) corresponding to Day 1 of the top five cool-season precipitation events in the Northeast associated with positive-to-negative NAO regime transitions. Geopotential heights are contoured every 6 dam; anomalies are contoured every 6 dam and are shaded as indicated.

Fig. 4.4b. Composite 300 hPa geopotential heights (dam) and wind speed ($m\ s^{-1}$) corresponding to Day 1 of the top five cool-season precipitation events in the Northeast associated with positive-to-negative NAO regime transitions. Geopotential heights are contoured every 12 dam. Wind speed is contoured every 5 $m\ s^{-1}$ starting at 30 $m\ s^{-1}$; shading begins at 35 $m\ s^{-1}$.

Fig. 4.4c. Composite 1000–500 hPa thickness (dam), 700 hPa absolute vorticity ($10^{-5}\ s^{-1}$), and sea level pressure (hPa) corresponding to Day 1 of the top five cool-season precipitation events in the Northeast associated with positive-to-negative NAO regime transitions. Thickness is contoured every 6 dam in blue, except for the 510 dam, 540 dam, and 570 dam thickness contours, which are red. Sea level pressure is contoured every 4 hPa in black. Absolute vorticity is contoured in intervals of $2 \times 10^{-5}\ s^{-1}$; shading begins at $12 \times 10^{-5}\ s^{-1}$.

Fig. 4.5a. Same as in Fig. 4.4a, except for Day 2 of a seven-day positive-to-negative NAO regime transition.

Fig. 4.5b. Same as in Fig. 4.4b, except for Day 2 of a seven-day positive-to-negative NAO regime transition.

Fig. 4.5c. Same as in Fig. 4.4c, except for Day 2 of a seven-day positive-to-negative NAO regime transition.

Fig. 4.6a. Same as in Fig. 4.4a, except for Day 3 of a seven-day positive-to-negative NAO regime transition.

Fig. 4.6b. Same as in Fig. 4.4b, except for Day 3 of a seven-day positive-to-negative NAO regime transition.

List of Tables

References

Ambaum, M. H. P., B. J. Hoskins, and D. B. Stephenson, 2001: Arctic Oscillation or North Atlantic Oscillation? *J. Climate,* **14**, 3495–3507.

Atallah, E. H., and L. F. Bosart, 2003: The extratropical transition and precipitation distribution of Hurricane Floyd (1999). *Mon. Wea. Rev.,* **131,** 1063–1081.

Barnston, A. G., and R. E. Livezey, 1987: Classification, seasonality and persistence of low-frequency atmospheric circulation patterns. *Mon. Wea. Rev.,* **115**, 1083–1126.

Benedict, J. J., S. Lee, and S. B. Feldstein, 2004: Synoptic view of the North Atlantic Oscillation. *J. Atmos. Sci.,* **61**, 121–144.

Branstator, G., 1995: Organization of storm track anomalies by recurring low-frequency circulation anomalies. *J. Atmos. Sci.,* **52,** 207–226.

Bosart, L. F., G. J. Hakim, K. R. Tyle, M. A. Bedrick, W. E. Bracken, M. H. Dickinson, and D. M. Schultz, 1996: Large-scale antecedent conditions associated with the 12–14 March 1993 cyclone ("superstorm '93") over eastern North America. *Mon. Wea. Rev.,* **124,** 1865–1891.

——, L. F., W. E. Bracken, A. Seimon, 1998: A study of cyclone mesoscale structure with emphasis on a large-amplitude intertia-gravity wave. *Mon. Wea. Rev.,* **126,** 1497–1527.

Cai, M., and M. Mak, 1990: Symbiotic relation between planetary and synoptic-scale waves. *J. Atmos. Sci.,* **47,** 2953–2968.

Cash, B. A., and S. Lee, 2001: Observed nonmodal growth of the Pacific–North American teleconnection pattern. *J. Climate,* **14**, 1017–1028.

Colucci, S. J., 1985: Explosive cyclogenesis and large-scale circulation changes: Implications for atmospheric blocking. *J. Atmos. Sci.,* **42**, 2701–2717.

——, 1987: Comparative diagnosis of blocking versus nonblocking planetary-scale circulation changes during synoptic-scale cyclogenesis. *J. Atmos. Sci.,* **44,** 124–139.

Crantz, D., 1765: Historie von Grönland. Barny und Leipzig. [Translation: History of Greenland, 2nd ed., 2 vols. London, 1820, see p. 42.]

DeLuca, D. P., 2004: The distribution of precipitation over the Northeast accompanying landfalling and transitioning tropical cyclones. M.S. thesis, Department of Earth and Atmospheric Sciences, University at Albany, State University of New York, 177 pp.

Dickinson, M. J., L. F. Bosart, W. Bracken, G. J. Hakim, D. M. Schultz, M. A. Bedrick, and K. R. Tyle, 1997: The March 1993 superstorm cyclogenesis: Incipient phase synoptic- and convective-scale flow interaction and model performance. *Mon. Wea. Rev.,* **125,** 3041–3072.

Dole, R., 1986: Persistent anomalies of the extratropical Northern Hemisphere wintertime circulation: Structure. *Mon. Wea. Rev.,* **114,** 178–207.

Feldstein, S. B., 2003: The dynamics of NAO teleconnection pattern growth and decay. *Quart. J. Roy. Meteor. Soc.,* **129,** 901–924.

Franzke, C., S. Lee, and S. B. Feldstein, 2003: Is the North Atlantic Oscillation a breaking wave? *J. Atmos. Sci.,* **61,** 145–160.

Groenert, D., 2002: Large-scale circulation anomaly indices in relation to cool-season precipitation events in the Northeastern United States. M.S. thesis, Department of Earth and Atmospheric Sciences, University at Albany, State University of New York, 144 pp.

Gyakum, J. R., and P. J. Roebber, 2001: The 1998 ice storm—analysis of a planetary-scale event. *Mon. Wea. Rev.,* **129,** 2983–2997.

Higgins, R. W., W. Shi, E. Yarosh, and R. Joyce, 2000: *Improved United States Precipitation Quality Control System and Analysis*. NCEP/CPC Atlas No. 7, 40 pp.

——, and S. D. Schubert, 1994: Simulated life cycles of persistent anticylonic anomalies over the North Pacific: Role of synoptic-scale eddies. *J. Atmos. Sci.,* **51**, 3238–3260.

——, and H. Nakamura, 2001: Interannual seesaw between the Aleutian and Icelandic lows. Part II: Its significance in the interannual variability over the wintertime Northern Hemisphere. *J. Climate*, **14**, 4512–4529.

Hurrell, J. W., 1995: Decadal trends in the North Atlantic oscillation: Regional temperatures and precipitation. *Science,* **269**, 676–679.

Kalnay, E., M. Kanamitsu, R. Kistler, W. Collins, D. Deaven, L. Gandin, M. Iredell, S. Saha, G. White, J. Woollen, Y. Zhu, A. Leetmaa, B. Reynolds, M. Chelliah, W. Ebisuzaki, W. Higgins, J. Janowiak, K. C. Mo, C. Ropelewski, J.

Wang, R. Jenne, and D. Joseph, 1996: The NCEP/NCAR 40-year reanalysis project. *Bull. Amer. Meteor. Soc*., **77**, 437–471.

Kanamitzu, M., J.C. Alpert, K.A. Campana, P.M. Caplan, D.G. Deaven, M. Iredell, B. Katz, H.-L. Pan, J. Sela, and G.H. White, 1991: Recent changes implemented into the Global Forecast System at NMC. *Wea. Forecasting*, **6,** 426–435.

Kimoto, M., H. Mukougawa, and S. Yoden, 1992: Medium-range forecast skill variation and blocking transition: A case study. *Mon. Wea. Rev.,* **120,** 1616–1627.

Kocin, P. J., and L. W. Uccellini, 2004: *Northeast Snowstorms. Meteor. Monogr.,* No. 54, Amer. Meteor. Soc., 818 pp.

Konrad, C. E., II, and S. J. Colucci, 1989: An examination of extreme cold air outbreaks over eastern North America. *Mon. Wea. Rev.,* **117,** 2687–2700.

Lackmann, G. M., L. F. Bosart, and D. Keyser, 1996: Planetary- and synoptic-scale characteristics of explosive wintertime cyclogenesis over the western North Atlantic Ocean. Mon. Wea. Rev., **124**, 2672–2702.

Leathers, D. J., B. Yarnal, and M. A. Palecki, 1991: The Pacific/North American teleconnection pattern and United States climate. Part I: Regional temperature and precipitation associations. *J. Climate,* **4**, 517–528.

Lejenäs, H., and H. Økland, 1983: Characteristics of Northern Hemisphere blocking as determined from a long time series of observational data. *Tellus,* **35A**, 350–362.

Mullen, S. L., 1987: Transient eddy forcing of blocking flows. *J. Atmos. Sci.,* **44**, 3–22.

Namias, J., 1950: The index cycle and its role in the general circulation. *J. Atmos. Sci.,* **7**, 130–139.

——, and P. F. Clapp, 1949: Confluence theory of the high tropospheric jet stream. *J. Meteor.,* **6,** 330–336.

Nicosia, D. J., and R. H. Grumm, 1999: Mesoscale band formation in three major Northeast United States snowstorms. *Wea. Forecasting,* **14,** 346–368.

Novak, D. R., L. F. Bosart, D. Keyser, and J. S. Waldstreicher, 2004: An observational study of cold season–banded precipitation in Northeast U.S. cyclones. *Wea. Forecasting,* **19,** 993–1010.

Oortwijn, J., 1998: Predictability of the onset of blocking and strong zonal flow regimes. *J. Atmos. Sci.,* **55**, 973–994.

Palmén, E., and C. W. Newton, 1969: *Atmospheric Circulation Systems: Their Structure and Physical Interpretation.* Academic Press, 603 pp.

Pelly, J. L., and B. J. Hoskins, 2003a: A new perspective on blocking**.** *J. Atmos. Sci.,* **60**, 743–755.

——, and ——, 2003b: How well does the ECMWF Ensemble Prediction System predict blocking? *Quart. J. Roy. Meteor. Soc.,* **129**, 1683–1702.

Quadrelli, R., and J. M. Wallace, 2004a: A simplified linear framework for interpreting patterns of Northern Hemisphere wintertime climate variability. *J. Climate,* **17**, 3728–3744.

——, and ——, 2004b: Varied expressions of the hemispheric circulation observed in association with contrasting polarities of prescribed patterns of variability. *J. Climate,* **21**, 4245–4253.

Reinhold, B. B., and R. T. Pierrehumbert, 1982: Dynamics of weather regimes: Quasi-stationary waves and blocking. *Mon. Wea. Rev.,* **110**, 1105–1145.

——, and S. Yang, 1993: The role of transients in weather regimes and transitions. *J. Atmos. Sci.,* **50**, 1173–1180.

Rex, D.P., 1950a: Blocking action in the middle troposphere and its effects on regional climate (I). An aerological study of blocking. *Tellus,* **2**, 196–211.

——, 1950b: Blocking action in the middle troposphere and its effects on regional climate (II). The climatology of blocking actions. *Tellus,* **2**, 275–301.

Rossby, C.-G., 1939: Relations between variations in the intensity of the zonal circulation and the displacements of the semi-permanent centers of action. *J. Mar. Res.,* **2**, 38–55.

——, and H. C. Willett, 1948: The circulation of the upper troposphere and lower stratosphere. *Science,* **108**, 643–652.

Sanders, F., and J. R. Gyakum, 1980: Synoptic-dynamic climatology of the “bomb”. *Mon. Wea. Rev.,* **108**, 1589–1606.

Shabar, A., J. Huang, and K. Higuchi, 2001: The relationship between the wintertime North Atlantic Oscillation and blocking episodes in the North Atlantic. *Int. J. Climatol.,* **21**, 355–369.

Sutcliffe, R. C., 1947: A contribution to the problem of development: *Quart. J. Roy. Meteor. Soc.,* **73**, 370–383.

Tibaldi, S., and F. Molteni, 1990: On the operational predictability of blocking. *Tellus,* **42A**, 343–365.

——, F. D'Andrea, E. Tosi, and E. Roeckner, 1997: Climatology of northern hemisphere blocking in the ECHAM model. *Clim. Dyn.*, **13,** 649–666.

Thorncroft, C. D., B. J. Hoskins, and M. E. McIntyre, 1993: Two paradigms of baroclinic-wave life-cycle behavior. *Quart. J. Roy. Meteor. Soc.,* **119,** 17–55.

Tracton, M. S., 1990: Predictability and its relationship to scale interaction processes in blocking. *Mon. Wea. Rev.,* **118**, 1666–1695.

——, K. Mo, W. Chen, E. Kalnay, R. Kistler, and G. White, 1989: Dynamical extended range forecasting (DERF) at the National Meteorological Center. *Mon. Wea. Rev.,* **117**, 1606–1637.

Trenberth, K. E., 1978: On the interpretation of the diagnostic quasi-geostrophic omega equation. *Mon. Wea. Rev.,* **106**, 131–136.

Uccellini, L. W., and P. J. Kocin, 1987: The interaction of jet streak circulations during heavy snow events along the east coast of the United States. *Wea. Forecasting,* **2,** 289–308.

van Loon, H., and J. C. Rogers, 1978: The seesaw in winter temperatures between Greenland and Northern Europe. Part I: General description. *Mon. Wea. Rev.,* **106**, 296–310.

Walker, G. T., and E. W. Bliss, 1932: World Weather V. *Mem. Roy. Meteor. Soc.,* **4,** 53–84.

Wallace, J. M., 2000: North Atlantic Oscillation/annular mode: Two paradigms—one phenomenon. *Quart. J. Roy. Meteor. Soc.,* **126**, 791–805.

——, and D. S. Gutzler, 1981: Teleconnections in the geopotential height field during the Northern Hemisphere winter. *Mon. Wea. Rev.,* **109**, 784–812.

Wilks, D. S., 1995: *Statistical Methods in the Atmospheric Sciences*. Academic Press, 467 pp.

Abstract

Past research has indicated that reconfigurations of large-scale flow regimes can alter regional weather patterns due to shifts in storm tracks and associated eddy transports of heat, momentum, and vorticity. Conventional wisdom also suggests that high-impact weather events tend to occur during large-scale regime transitions. Motivated by these considerations, this research investigates relationships between large-scale regime transitions and Northeast precipitation in the cool season (November–April) from a statistical and synoptic perspective.

In this study, a regime transition is defined as a two-standard-deviation change centered on zero in the North Atlantic Oscillation (NAO) index or Pacific/North American (PNA) pattern index over a seven-day period. To identify regime transitions, a 56-year database (1948–2003) of daily NAO and PNA indices was generated from the National Centers for Environmental Prediction (NCEP)–National Center for Atmospheric Research (NCAR) reanalysis dataset. A daily precipitation anomaly database for the Northeast was derived from the Unified Precipitation Dataset (UPD) for the same 56-year period.

Key statistical results indicate that transitions from positive to negative NAO regimes and from negative to positive PNA regimes are associated with enhanced precipitation in the Northeast. Conversely, transitions from negative to positive NAO regimes and from positive to negative PNA regimes are associated with suppressed Northeast precipitation. Results also show that during periods

surrounding major Northeast precipitation events in the cool season, the NAO index tends to decrease and the PNA index tends to increase.

To interpret these relationships synoptically, composite analyses were created of cool-season regime transitions surrounding major precipitation events in the Northeast. The analyses suggest that synoptic-scale features are important in these types of large-scale regimes transitions. A positive-to-negative NAO regime transition (a weakening of the North Atlantic jet) surrounding a major Northeast precipitation event appears to be related to strong warm air advection in the western North Atlantic downstream of a surface low associated with the Northeast precipitation event. In the case of a negative-to-positive PNA regime transition [an amplification of a trough (ridge) over eastern (western) North America] surrounding a major Northeast precipitation event, two synoptic-scale features appear to be important. One feature is persistent warm air advection that amplifies a ridge over western North America, and the other feature is a weak cold surge in the Northeast in the wake of the precipitation event that acts to precondition the atmosphere for a second, stronger cold surge over eastern North America.